Ministère de l'Enseignement Supérieur et de la Recherche Scientifique

Université Hassiba Benbouali de Chlef

Faculté des Sciences et de la technologie

Département d' Électrotechnique

THÈSE

Présentée pour l'obtention du diplôme de

DOCTORAT

Filière : Électrotechnique

Spécialité : Commande Électrique

Par

Abderrahim SAKOUCHI

Thème:

Commande par Backstepping d'un Système de Conversion d'Énergie Eolienne Multi-machine (Backstepping Control of a Multi-Machine Wind Energy System)

Soutenue le 24/02/2025, devant le jury composé de :

BOUNADJA Mohammed	Professeur	Université de Chlef	Président
DJAHBAR Abdelkader	Professeur	Université de Chlef	Rapporteur
BOUNADJA Elhadj	Professeur	Université de Chlef	Co-rapporteur
HAMZAOUI Ihssen	MCA	Université de Khemis Miliana	Examinateur
YAHDOU Adil	MCA	Université de Chlef	Examinateur
BENBOUALI Abderrahman	MCA	Université de Chlef	Examinateur
HELAIMI M'hamed	Professeur	Université de Chlef	Invité

Dedication

This thesis is dedicated to my remarkable parents, whose unwavering support and guidance have shaped me into the person I am today. I am profoundly grateful for their unconditional love and encouragement throughout my journey. Their sacrifices and belief in my potential have been instrumental in my achievements. I sincerely appreciate everything they have done for me.

This work is dedicated to the cherished memory of my beloved grandfather and my uncle El Khemici, whose influence continues to inspire me. I extend my heartfelt gratitude to my grandmother, who has always been a nurturing and compassionate second mother to me. I am also thankful for the love and support of my sisters, as well as the joy brought by my sister's children. My appreciation goes to my brother-in-law for his encouragement.

I would like to acknowledge my family, the Sakouchi family, for their unwavering support. Special thanks are due to my friends Yahia, Hatem, Fathy, and Khaled, whose assistance has been invaluable. I also express my gratitude to all my friends and colleagues who have accompanied me on this journey.

Furthermore, I would like to extend my sincere appreciation to all the educators who have guided me throughout my academic career, particularly the faculty members in the Department of Electrical Engineering at Chlef and Medea. Their knowledge and mentorship have played a significant role in my development and success.

SAKOUCHI Abderrahim

Acknowledgments

Praise to "Allah" for bestowing upon me the faith, courage, and patience necessary to successfully complete this research under better favorable conditions.

At the conclusion of this research, I would like to extend my sincere gratitude to my supervisors, **Pr. Djahbar Abdelkader** and **Pr. Bounadja Elhadj**, from the Department of Electrical Engineering at Chlef University. Additionally, I would like to express my appreciation to **Dr. Benbouhenni Habib**, **Pr. Moualdia Abdelhafidh**, and **Dr. Kabache Nadir** for their invaluable support and guidance.

I would like to extend my heartfelt appreciation to the members of my graduate study committee: the committee chair, **Pr. Mohammed Bounadja** from the University of Chlef, and the jury members, **Dr. Ihssen Hamzaoui** from the University of Khemis Miliana, **Dr. Adil Yahdou**, and **Dr. Abderrahman Benbouali**, all from the University of Chlef, as well as **Pr. M'hamed Helaimi** from the University of Chlef and **Pr. Abdelhafidh Moualdia** from the University of Medea. I am grateful for their time and effort in reviewing my thesis and serving on my committee, as well as for their invaluable advice and assistance. I sincerely appreciate their willingness to be part of the reading committee despite their numerous commitments.

I also wish to express my gratitude to all those who contributed to the development and realization of this thesis, including everyone who supported me, both directly and indirectly, in completing this work, with special thanks to **Mr. Selma Belkacem.**

Lastly, I would like to extend my deepest appreciation to my parents for their unwavering support throughout my extensive years of study.

List of Publications

Journal Publications

1. **Sakouchi A,** Bounadja E, Djahbar A, Moualdia A. Artificial intelligent-based backstepping control of parallel-connected multi-machine wind generation system using a new fifteen-switch rectifier. Wind Engineering. 2024 Oct 7:0309524X241270424.
2. **Sakouchi A,** Djahbar A, Bounadja E, Benbouhenni H, Iqbal A, Moualdia A, Kechida A. Enhanced control of grid-connected multi-machine wind power generation systems using fuzzy backstepping approaches. Energy Reports. 2024 Dec 1;12:4208-31.
3. **Sakouchi, A.,** Djahbar, A., Bounadja, E., & Moualdia, A. (2025). Intelligent backstepping control of power grid-connected wind power generation system using two five-phase PMSGs controlled through the fifteen-switch rectifier. Measurement and Control, 00202940251318995.

Conference Proceedings

1. **Sakouchi A,** Bounadja E, Djahbar A. Direct Power Control based on Second Order Sliding Mode Controller of a five-phase PMSG Wind Turbine. In2023 1st International Conference on Renewable Solutions for Ecosystems: Towards a Sustainable Energy Transition (ICRSEtoSET) 2023 May 6 (pp. 1-6). IEEE.
2. **Sakouchi A,** Bounadja E, Djahbar A. Nonlinear control via Backstepping for five-phase permanent magnet synchronous generator-based wind generation system. In2023 2nd International Conference on Electronics, Energy and Measurement (IC2EM) 2023 Nov 28 (Vol. 1, pp. 1-6). IEEE.
3. **Sakouchi, A**., Djahbar, A., & Bounadja, E. (). Enhanced Performance of Wind Farm Systems with Multi-phase PMSGs using Backstepping Control. In 2024 International Conference on Advances in Electrical and Communication Technologies (ICAECOT) 2024 October (pp. 1-6). IEEE.

Abstract

This thesis presents a methodology to improve the performance of a multi-machine wind power generation system (WPGS) by incorporating nonlinear and intelligent control techniques. The primary objective is to optimize the system's performance, which utilizes permanent magnet synchronous generators (PMSGs) connected to the electrical grid. To enable this grid interconnection, a novel back-to-back converters (NBTBCs) configuration is employed, comprising a fifteen-switch rectifier (FSR) and a conventional inverter, with control implemented using pulse width modulation (PWM).

The control algorithm has been meticulously designed to efficiently control the system while concurrently minimizing fluctuations in both active and reactive power. Initially, a thorough model of the wind power generation system is presented. This is then followed by a comprehensive exposition of the fuzzy backstepping control (FBC) law, which seamlessly incorporates the Lyapunov stability technique. The utilization of fuzzy logic (FL) serves to adaptively adjust the gains within the backstepping (BC) framework, thereby ensuring that the control system is capable of effectively responding to disturbances and variations in system parameters. Consequently, this adaptive control strategy significantly enhances the overall efficiency of the system in both static and dynamic operational modes.

The conducted simulation tests employing MATLAB have yielded a comparative analysis of the proposed strategy against the traditional backstepping control (BC) approach. The findings demonstrate that the fuzzy backstepping control (FBC) methodology exhibits robust performance and superior reference tracking capabilities, successfully mitigating speed overshoot under diverse wind conditions. These results validate the effectiveness and advantages of the proposed control strategy over conventional methods in managing the inherent complexities associated with wind power generation systems (WPGSs).

Keywords: Permanent magnet synchronous-generators, wind power generation system, fifteen-switch rectifier, Multi-machine, backstopping control, fuzzy logic, fuzzy backstopping control.

Résumé

Cette thèse présente une méthodologie visant à améliorer la performance d'un système de génération d'énergie éolienne (SGEE) à multi machine en intégrant des techniques de contrôle non linéaires et intelligentes. L'objectif principal est d'optimiser la performance du système, qui utilise des générateurs synchrones à aimants permanents (GSAP) connectés au réseau électrique. Pour permettre cette interconnexion au réseau, une configuration novatrice de convertisseurs à double conversion (NCDC) est employée, comprenant un redresseur à quinze interrupteurs (RQI) et un onduleur conventionnel, avec un contrôle mis en œuvre à l'aide de la modulation de largeur d'impulsion (MLI).

L'algorithme de contrôle a été méticuleusement conçu pour gérer efficacement le système tout en minimisant simultanément les fluctuations de la puissance active et réactive. Dans un premier temps, un modèle complet du système de génération d'énergie éolienne est présenté. Cela est ensuite suivi par une exposition exhaustive de la loi de contrôle par backstepping flou (CBF), qui intègre de manière fluide la technique de stabilité de Lyapunov. L'utilisation de la logique floue permet d'ajuster de manière adaptative les gains au sein du cadre de backstepping (BC), garantissant ainsi que le système de contrôle est capable de répondre efficacement aux perturbations et aux variations des paramètres du système.

Par conséquent, cette stratégie de contrôle adaptatif améliore considérablement l'efficacité globale du système tant en modes opérationnels statiques que dynamiques. Les tests simulation réalisés avec MATLAB ont permis d'effectuer une analyse comparative de la stratégie proposée par rapport à l'approche traditionnelle de BC. Les résultats montrent que la méthodologie de CBF présente des performances robustes et des capacités de suivi de référence supérieures, atténuant avec succès les dépassements de vitesse dans diverses conditions de vent. Ces résultats valident l'efficacité et les avantages de la stratégie de contrôle proposée par rapport aux méthodes conventionnelles dans la gestion des complexités inhérentes aux SGEE.

Mots-clés : Générateurs Synchrones à Aimants Permanents, Système de Génération d'énergie éolienne, Redresseur à Quinze Interrupteurs, Multi machine, Contrôle par Backstepping, Logique Floue, Contrôle par Backstepping Flou.

ملخص

تقدم هذه الأطروحة استراتيجية تحكم قوية لتحسين قدرة نظام توليد (WPGS) طاقة الرياح متعدد الآلات من خلال دمج تقنيات التحكم الغير خطية و الذكية معا. الهدف تحسين أداء النظام، الذي يستخدم مولدات متزامنة ذات مغناطيس دائم (PMSGs) متصلة بالشبكة الكهربائية. لتمكين هذا الاتصال بالشبكة، يتم استخدام تكوين مبتكر لمحولين متتاليين (NBTBCs)، يتكون من مقوّم بخمسة عشر مفتاحًا (FSR) ومحوّل تقليدي، مع تنفيذ التحكم باستخدام تعديل عرض النبضة (PWM).

تم تصميم خوارزمية التحكم بدقة للتحكم الفعال في النظام مع تقليل التقلبات في كل من الطاقة النشطة و المتفاعلة. في البداية، يتم تقديم نموذج شامل لنظام توليد الطاقة الرياح (WPGS). ثم يتبعه عرض شامل لقانون التحكم الغير خطي الضبابي (FBC)، الذي يدمج بسلاسة تقنية استقرار ليوبونوف. تُستخدم المنطق الضبابي (FL) لضبط المكاسب بشكل تكيفي ضمن إطار استراتيجية التحكم التحكم بالتراجع (BC) ، مما يضمن أن نظام التحكم قادر على الاستجابة بفعالية للاضطرابات والتغيرات في معلمات النظام.

أسفرت الاختبارات التجريبية التي تم اجرائها باستخدام (MATLAB) عن تحليل مقارن للاستراتجية المقترحة مقابل نهج التحكم التقليدي (BC). تظهر النتائج ان استراتيجية التحكم التحكم الضبابي بالتراجع (FBC) تظهر آداءً قويًا في تتبع القيم المرجعية بتفوق، مما يخفف بنجاح من تجاوزات السرعة في ظل تقلبات الرياح المتنوعة. تثبت هذه النتائج فعالية ومزايا استراتيجية التحكم المقترحة مقارنة بالطريقة التقليدية في ادارة التعقيدات الكامنة المرتبطة بنظم توليد طاقة الرياح (WPGS).

الكلمات المفتاحية: مولدات متزامنة ذات مغناطيس دائم، نظام توليد طاقة الرياح، مقوّم بخمسة عشر مفتاحًا، متعدد الآلات ، التحكم الضبابي ، التحكم بالتراجع ،التحكم بالتراجع الضبابي.

List of Abbreviations

RE	Renewable Energy
WE	Wind Energy
SE	Solar Energy
EE	Electrical Energy
WTs	Wind Turbines
WS	Wind Speed
PV	Photovoltaic
MM	Mathematical Model
IRENA	International Renewable Energy Agency
LCOE	Levelized Cost Of Electricity
WPGS	Wind Power Generation System
PMSM	Permanent Magnet Synchronous Machine
PMSG	Permanent Magnet Synchronous Generator
DFIG	Doubly-Fed Induction Generator
AC	Alternative Current
DC	Direct Current.
BTBCs	Back-To-Back converters
MSC	Machine Side Converter
GSC	Grid Side Converter
NSI	Nine-Switch Inverter
FSR	Fifteen-Switch Rectifier
MPC	Model Predictive Control
SMC	Sliding Mode Control
LF	Lyapunov Function
BC	Backstepping Control
FL	Fuzzy Logic
FBC	Fuzzy Backstepping Control
MFs	Membership Functions
PWM	Pulse Width Modulation
SVM	Space Vector Modulation
THD	Total Harmonic Distortion
SSE	Steady-State Error

List of Symbols

P_v	Aerodynamic energy
ρ	Air density
V_W	Wind speed.
C_p	Power coefficient.
A	Swept area by the wind
R	Blades' radius.
λ	Tip velocity ratio.
β	Pitch angle of the propeller blades
V_{abcde}	Voltages.
I_{abcde}	Currents
Φ_{abcde}	Flux linkage
R_s	Stator resistance
Φ_f	Amplitude of fundamental of the permanent magnet flux linkages
L_s	Stator inductance
L_{ls}	Leakage inductance
$L_{ls} + L_{ms}$	Self-inductance of phase
θ_m	Rotor position.
$V_{\alpha s}, V_{\beta s}, V_{xs}, V_{ys}$	Stator voltages in the α-β-x-y axes.
$I_{\alpha s}, I_{\beta s}, I_{xs}, I_{ys}$	Stator currents in the α-β-x-y axes.
$\Phi_{\alpha s}, \Phi_{\beta s}, \Phi_{xs}, \Phi_{ys}$	Flux linkage in the α-β-x-y frame.
$V_{ds}, V_{qs}, V_{xs}, V_{ys}$	Stator voltages in the d-q-x-y axes
$I_{ds}, I_{qs}, I_{xs}, I_{ys}$	Stator currents in the d-q-x-y axes
$\Phi_{ds}, \Phi_{qs}, \Phi_{xs}, \Phi_{ys}$	Flux linkage in the d-q-x-y frame.
L_d, L_q	Inductances in the d-q axes
w_m	Electrical speed
Ω_m	Mechanical speed.
T_{em}	Electromagnetic Torque
T_m	Turbine's mechanical torque
J	Inertia coefficient

K_f	Friction coefficient
P	Number of poles pairs
S_a S_b S_c S_d S_e	Switching signals
j	machine's number
$\xi_{\Omega j}$	Speed error
ξ_{dj} ξ_{dj} ξ_{xj} ξ_{yj}	Currents error
V	Lyapunov function
k_Ω	Speed regulator gain
k_d k_q k_x k_y	Currents regulators gains (MSC)
V_{gd}, V_{gq}	Grid voltages in the d-q axes.
V_{id}, V_{iq}	The voltage vector of the inverter in the d-q
I_{gd}, I_{gq}	Grid currents in the d-q axes.
w_g	The grid's angular frequency.
R_g	The resistance of the grid filter
L_g	The inductance of the grid filter
V_{dc}	DC-link voltage
P_g	Grid active power
Q_g	Grid reactive power
e_{dc}	DC-link voltage error
e_d e_q	Grid currents error
k_{dc}	DC-link voltage regulator gain.
K_{dg} K_{qg}	Grid currents regulators gains.

List of Figures

Fig. (1.1): Wind atlas of Algeria at 10 m above ground level.....9

Fig. (1.2): Comparison of average wind speeds at windy sites 9

Fig. (1.3): Recoverable and usable power at 10m and 25m in various zones 11

Fig. (1.4): The WT system. 12

Fig. (1.5): WE capacity (in Megawatts) installed in 2023 13

Fig. (1.**6):** Types of the three vertical axis wind turbines. 14

Fig. (1.7): Horizontal axis wind turbine (HAWT). 14

Fig. (1.8): Upwind and Downwind wind turbines. 15

Fig. (1.9): The wind turbine tower.. 17

Fig. (1.10): The rotor of a wind turbine. 17

Fig. (1.11): The nacelle of a wind turbine. 18

Fig. (1.12): The key elements 18

Fig. (1.13): The increase in annual installed capacity of onshore and offshore wind farms globally from 2010 to 2022 19

Fig. (1.14): Onshore wind system 20

Fig. (1.15): Offshore wind system 20

Fig. (1.16): Statistics on the world's wind power production in 2020. 21

Fig. (1.17): Stages of energy conversion in a contemporary wind generation system 22

Fig. (1.18): DFIG (Doubly Fed Induction Generator). 23

Fig. (1.19): PMSG (Permanent Magnet Synchronous Generator).. 24

Fig. (2.1): Machines type1. 34

Fig. (2.2): Machines type 2. 35

Fig. (2.3): Internal architecture of a PMSM 37

Fig. (2.4): Two different model of PM machine based on field flux 38

Fig. (2.5): Simple axial structure with a rotor and stator. 38

Fig. (2.6): Axial flux structure with double rotor and one stator. 39

Fig. (2.7): Axial flux structure with double stator and rotor.....39

Fig. (2.8): Radial flux configuration: a) external rotor, b) internal rotor. 40

Fig. (2.9): The machine's model: (a) SPM machine model; (b) The SPM machine's rotor structure; (c) IPM machine model; (d) The IPM machine's rotor structure. 41

Fig. (2.10): Characteristic of the electric torque-angle. 42

Fig. (2.11): Diagrammatic illustration of a five-phase PMSG.....43

Fig. (2.12): d-q-x-y frame. 46

Fig. (2.13): Configuration of a WS utilizing two parallel PMSGs. 48

Fig. (2.14): Configuration of a WS utilizing three parallel PMSGs 48

Fig. (2.15): The connection of 2 machines to the FSR.. 49

Fig. (3.1): Traditional multiphase rectifier based multi-machine system 54

Fig. (3.2): The architecture of a fifteen-switch rectifier (FSR) based multi-machine system 54

Fig. (3.3): Scheme for generating gate signals.....56

Fig. (3.4): Control signals for a FSR.....56

Fig. (3.5): Conventional 5-phase rectifier.....57

Fig. (3.6): The 5-phase rectifier space vectors in two two-dimensional subspaces.....58

Fig. (3.7): FSR's Operational Strategy. 62

Fig. (3.8): Control inputs for the upper and lower stages are applied sequentially to the FSR....62

Fig. (3.9): The FSR's Simulink diagram. 63

Fig. (3.10): The carrier and references control signals.. 64

Fig. (3.11): The dc-bus voltages. 64

Fig. (4.1): The control design of FSR. 71

Fig. (4.2): Self-tuning structure of the FBC technique.. 75

Fig. (4.3): Fuzzy controller's structural diagram. 76

Fig. (4.4): MF of the error($\boldsymbol{e}$) and the rate of error ($\dot{\boldsymbol{e}}$).....77

Fig. (4.5): The tuned $\boldsymbol{K}_{\Omega \boldsymbol{J}}$ gains' MF.. 77

Fig. (4.6): The control design of GSC. 79

Fig. (4.7): WPGS's general command structure.. 81

Fig. (4.8): Budd curve for BC technique.. 83

Fig. (4.9): Budd curve for FBC strategy.. 84

Fig. (4.10): Steps wind velocity profiles.. 86

Fig. (4.11): Generators' mechanical speed. 86

Fig. (4.12): PMSGs' electromagnetic torque.. 86

Fig. (4.13): I_d- I_q currents: (a, b) PMSG-1, (c, d) PMSG-2. 87

Fig. (4.14): DC-link voltage, power, and THD of the suggested methods.. 88

Fig. (4.15): Variable WS profile.. 90

Fig. (4.16): Block Simulation outcomes of WPGS controlled by FBC: a)Total mechanical power; b) Total torque. 90

Fig. (4.17): PMSGs' mechanical speed.. 91

Fig. (4.18): The simulation outcomes of test 2.. 92

Fig. (4.19): PMSGs' mechanical speed (Robust test). 94

Fig. (4.20): The results of test 3.. 95

List of Table

Table (1.1): Overview of the leading countries in WE 12

Table (1.2): Advantages and disadvantages of fixed-speed and variable-speed wind turbines. 16

Table (2.1): The connection method of the 5-phase machines to the FSR.....49

Table (3.1): The switching state of the FSR and the voltage of its poles.....55

Table (3.2): The rectifier's switching states.....59

Table (3.3): Switching state of FSR 61

Table (3.4): Comparison between the suggested rectifier and the conventional one. 65

Table (4.1): Table containing FLC system rules. 76

Table (4.2): The response time, overshoot, ripples, and SSE ratios of the five-phase PMSG energy (test 1). 89

Table (4.3): The response time, overshoot, ripples, and SSE ratios of the five-phase PMSG energy (Test 2). 93

Table (4.4): The response time, ripples, overshoot, and SSE ratios of the five-phase PMSG energy (Test 3). 96

Table (4.5): Comparative analysis of performance among several control techniques.....97

Table of Contents

General Introduction 1

Chapter 1 State of the art of wind energy conversion

1.1 Introduction 7
1.2 Wind Energy Potential in Algeria 8
1.3. The Preamble of the Wind Energy System 10
1.3.1 History 11
1.3.2 Type of wind turbines 13
1.3.2.1 Vertical Axis Wind Turbine (VAWT) 13
1.3.2.2 Horizontal Axis Wind Turbine (HAWT) 14
1.3.2.3 The Two Type of Wind Turbine 15
1.4 The Architecture of a Wind Turbine 16
1.4.1 The Tower 16
1.4.2 The Rotor 17
1.4.3 The Nacelle 17
1.5 The Categories of Wind Turbines 18
1.5.1 Onshore Wind Energy 19
1.5.2 Offshore Wind Energy 20
1.6 The wind Energy Conversion Chain 21
1.6.1 Asynchronous Generator 22
1.6.1.1 Squirrel Cage Induction Generator (SCIG) 22
1.6.1.2 Squirrel Doubly Fed Induction Generator (DFIG) 22
1.6.2 Synchronous Generator 23
1.6.2.1 Wound Rotor SG 23
1.6.2.2 Permanent Magnet Synchronous Generator (PMSG) 23
1.7 Wind Energy: Its Advantages and Disadvantages 24
1.7.1 Advantages 24
1.7.2 Disadvantages 24
1.8 WT Model 25
1.8.1 Power coefficient 26
1.8.2 WS model 26
1.9 Conclusion 26
References 27

Chapter 2 Modeling of Parallel multi-machine system

2.1 Introduction....33
2.2 Multi-phase Machine....33
2.2.1 Type 1....34
2.2.2 Type 2....35
2.3 Multiple-Phase Machines: Pros and Cons....35
2.3.1 Advantages....35
2.3.2 Disadvantages....36
2.4 Overview of Five-phase PMSM....36
2.4.1 Based on the orientation of the field flux....37
2.4.2 Based on the configuration of the magnets....40
2.5 The operational principal of Permanent Magnet Synchronous Machines....41
2.5.1 The operational concept in generator mode....42
2.5.2 The operational concept in motor mode....42
2.6 Modeling of the Five-Phase PMSG....43
2.6.1 Five-Phase PMSG Model in Stationary Frame....44
2.6.2 Five-Phase PMSG Model in Synchronous Frame....45
2.7 Configuration of multi-machine wind system....47
2.8 The novel configuration of multi-machine wind system....48
2.9 Conclusion....50
References....50

Chapter 3 Fifteen-Switch Rectifier

3.1 Introduction....53
3.2 Structure of Fifteen-Switch Rectifier....53
3.3 Operating Principles of the Fifteen-Switch Rectifier....54
3.4 Implementation of the PWM control technique....55
3.5 The five-phase PWM rectifier's operational principle....56
3.6 The FSR's operational principle....60
3.7 Dynamic Analysis of a Fifteen-Switch Rectifier....62
3.8 Comparative Analysis of the suggested and conventional converter....65
3.9 Conclusion....65
References....66

Chapter 4 Fuzzy Backstepping Control of Multi-Machine Wind Power Generation System

4.1 Introduction....67
4.2 Overview of Backstepping Control Techniques....67
4.2.1 Primary concepts....67
4.2.2 Affine Form....68
4.2.3 Lyapunov Function....68
4.2.4 The Lower Triangular Shape....69
4.3 Overview of Fuzzy Logic Techniques....69
4.4 Implementation of Fuzzy Backstepping Control....70
4.4.1 MSC control....70
4.4.1.1 Backstepping control design....70
4.4.1.2 FBC approach....75
4.4.2 GSC control....78
4.4.3 System stability study....81
4.5 Results....84
4.5.1 Steps WS test....84
4.5.2 Variable wins velocity test....89
4.5.3 Robustness test....193
4.6 Conclusion....97
General Conclusion....100
APPENDIX A....102
APPENDIX B....103
References....104

General Introduction

General Introduction

a) Antecedents

The renewable energy (RE) revolution has emerged as one of the most significant transitions of the contemporary period, notable for its quick development and growth. Renewable sources are those that are found in nature, are affordable, and do not contribute to the spread of hazardous gases, therefore their usage may assist in combating the problem of global warming. Wind energy (WE), solar energy (SE), and hydropower are among the most common renewable energy sources (REs) utilized across the globe to generate electrical energy (EE) [1]. Using these RE sources enables us to meet the growing demand for electrical EE while reducing reliance on conventional sources. According to the research in [2], the WE system is regarded as one of the most significant and pervasive energy generation systems on land and sea levels. This energy system uses wind turbines (WTs) to transform WE into mechanical energy. According to the author in [3], the resultant energy is correlated with both wind speed and WT size; the bigger the WT dimensions, the higher the resulting energy. Additionally, the produced energy is correlated with changes in wind speed (WS); that is, as WS rises or falls, so does the resulting energy. Numerous studies addressed the problem of using WE to generate EE [4-6], addressing both the advantages and disadvantages while developing suitable methods to enhance the quality of the energy produced. The author of the research [7] asserts that the quality of EE and current are among the most significant challenges and shortcomings in WE systems. In 2010, the global average levelized cost of electricity (LCOE) for onshore wind energy was $0.107 per kWh, exceeding the lowest cost of fossil fuel generation, which was $0.056 per kWh, by 95%. By 2022, the average LCOE for new onshore wind projects saw a substantial decline to $0.033 per kWh [8]. This signifies an impressive 52% reduction compared to the lower-cost fossil fuel alternative, which was priced at $0.069 per kWh. In comparison to WE, SE is regarded as the primary competitor in the realm of EE generation due to its widespread adoption and utilization [9]. Solar energy systems rely on photovoltaic cells to transform light into electrical current, with these cells being highly responsive to environmental conditions [10]. Typically, these cells are arranged in panels, and large installations comprising thousands of such panels are referred to as solar farms. According to the study [11], natural elements influence the production of EE from SE, resulting in network disruptions that are unwanted. To meet the growing demand for EE, solar farms with big areas and a great number of solar panels must be used, which incurs additional expenditures. As is well known, the expansion of SE farms at the cost of agricultural areas produces a variety of social, political, economic, and even financial issues. Notably, the progress

in cost reduction for solar photovoltaic (PV) technology has outpaced that of onshore wind energy. In 2010, the global average LCOE for solar PV was 0.445 USD/kWh, making it substantially more expensive—by 710%—than the least expensive fossil fuel option. By 2022, solar PV costs had significantly declined to 0.049 USD/kWh, resulting in a global average LCOE that was 29% lower than that of the most affordable fossil fuel-fired alternative.

Different nations and regions are expected to adopt varied strategies to accelerate the deployment of alternative energy sources. Countries with favorable conditions, such as lower investment barriers, abundant RE resources, and well-developed power markets, should aim for substantial increases in renewable energy and the decarbonization of their economies. By doing so, they can significantly contribute to the global effort by sharing their experiences, technological expertise, and insights necessary for scaling up renewable energy. The G20 nations are projected to lead the global solar PV market. In the realm of WE, countries such as China, the United States, Canada, Brazil, and several European nations hold considerable onshore wind potential. Moreover, it is anticipated that the majority of offshore wind expansion will take place in four major markets: China, the EU-27, the US, and India, which together are expected to account for over 60% of the total projected deployment by 2030.

According to the International Renewable Energy Agency (IRENA) scenario outlined in the global energy transitions forecast, the world's RE generation capacity must triple by 2030, exceeding 11,000 GW. Solar PV and WE are anticipated to account for approximately 90% of this additional RE capacity. The overall installed capacity for alternative power generation is expected to increase from 3,382 GW in 2022 to 11,174 GW by 2030. Specifically, solar PV capacity is projected to rise from 1,055 GW in 2022 to over 5,400 GW, while wind energy installations are expected to surpass 3,500 GW (comprising 3,040 GW from onshore and 500 GW from offshore) compared to 899 GW in 2022. The share of variable RE, including solar PV and wind energy, in total electricity generation is predicted to grow from 10% in 2021 to 46% by 2030, necessitating enhanced resilience in energy system operations. Following solar PV and wind energy, hydropower is projected to experience the third-largest growth in generation capacity, with an anticipated increase of nearly 17% from the 2022 level, reaching 1,465 GW under the IRENA 1.5°C Scenario.

Wind energy (WE) is regarded as a highly reliable solution for EE generation, as it is consistently available throughout the year across various regions worldwide. The implementation of this energy source relies on WTs [12], which can be effectively utilized at sea level, thus enabling cost reductions compared to SE, which is not feasible at sea level [13]. Consequently, WE is viewed as a promising option for the future, aimed at decreasing the costs associated with the production and consumption of

EE. Additionally, the deployment of large WTs can address the challenge of high energy demand; for instance, one or two giant WTs with a capacity of 50 megawatts each can sufficiently meet the electrical energy requirements of a city [14]. The energy output from a single large WT can match or exceed that produced by a solar farm.

According to two studies [15, 16], there has been significant growth and increased utilization of WTs in recent years, accompanied by notable technological advancements that have led to cost reductions compared to earlier periods. To optimize the performance of WE systems, careful attention has been given to their components, particularly the generator. Since the introduction of these systems, various generator types have been utilized, with the permanent magnet synchronous generator (PMSG) emerging as a leading option. The PMSG has attracted considerable interest from investors due to its many advantages, including the ability to operate at low rotational speeds and the potential for gearbox-free designs. These characteristics contribute to reduced production and maintenance costs, while also minimizing rotor losses and achieving substantial torque [17-23]. The PMSG is integrated into the electrical grid through two distinct converters. The first converter transforms alternating voltage into direct voltage, while the second inverter converts direct voltage back into alternating voltage. The implementation of these two converters facilitates the regulation of voltage and frequency within the network. However, a notable drawback of using a PMSG is its limited control over output power, unlike the doubly-fed induction generator (DFIG). Additionally, under conditions of variable wind speed, the PMSG exhibits lower efficiency compared to the DFIG. The deployment of a three-phase PMSG in energy systems often fails to yield sufficient energy output. To achieve higher energy levels, a larger generator is required, which consequently increases its weight, leading to several challenges for WTs. Additionally, the increased weight of the generator results in higher costs, which is not desirable. In this context, a multi-phase PMSG offers several significant advantages that are absent in a three-phase system. These advantages include enhanced reliability, reduced capacitance, and a greater frequency of torque pulses. As a result, a multi-phase PMSG represents an excellent option for WE applications [24, 25].

b) Motivation

When addressing the essential components of WPGSs, it is necessary to go into the world of power electronics, a critical technology in the area of electrical engineering. Power electronics converters act as sophisticated interfaces for these systems, providing a variety of functions such as frequency control, power, and voltage [26]. Back-to-back converters (BTBCs) are a popular option because they have exhibited a variety of characteristics, including good control and management of bidirectional power

flow, as well as rapid power injected into the network [27–29].

c) Literature review

Our research introduces a novel type of converter that has not seen widespread application. Initially implemented as a nine-switch inverter (NSI), this converter facilitates independent control of machines or loads, accommodating either two three-phase loads or a single six-phase load without complicating control techniques. A wealth of literature has explored various methods associated with these converters [30-37]. Furthermore, studies [38-40] have presented different control strategies employing model predictive control (MPC) to effectively manage load dynamics in scenarios involving two independent multiphase loads powered by the NSI. Moreover, [41] utilized the same topology and employed the sliding mode control (SMC) technique. The findings from these studies indicate that the nine-switch inverter (NSI) has exhibited commendable performance, especially regarding load separation. To explore an alternative application of this topology as a rectifier instead of an inverter, the author in [29] introduced a novel configuration known as the FSR, which is closely related to our research focus. This approach involved a modified arrangement of BTBCs, substituting the conventional rectifier with the FSR while ensuring that the functionality of all system components remained intact. The results indicated satisfactory overall system performance, with particular emphasis on the FSR. Importantly, the control technology implemented did not introduce complexity, and the FSR design notably reduced the number of switches compared to the conventional topology discussed in [18, 19], thereby minimizing switching losses.

The Backstepping control (BC) strategy is traditionally regarded as one of the most renowned nonlinear strategies due to its exceptional robustness and exceptional performance in comparison to other strategies, such as DPC [42]. This method has the ability to greatly enhance system attributes, since it involves knowledge of the system's mathematical model (MM). This study focuses on applying the enhanced BC approach to regulate an energy system that relies primarily powered by 5-phase PMSG. In contrast, this thesis centers on a multi-machine wind system as its primary focus. This multi-machine wind system represents a significant contribution to the research, as it is designed to generate energy and address the challenges posed by rising energy demand. The thesis provides a detailed structure and MM for the proposed system, which primarily incorporates two five-phase permanent magnet synchronous generators (PMSGs) to convert mechanical energy produced by WTs into EE. Thus, the implementation of five-phase PMSGs constitutes the second major contribution of this work. To control these generators, a hybrid control technique has been employed, integrating BC and FLC methods. This strategy utilizes pulse width modulation (PWM) to control the machine-side converter,

thereby simplifying the overall system, enhancing control, and reducing total system costs. A self-tuning BC with FL parameters has been developed to allow for adaptive adjustments of the generators' speed control gains.

d) Objectives

The primary aims of the research conducted in this thesis involve the following:

- Improving the performance and efficiency of the BC strategy of five-phase PMSG.
- Significantly improve the value of THD of current compared to using the BC strategy.
- Significant reduction in power and current ripples compared to using the BC technique.
- Increasing the durability of the proposed energy system.
- Improving the dynamic response of power.
- Improvement of both overshoot and Steady-state error (SSE) of five-phase PMSG power.

e) Organization

Following the general introduction, which offers an overview of the various control methods and multi-machine systems, the proposed approach for controlling the multi-machine WPGS will be addressed in this thesis. The main body of the thesis is structured as outlined below.

Chapter 1 provides an overview of WE and the physical principles that govern its operation. It begins with a general introduction, followed by a review of the various methods employed to generate electricity from wind. The chapter then describes WTs, including their different types, components, and operational methods (fixed speed and variable speed), as well as their classifications (onshore and offshore). The final section examines the combinations of different electric machines used to convert WE, discusses their respective advantages and disadvantages, and models the WTs.

Chapter 2 focused on the generator technology used in the research. It defined multiphase machines, discussed their key applications, and examined their various types, advantages, and disadvantages. The chapter then provided an overview of five-phase PMSMs, including their key components, essential elements, and different applications. It also explained the modeling procedure for the five-phase PMSG, establishing the theoretical foundation for understanding its operation. Additionally, the chapter included a discussion on the modeling of two parallel PMSGs within the WS.

Chapter 3 discussed the FSR in the conversion system. It provided a definition and explanation of the general engineering of this transformer. The text then described how the rectifier works, including

the use of the PWM unit. To give a comprehensive explanation, it compared the operation of the traditional five-phase rectifier to the FSR, covering all operating cases. Finally, the key strengths and weaknesses of the FSR were discussed in comparison to using two conventional rectifiers in parallel.

Chapter 4 discusses the implementation of FBC for a multi-machine WPGS that utilizes two 5-phase PMSGs. This chapter also compares the effectiveness of this approach with traditional BC strategy.

The thesis will conclude with a comprehensive summary of the various achievements achieved and the challenges faced. Furthermore, we will present potential directions for further research.

Chapter 1

State of the art of wind energy conversion

1.1 Introduction

Fossil fuels are accused of being the primary cause of climate change and significantly contribute to biodiversity loss and global pollution. Transitioning from fossil fuels to RE is a necessary step, and making renewable energy the norm is not a matter of technology or cost.

The electricity sector has made remarkable progress. Today, almost all new electrical equipment is renewable. More than 256 GW were added globally in 2020, surpassing the previous record by nearly 30%. In a growing number of regions, including parts of China, the European Union, India, and the United States, it is now cheaper to build new wind or solar power plants than to operate existing coal plants. These advancements can and must be reflected in all other sectors.

The rise in global energy demand has offset the growth in renewable energy deployment. As a result, the share of fossil fuels in total final energy consumption (TFEC) has remained nearly unchanged since 2009. RE accounted for just over 12.6% of the world's final energy demand in 2020, up from only 10.6% in 2009. Even the share of renewables in final electricity demand stagnated in 2020 compared to 2019.

Despite record additions to RE capacity in 2021, the increase in global electricity demand was mainly met by fossil fuels. Coal consumption for electricity production rose by 9%, compared to a 5% increase for renewables. Moreover, progress has been uneven across regions. In 2019, only 3 out of 80 countries – Iceland, Norway, and Sweden – had renewable energy shares in TFEC of over 50%. Additionally, 20 countries, mainly in Europe and Latin America, achieved at least a quarter of their total final energy consumption through renewable energy sources.

This chapter first provides an overview of energy supply prospects, renewable energy production, and particularly wind energy. The second part describes wind turbines, their components, different types, and operational strategies (fixed speed (FS), variable speed (VS)).

The final section addresses the combinations of different electrical machines used to convert wind energy, which will be studied and compared according to their various advantages and disadvantages. The different techniques for limiting or controlling wind power are then briefly explained, along with the various generator designs available on the market.

Lastly, we will specify the choice of wind turbine type, which will help define the framework of our work, focusing on the complexity of control systems for both the turbine and the wind turbine generator.

1.2 Wind Energy Potential in Algeria

Algeria has the greatest wind energy production potential in North Africa. Preliminary studies of annual seasonal wind speed variations have allowed the identification of the windiest regions in Algeria. This wind speed mapping serves two main purposes:

- Identifying large areas with promising prospects for wind energy development: These maps highlight regions that are favorable for wind power projects.
- Emphasizing the relative fluctuations in Algerian wind resources: This helps better understand the wind distribution across the country.

The Center for RE Development (CRED) provides wind potential estimates based on hourly and tri-hourly WS data, recorded continuously over ten years (2004-2014) at 74 meteorological stations of the National Meteorological Office (NMO), along with 21 additional meteorological stations from neighboring countries (as shown in Fig. (1.1)) [43].

The geographic distribution of winds is relatively uniform between northern and southern Algeria. According to the new wind atlas installed at 10 meters above ground, significant changes in wind resource estimates are observed, especially in the Sahara.

- For example, Insalah records an average WS of 6 m/s, while Adrar has a slightly higher average speed of 6.3 m/s.
- The Illizi region, with numerous stations, registers average wind speeds exceeding 5 m/s.
- Hassi R'Mel stands out with an average wind speed of 6.5 m/s, which is considered quite high.

Moving north, some microclimates in the western and eastern parts of the country also exhibit significant wind potential. In the regions of Mescheria, Tiaret, and Djelfa, average wind speeds of 5.6 m/s are recorded. A bit further east, similar speeds are measured at 5.6 m/s and 5.1 m/s respectively. Additionally, M'Sila emerges as an interesting zone with an average annual wind speed of 5.3 m/s.

Sites such as Tébessa, Ksar-Chellala, and Bou Saada have a significant percentage of low wind speed values, with over 50% of their recorded data showing minimal wind speeds. This indicates that these areas may not be as promising for large-scale wind energy development due to the relatively low and inconsistent wind speeds, which could limit their potential for efficient wind power generation.

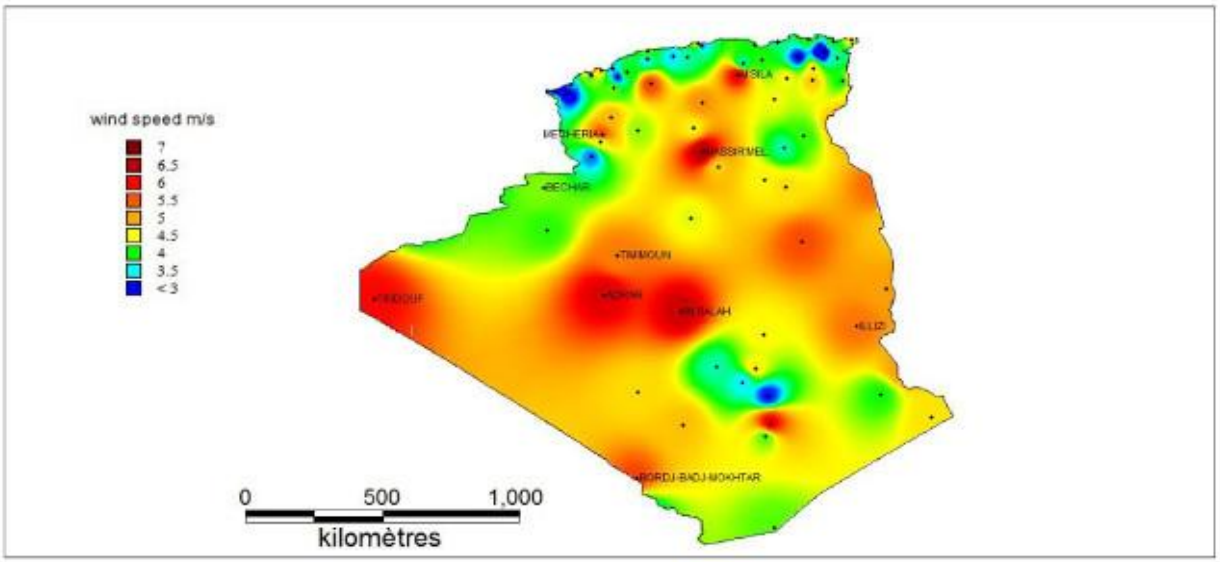

Fig. (1.1): Wind atlas of Algeria at 10 m above ground level, produced by [43].

Even the information provided by the wind atlas of Algeria, which quantifies the existing potential, remains insufficient to select appropriate locations for wind farm construction. The search for these sites, capable of ensuring profitability and providing competitive wind power, is still ongoing. The Geographic Information System (GIS) method, based on the layering of strata [44] (Fig. (1.2)), is used to determine ideal locations in Algeria.

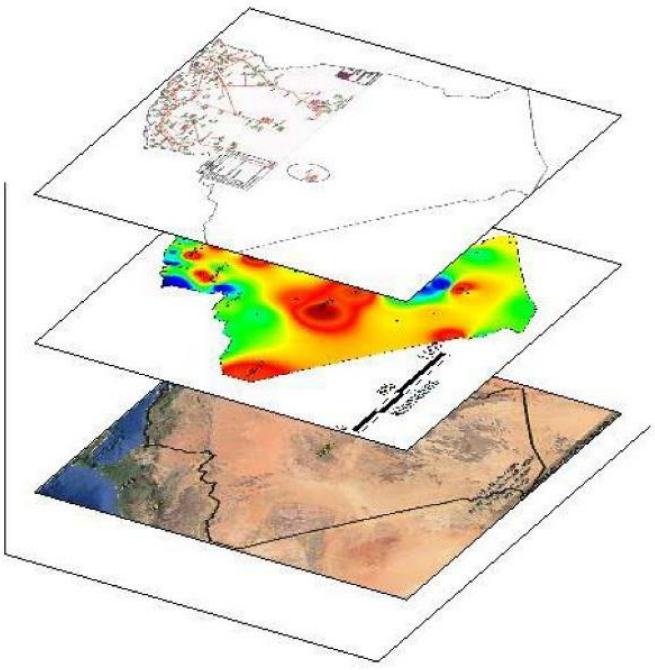

Fig. (1.2): Comparison of average wind speeds at windy sites [43].

Adrar is located in a wind corridor with a speed of 6 m/s, and research has shown that it can reach up to 20 m/s, making the energy potential substantial and very promising. The WT in Adrar, the first in

Algeria, was installed in 1953 on the INRAA grounds, a few kilometers from Adrar at a place called Ouled Aissa in the commune of Ould Brahim.

The total installed wind WE capacity by 2030 is set at 5010 MW, with a target of 1 GW between 2015 and 2020. It should also be noted that by 2020, the Adrar network will be connected to the northern grid. According to the implementation report presented by SKTM, the total installed capacity is 10 MW (Kaberten wind farm). Additionally, there is potential in Janet and Insalah. A more in-depth study of these new areas is necessary, with ten wind measurement masts to be installed for this purpose. Therefore, the choice of the location for the future wind farm will be made at a later stage.

Kaberten is the first central power plant site in Algeria, located 72 km north of the capital of Adrar. This wind farm was commissioned in early June 2014 and inaugurated on July 3, 2014. The project was developed to provide a total wind power capacity of 10.2 MW, consisting of 12 Gamesa G52 turbines with a diameter of 52 meters and a mast height of 55 meters. The turbines are installed on a site with a total area of 33 hectares. The project was carried out by two SONELGAZ groups under the expertise of CEGELEC (ETTERKIB Equipment Assembly and ENERGA Civil Engineering), with a total investment of 2.8 billion dinars [45,46].

This project supplies electrical energy to the local grid. The WE production records show that the amount of energy produced on any given day reached the nominal output power of the farm. The SCADA system provides control, and communication between the control room and the turbines is done via fiber optic cables. The Kaberten wind farm is a first in Algeria. It is, therefore, a pilot project where general feedback is expected, particularly regarding the behavior of the turbines under the influence of high temperatures and dust storms [47,48]. The figure below (Fig. (1.3)) shows the achievable and usable WE at 10 and 25 meters for various sites, including Adrar.

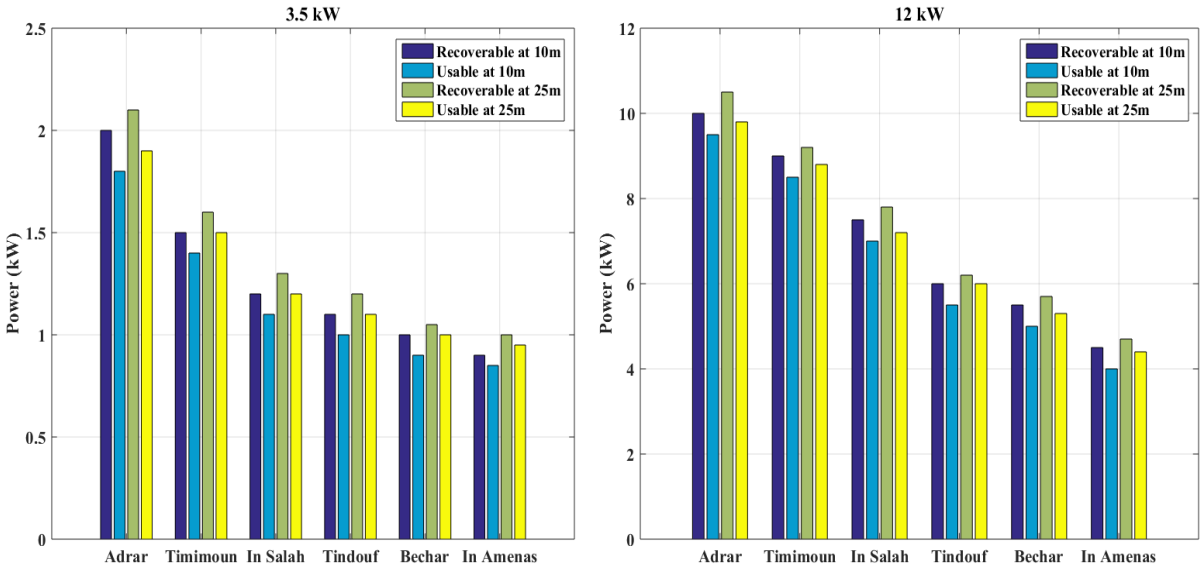

Fig. (1.3): Recoverable and usable power at 10m and 25m in various zones [49].

1.3. The Preamble of the Wind Energy System

1.3.1 History

For centuries, humans have harnessed wind energy to propel boats, grind grain, or pump water. This ancient technology is now being used to generate electricity.

The production of WE, which has been technically well developed, is currently booming. Whether on a small scale with small wind turbines or on a large scale with large WTs, WE can contribute to diversifying electricity production in a decentralized manner, directly generating zero pollution or CO2 emissions [50].

Wind resources originate from the movement of air masses indirectly caused by the Earth's solar radiation. When some regions of the planet are hot while others are cold, pressure differences occur, causing air masses to move consistently (Fig. (1.4)) [41].

Fig. (1.4): The WT system.

Preliminary data released on March 18, 2022, by the WWEA (World Wind Energy Association) indicates that the global wind turbine industry achieved a new high in 2021, with a total of 97.5 gigawatts installed globally, an increase from 92.7 gigawatts in 2020. The total capacity of all wind turbines globally has surpassed 840 gigawatts, an increase from 742.5 gigawatts in 2020, sufficient to provide over 7% of the world's power demand. In 2023, there was an augmentation of 10 megawatts relative to the 839,730 gigawatts recorded in 2021.

The Table (1.1) ranks the countries using the most wind-generated energy worldwide in 2023. Fig. (1.5) shows the energy produced by WTs installed worldwide.

Table (1.1): Overview of the leading countries in WE [52,53].

Rank	Country	Installed Wind Turbine Capacity (Megawatts)		Annual Growth Rate 2013-2023
		In 2021	In 2023	
1	China	343,829	441,895	+19.1%
2	US	134,846	148,020	+9.4%
3	Germany	63,924	69,459	+7.6%
4	India	40,100	44,736	+9.3%
5	Spain	28,196	31,028	+3.1%
6	UK	26,812	30,215	+10.4%
7	Brazil	21,365	29,135	+29.5%
8	France	19,081	22,196	+10.5%
9	Canada	14,304	16,989	+8.1%
10	Sweden	12,097	16,252	+14.5%

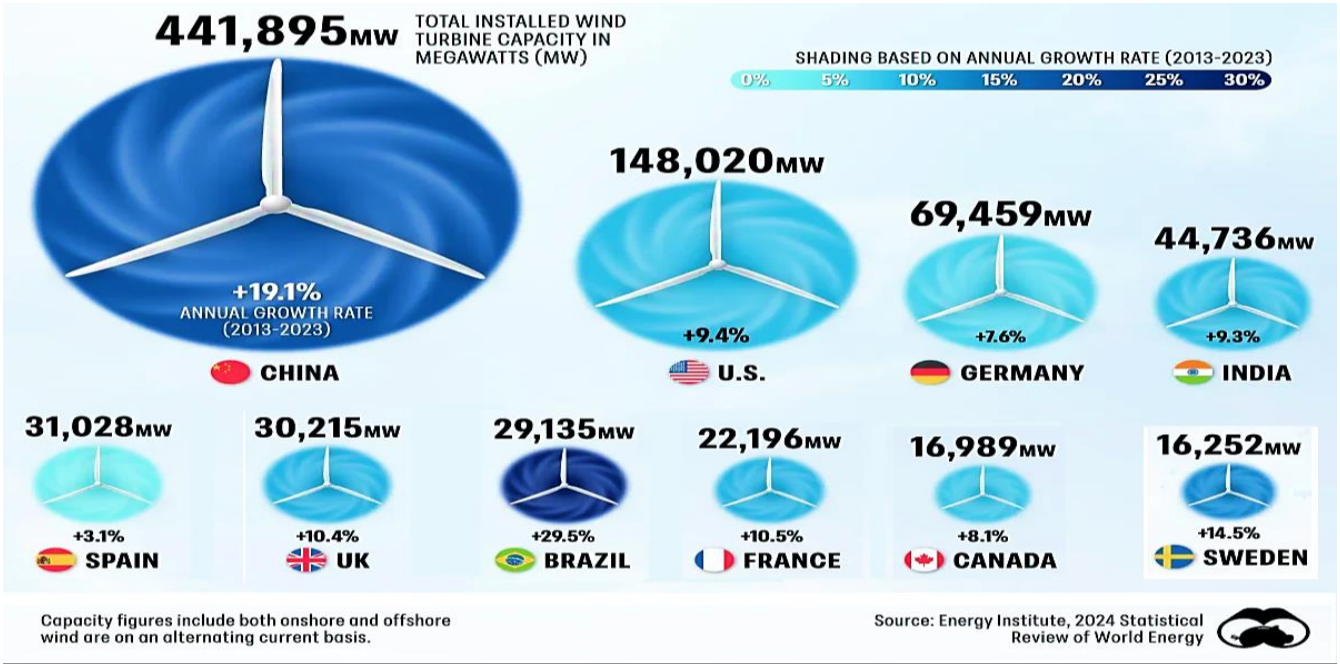

Fig. (1.5): WE capacity (in Megawatts) installed in 2023 [53].

1.3.2 Types of Wind Turbines

WTs, often referred to as turbines, are essential components of energy conversion systems. Over the years, various types of turbines have been developed. This section provides an overview of turbine technology [54,55].

Synchronous machines include all the machines that the rotor speed is equal to the speed of the rotating stator field. In case of PMSM, the rotor excitation is provided by permanent magnets (PM) [45]. The PMSM does not need extra DC power supply or field windings in order to provide rotor excitation. Therefore, the power losses related to the filed windings are eliminated in this kind of machines. In addition, the magnets and redundant teeth in stators allow magnetic decoupling from the different groups of windings [7-8][46].

1.3.2.1 Vertical Axis Wind Turbine (VAWT)

Vertical Axis WTs (VAWTs) were the first structures developed to generate electricity, in contrast to traditional horizontal axis wind turbines. One of their main advantages is that the controller and generator are located at ground level, making them easily accessible [54]. Several prototypes have been developed, but three types have reached the industrialization stage, as shown in Fig. (1.6) [56].

a. Savonius

b. Darrieus

c. Musgrove

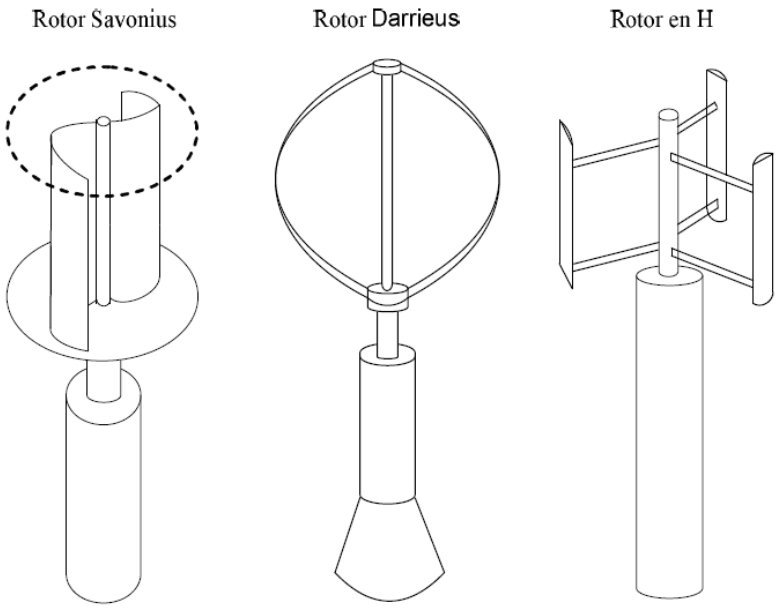

Fig. (1.6): Types of the three vertical axis wind turbines.

1.3.2.2 Horizontal Axis Wind Turbine (HAWT)

Horizontal Axis WTs (HAWTs), shown in Fig. (1.7), are the most common type of WT. The rotor blades are positioned to capture the airflow, which generates torque. This torque drives generators that produce electricity. These turbines are fully autonomous at startup, economical, and take up less ground space. Typically featuring three blades, HAWTs can deliver power in the megawatt range [57].

The turbine can be positioned either at the front of the nacelle or at the rear, as shown in Fig. (1.8): facing the wind (Upwind) or behind the wind (Downwind) [56].

HAWTs are the most commonly used because they experience fewer mechanical constraints and are less expensive compared to VAWTs.

Fig. (1.7): Horizontal axis wind turbine (HAWT).

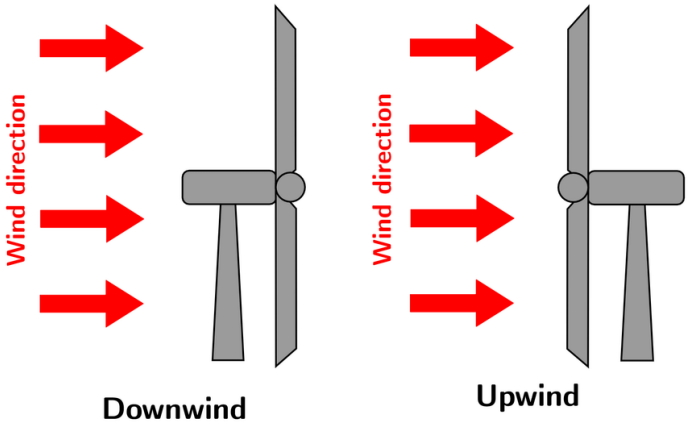

Fig. (1.8): Upwind and Downwind wind turbines.

1.3.2.3 The Two Types of Wind Turbines

WTs are also classified into two types based on their rotational speed: fixed speed and variable speed. A fixed-speed wind turbine (FSWT) operates at an almost constant speed, determined by factors such as the gearbox ratio, the number of poles in the generator, and the grid frequency.

The maximum energy conversion efficiency can only be achieved at specific (constant) WSs, while other wind speeds result in lower system efficiency. Aerodynamic guides on the blades protect the turbine from potential damage caused by strong wind gusts. Additionally, since the turbine operates at a low speed, a gearbox (multiplier) is required to increase the rotational speed for energy generation.

FSWTs generate highly variable output energy to the grid, causing disturbances. This type of turbine also requires a robust mechanical design to withstand high mechanical loads [58].

On the other hand, VSWTs can achieve maximum power conversion efficiency over a wide range of WSs. The regulation of the wind turbine's speed is done via static converters that control the alternator's speed, which is mechanically coupled to the turbine's rotor (blade) connected to the electrical grid.

Table (1.2) demonstrates the main advantages of VSWTs. The table highlights how the variable-speed mode improves energy production efficiency and the quality of the energy developed through power conversion technology. This mode also reduces mechanical stress. However, using power converters in the WE conversion chain increases both system costs and power losses (due to rectification and conduction). Nevertheless, these additional costs are offset by greater operational flexibility and autonomy.

Table (1.2): Advantages and disadvantages of fixed-speed and variable-speed wind turbines.

Speed Mode	Advantages	Disadvantages
Fixed Speed	• Simple design • Low cost and low maintenance	• Low energy conversion efficiency • High mechanical stress • Large power fluctuations to the grid
Variable Speed	• High energy conversion efficiency • Improved power quality • Reduced mechanical stress	• Higher system cost • Power losses due to conversion (rectification) • More complex system control

1.4 The Architecture of a Wind Turbine

Today, almost all grid-connected wind turbines are horizontal-axis turbines with three blades. In this regard, this section highlights the key components of horizontal-axis WTs.

Horizontal-axis wind turbines consist of three basic elements:

- Tower or mast;
- Rotor;
- Nacelle, which houses the components that convert mechanical energy into electrical energy, primarily the generator [59].

1.4.1 The Tower

The tower (Fig. (1.9)) is the structure that supports the main elements: the rotor and the nacelle. It is typically made of steel to provide the necessary strength for the entire structure. The tower must be as tall as possible to avoid wind disturbances near the ground. However, the weight of the tower must be sufficient to support all the components of the WT. The higher the rotor is positioned, the better the turbine's performance.

Fig. (1.9): The wind turbine tower.

1.4.2 The Rotor

The rotor (Fig. (1.10)) is the mechanical part that converts the wind's driving force, captured by the rotor blades, into rotational energy, which is then converted into electricity inside the nacelle. It typically consists of three blades and is positioned in front of the nacelle [60].

Fig. (1.10): The rotor of a wind turbine.

1.4.3 The Nacelle

The nacelle (Fig. (1.11)) houses all the mechanical components that connect the WT to the generator. These include the low-speed shaft (LSS), high-speed shaft (HSS), bearings, gears, and a braking system (which can consist of disk brakes and aerodynamic brakes used to stop the turbine in

case of overload). The generators are typically either synchronous or asynchronous machines.

Fig. (1.11): The nacelle of a wind turbine.

Fig. (1.12) depicts the essential elements included inside the nacelle. This assembly is critical for the overall functionality of the system, as it typically includes essential elements such as the gearbox, generator, and control systems. Each of these components plays a vital role in converting mechanical energy into EE. Understanding the layout and function of these elements is crucial for optimizing performance and facilitating maintenance in various applications.

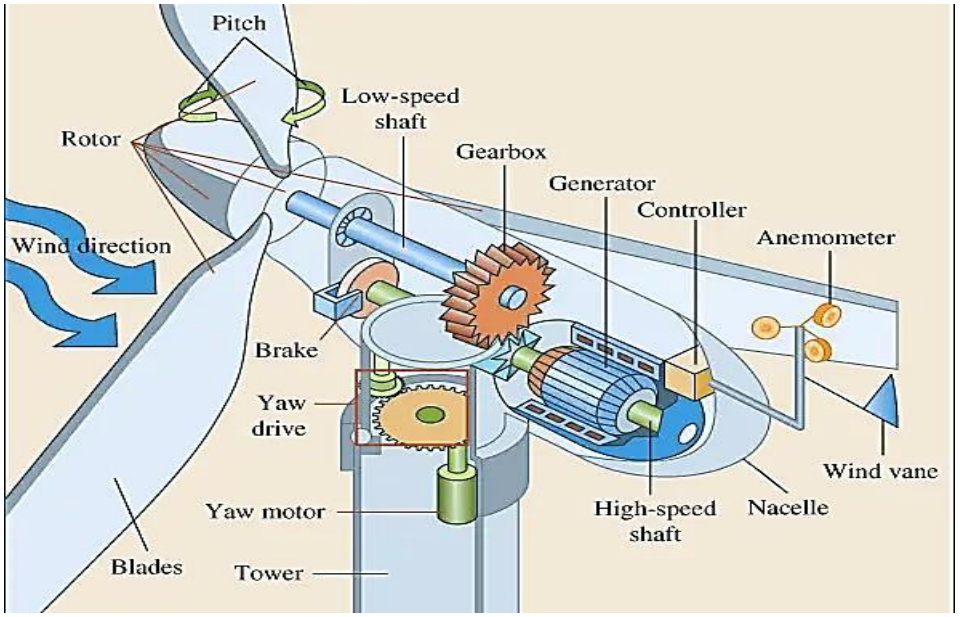

Fig. (1.12): The key elements

1.5 The Categories of Wind Turbines

The global wind resources can be generally divided into two principal categories based on their geographical locations: onshore and offshore wind resources. This classification is essential for

comprehending the potential for wind energy extraction, which is significantly dependent on the establishment of both onshore and offshore wind farm industries [61].

The data presented in Fig (1.13) demonstrates the growth in the annual installed capacity of various types of wind farms worldwide from 2010 to 2022.

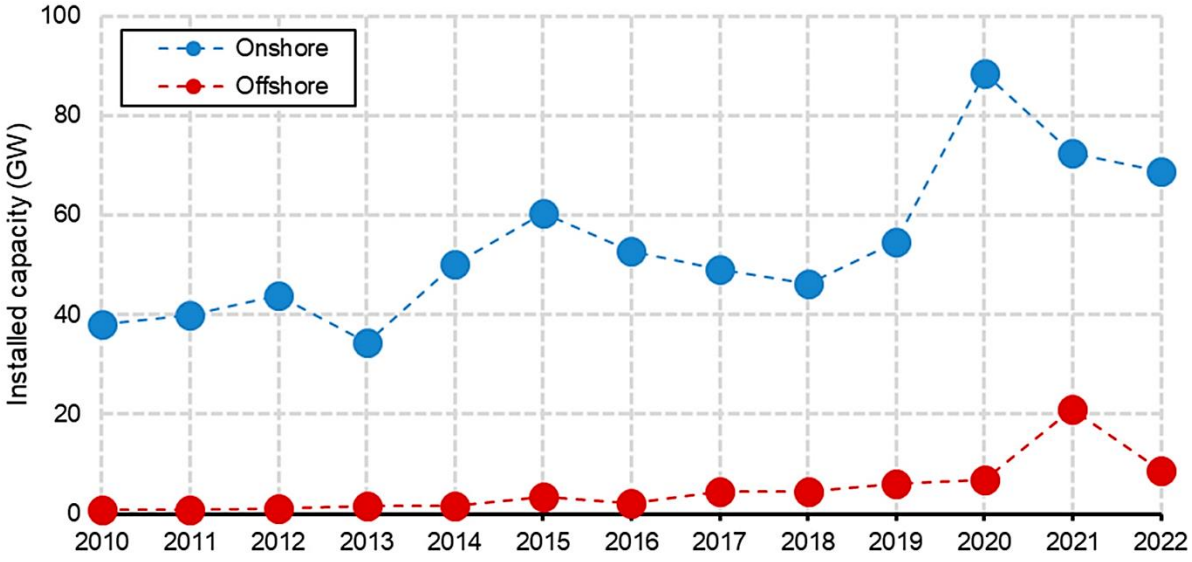

Fig. (1.13): The increase in annual installed capacity of onshore and offshore wind farms globally from 2010 to 2022 [62].

1.5.1 Onshore Wind Energy

Onshore wind power facilities have served as a substantial source of wind-derived energy for numerous decades. These installations are customarily situated in locations possessing advantageous wind conditions, such as plains, hillsides, and coastal zones (Fig. (1.14)). The associated infrastructure and technology have rendered onshore wind power facilities a dependable and well-entrenched alternative for optimizing wind-based electricity generation. Recent data indicates that onshore WE has contributed significantly to the worldwide energy portfolio, comprising a considerable segment of renewable energy production [62].

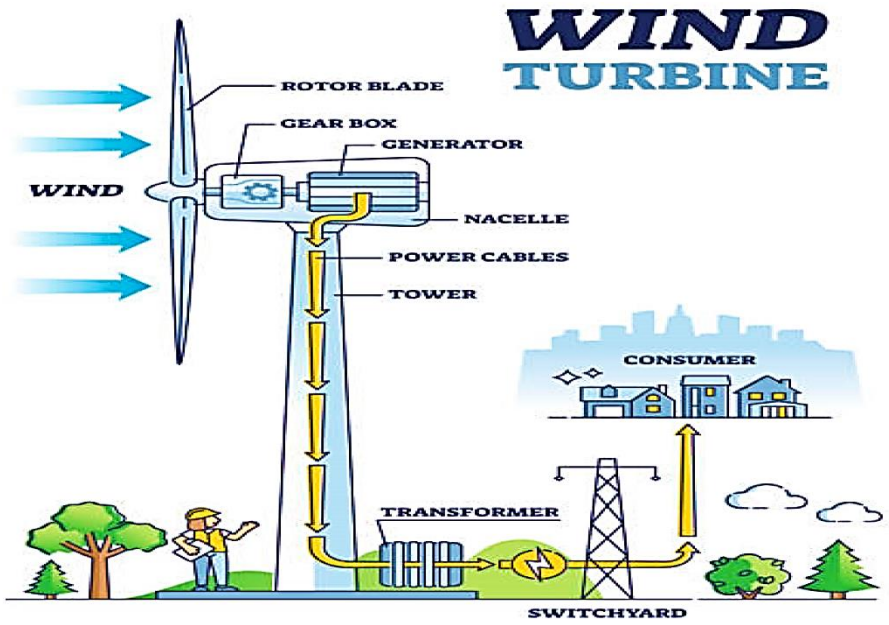

Fig. (1.14): Onshore wind system [62]

1.5.2 Offshore Wind Energy

The harvesting of offshore WE has garnered growing acknowledgment owing to its potential for higher and more consistent WSs. Offshore wind farms are typically situated in bodies of water, where wind conditions frequently prove more favorable than on land (Fig. (1.15)). The development of offshore WE is regarded as a promising avenue for expanding RE capacity, particularly in regions where land-based wind resources are limited or where energy demands are substantial. Recent advancements in technology and reductions in costs associated with offshore wind installations have further augmented interest in this sector [63].

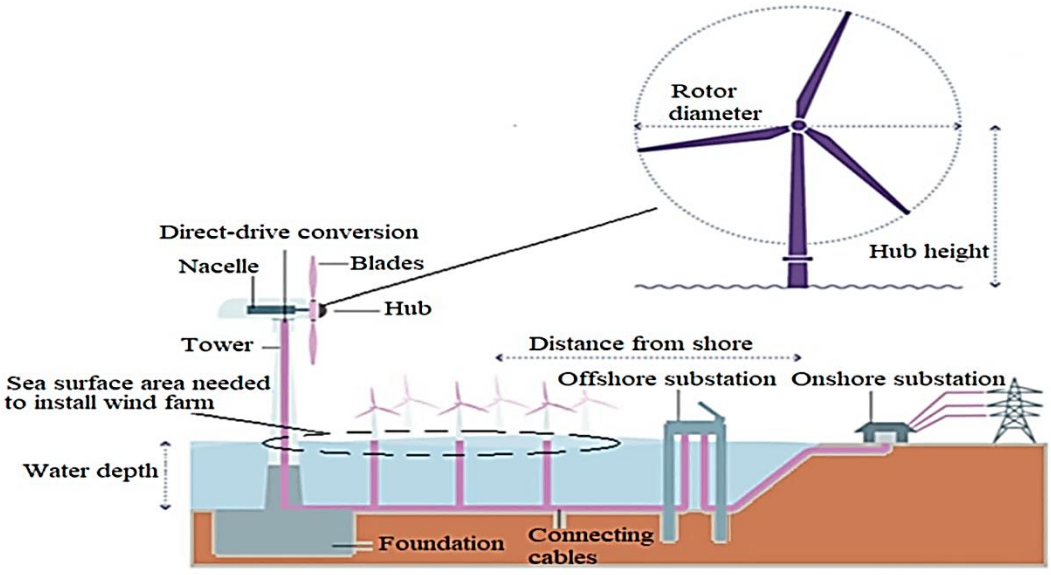

Fig. (1.15): Offshore wind system [62]

In the present context, numerous nations across the globe actively endeavor to invest in WE (Fig. (1.16)), harnessing their natural resources and capabilities. China has established itself as the preeminent global investor in onshore WE, capitalizing on its expansive land area and advantageous wind conditions to establish extensive wind farm infrastructure. This investment corresponds with China's overarching objectives of augmenting renewable energy capacity and mitigating carbon emissions.

Whereas the United Kingdom is the leading investor in offshore WE, especially via the advancement of projects in the North Sea, known for its continuously high wind speeds. The UK's strategic focus on offshore wind has positioned it as a leader in this sector, facilitating significant advancements in technology and infrastructure. By harnessing the robust wind resources available in these maritime regions, the UK aims to bolster its RE output and achieve ambitious climate targets. This competitive landscape highlights the global shift towards sustainable energy solutions and the varying approaches taken by different nations based on their unique geographical advantages.

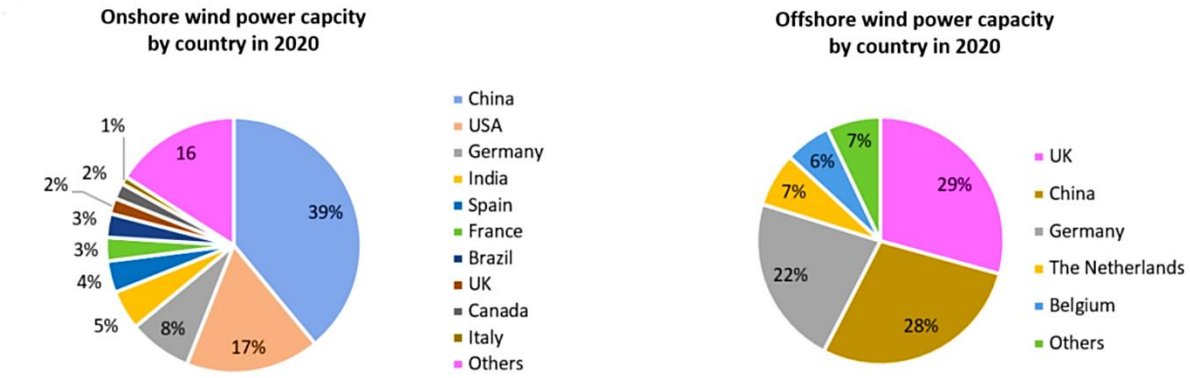

Fig. (1.16): Statistics on the world's wind power production in 2020 [63]

1.6 The Wind Energy Conversion Chain

The primary use of WTs today is the production of EE. Electromechanical systems are essential for this process (Fig. (1.17)). Various types of electrical machines are used to generate energy from turbines, with economic and technical factors determining the appropriate machine type for each application. For low power applications (<20 kW), the simplicity and low cost of PMSG give them an advantage. For high-power applications up to 2 MW, asynchronous generators are more popular and cost-effective [64,65].

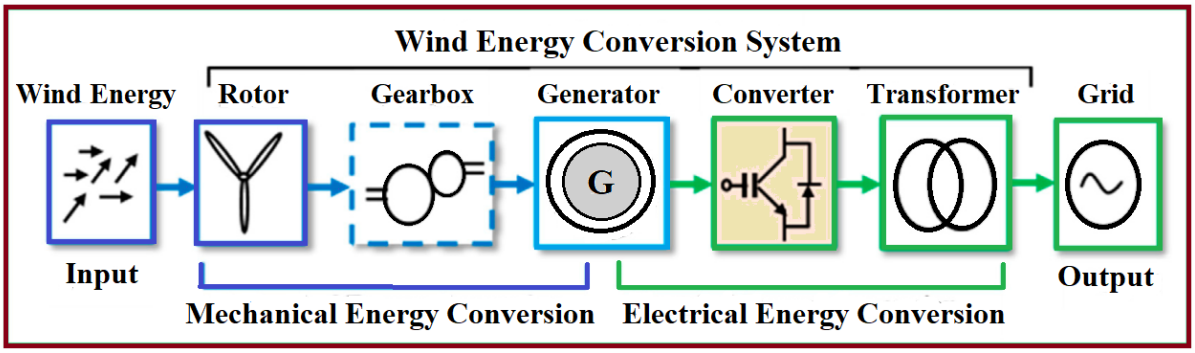

Fig. (1.17): Stages of energy conversion in a contemporary wind generation system [66]

1.6.1 Asynchronous Generator

Induction generators are frequently used in medium and large-capacity WTs due to their durability, simple mechanics, and low cost. The main drawback is the need for reactive current to magnetize the stator [67,68].

1.6.1.1 Squirrel Cage Induction Generator (SCIG)

The SCIGs are mainly chosen for their simplicity, high efficiency, and low maintenance. The reactive power demand is offset by connecting a capacitor bank in parallel with the generator or using a static power converter [69].

1.6.1.2 Doubly Fed Induction Generator (DFIG)

The DFIG (Fig. (1.18)) was developed to allow motor operation over a wide speed range. DFIG enables variable speed operation by adjusting the supply frequency to the rotor windings. This eliminates the need for a full converter between the grid and the rotor, reducing the system's size by approximately 70%.

In generator mode, DFIG works by matching the rotor circuit's frequency to provide a fixed frequency or variable speed at the stator. This feature has made DFIG an important alternative to traditional asynchronous machines in many distributed generation systems [60,68], such as:

- Power systems for ships or mobile machines;
- Hydropower plants with variable flow and speed;
- Wind turbines or tidal turbines with variable speed;
- The generator set has the ability to decelerate when there is low demand, significantly reducing fuel consumption.

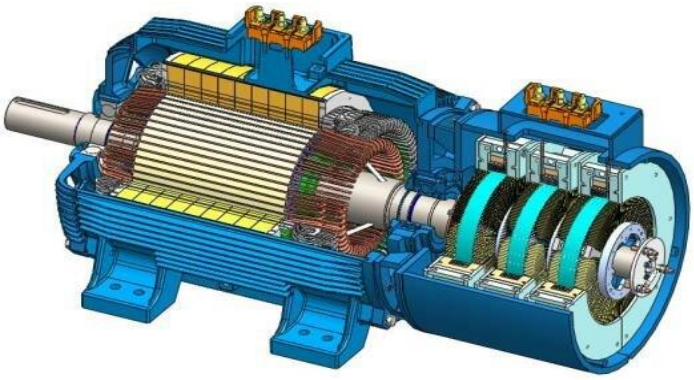

Fig. (1.18): DFIG (Doubly Fed Induction Generator).

1.6.2 Synchronous Generator (SG)

The advantage of synchronous generators over asynchronous generators is the absence of reactive current for magnetization. The magnetic field in synchronous generators can be generated either by permanent magnets or by conventional excitation windings. When the generator has enough poles, it can be used for direct-drive applications without the need for a gearbox. However, SGs are better suited for indirect grid connection via a static converter, allowing for variable-speed operation.

For small units, a PMSG is simpler and more cost-effective [70].

1.6.2.1 Wound Rotor SG

A direct connection to the grid means that the SG will operate at a constant speed. This speed is determined by the grid frequency and the number of poles in the machine. The excitation is either provided through slip rings and brushes or brushless with a rotary switch. Implementing a variable-speed drive in a multipole, gearless system allows for direct speed control. However, this solution requires oversized generators and converters to handle the system's full rated power [70].

1.6.2.2 Permanent Magnet Synchronous Generator (PMSG)

The PMSG (Fig. (1.19)) is the most used generator in small WTs due to its low cost, simplicity, and automatic features, which enable it to operate with a high-power factor and good efficiency. In direct-drive systems (without a mechanical gearbox), synchronous machines are used. Their design, especially regarding mass moments of inertia, becomes highly advantageous when the number of poles is large. When their operating frequency is not compatible with the grid frequency, a frequency converter is required. This is why direct-drive machines are typically variable speed [71-73].

The advantages of the PMSG are:

- Optimized power extraction for low and medium WSs;
- No gearbox required;

- Variable-speed operation across the entire speed range;
- Joule losses and iron losses are confined to the stator;
- No heating in the rotor.

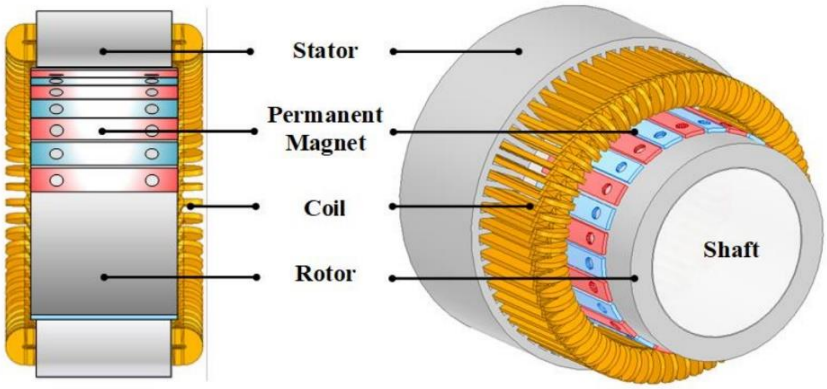

Fig. (1.19): PMSG (Permanent Magnet Synchronous Generator).

1.7 Wind Energy: Its Advantages and Disadvantages

The advantages of WE are closely tied to the technological developments enabling its use. However, this energy source also presents certain drawbacks, which must be carefully considered to avoid hindering its development [74,75].

1.7.1 Advantages

- No CO2 emissions during operation;
- RE source;
- No radioactive waste;
- Easy to stop;
- Simple to dismantle;
- Cost-effective in remote areas;
- High efficiency in winter (when energy demand is highest).

1.7.2 Disadvantages

- ❖ Visual impact;
- ❖ Noise;
- ❖ Impact on bird migration;

- ❖ The electrical power produced is not constant;
- ❖ High cost.

1.8 WT Model

The input and output of the WT are variable and can be summarized as follows:

- The primary energy received by the turbine is determined by wind speed.
- The specific quantities required by the machine come mainly from the geometry of the rotor and the swept area by the turbine blades.
- The blade pitch and the setting angle determine the speed of the turbine.
- The power or torque represents the output quantities of the turbine, which are controlled by varying the input quantities.

The turbine captures the wind's energy through its blades and converts it into mechanical energy. If the wind turbine is facing the wind, the mechanical power can be expressed as follows [75]:

$$P_V = \frac{1}{2}\rho C_p(\lambda, \beta) A {V_W}^3 \quad (1.1)$$

ρ: The air density (kg/m^3). It is specific to each region and depends on the altitude and temperature where the wind turbine is installed. For our case, we have set ρ to $1.225\ kg/m^3$.

V_W: The wind speed (m/s).

C_p: The power coefficient.

A: The swept area by the wind, expressed as $A = \pi R^2$.

1.8.1 Power coefficient

The power coefficient (C_p) is related to the quality of the wind turbine and depends on the shape of the blades. It can be modeled using a single equation that depends on the tip speed ratio (λ) and the pitch angle of the blades (β). The power coefficient is obtained through data zones or by approximating the coefficient using an analytical function [77].

In our case, the analytical function of the power coefficient used to model the turbine is given as follows:

$$C_p(\lambda, \beta) = C_1 . \left[\frac{C_2}{\lambda_i} - C_3 . \beta - C_4\right] exp\left(\frac{-C_5}{\lambda_i}\right) \quad (1.2)$$

The coefficients C_1 to C_5 can vary for different turbines. These six coefficients are adjusted to achieve a

maximum C_p.

The power coefficient C_p is variable and depends on the wind speed, the rotational speed of the turbine, and the parameters of the turbine blades, such as the angle of incidence and the pitch angle.

An experimental study to derive the value of the C_p coefficient is given by:

$$C_p(\lambda, \beta) = 0.5 \left[\frac{116}{\lambda_i} - 0.4\beta - 5\right] exp\left(\frac{-21}{\lambda_i}\right) \quad (1.3)$$

Where:

$$\frac{1}{\lambda_i} = \frac{1}{\lambda + 0.08.\beta} - \frac{0.035}{\beta^3 + 1} \quad (1.4)$$

1.8.2 WS model

The WS model requires a wind model, aerodynamic behavior of the blades, generators, power converters, and a control system. The input variable of the wind system comes from the wind itself. The exact height of the hub is quite difficult to measure. However, a random wind quantity is determined using statistical parameters. A scalar function that increases over time generally expresses WS [78]:

$$V_V = f(t) \quad (1.5)$$

The accuracy of WS estimation over time can be represented by an analytical function or generated through a statistical law measured for a specific location. For a theoretical model, the wind configuration must meet two standards:

- The duration of the profile should be limited to reduce simulation time.
- The wind profile should represent sediment characteristics (intensity, variation, statistical distribution, etc.).

This study represents the evolution of WS in a deterministic manner, using the sum of several harmonics, consistent with [79]:

$$V_V(t) = 9.5 + (\frac{1}{2} * sin(\omega t) - \frac{0.875}{2} * sin(\omega t) + \frac{0.75}{2} * sin(\omega t) - \frac{0.625}{2} * sin(\omega t) + sin(18.84t) + \frac{0.5}{2} * sin(\omega t) + \frac{0.375}{2} * sin(\omega t)) \quad (1.6)$$

1.9 Conclusion

Different types of WTs have been introduced in the design of energy conversion systems. To highlight this development, the chapter first presents the state of the art, explaining general terms related to wind energy and showcasing its evolution on both global and Algerian scales. Subsequently,

it outlines the stages of this energy challenge, demonstrated through various types of wind turbines, including fixed-speed, variable-speed, vertical-axis, and horizontal-axis turbines. The last part describes the main kinds of generators used in this field, highlighting their respective benefits. The next chapter will provide a comprehensive analysis of the chosen generator type for this research and investigate its utilization in a multi-machine system. This method seeks to improve comprehension of the generator's operating setting and its advantages within a wider framework.

References

[1] ZoltánVarga, PéterStumpf, Rafael K. Járdán, István Nagy, Application of Ultrahigh Speed Induction Machine for Waste or Renewable Energy Recovery, International Journal of Renewable Energy Research-IJRER, 1(4):200-211,2011. https://doi.org/10.20508/ijrer.v1i4.148.g77.

[2] Bayram Kilic, Evaluating of Renewable Energy Potential in Turkey, International Journal of Renewable Energy Research-IJRER, 1(4): 259-264, 2011. https://doi.org/10.20508/ijrer.v1i4.79.g64.

[3] Youcef Soufi, Sihem Ghoudelbourk, Tahar Bahi, Hichem Merabet, Harmonics Minimization of Multilevel Inverter Connecting Source Renewable Energy to Power System, International Journal of Renewable Energy Research-IJRER, 1(4): 265-270, 2011. https://doi.org/10.20508/ijrer.v1i4.80.g65

[4] Seifeddine Belfedhal, EL madjid Berkouk, Modeling and Control of Wind Power Conversion System With a Flywheel Energy Storage System, International Journal of Renewable Energy Research-IJRER,1(3):161-152 ,2011. https://doi.org/10.20508/ijrer.v1i3.48.g47.

[5] Mohamed Mansour, M.N. Mansouri, M.F. Mmimouni, Study and Control of a Variable-Speed Wind-Energy System Connected to the Grid. International Journal of Renewable Energy Research-IJRER, 1(2): 96-104,2011. https://doi.org/10.20508/ijrer.v1i2.38.g26.

[6] Zehra Yumurtaci, Kutlay Toprak, Analysis of Hydrogen Production Economy Using Wind Power and a Case Study. International Journal of Renewable Energy Research-IJRER,1(1):11-17, 2011. https://doi.org/10.20508/ijrer.v1i1.24.g10

[7] Benbouhenni, H., Colak, I., Bizon, N. et al. Power regulation of variable speed multi rotor wind systems using fuzzy cascaded control. Sci Rep 14, 16415 (2024). https://doi.org/10.1038/s41598-024-67194-4.

[8] Alliance GR, Presidency C. Tripling renewable power and doubling energy efficiency by 2030: Crucial steps towards 1.5° C.

[9] Ali Abd Elsalam Ibrahim, M.R.I. Ramadan, S. Aboul-Enein, A.Abdel-Azeem ElSebaii, S.M. El-Broullesy, Short Circuit Current Isc as a Real Non-Destructive Diagnostic Tool of a Photovoltaic Modules Performance. International Journal of Renewable Energy Research-IJRER, 1(3):168-162 ,2011. https://doi.org/10.20508/ijrer.v1i3.54.g48.

[10] Ali Abd Elsalam Ibrahim, Dark I-V Characteristics and Lock-in Thermography (LIT) Techniques as a Diagnostic Tools for Silicon Solar Cell After 4000 hours of Thermal Stress at 400K. International Journal of Renewable Energy Research-IJRER,1(3): 169-174, 2011. https://doi.org/10.20508/ijrer.v1i3.55.g49.

[11] Ali Djerioui, K. Aliouane, F. Bouchafaa, Sliding Mode Observer of a Power Quality in Grid Connected Renewable Energy System. International Journal of Renewable Energy Research-IJRER, 2(4):548-541 2012. https://doi.org/10.20508/ijrer.v2i4.270.g6059

[12] Temitope Raphael Ayodele, Adiasa Jimoh, Josial L Munda, Agee J Tehile, Challenges of Grid Integration of Wind Power on Power System Grid Integrity: A Review.International Journal of Renewable Energy Research-IJRER, 2(4):618-626 ,2012. https://doi.org/10.20508/ijrer.v2i4.317.g6069

[13] Abdel Ghani Aissaoui, Ahmed Tahour, Mohamed Abid, Najib Essounbouli, Frederic Nollet, Moulay Idriss Chergui, Variable Structure Control Applied in Wind Turbine Based on Induction Generator. International Journal of Renewable Energy Research-IJRER, 2(4):600-607, 2012. https://doi.org/10.20508/ijrer.v2i4.310.g6067

[14] Adel Khedher, Nihel Khemiri, Mohamed Faouzi Mimouni, Wind Energy Conversion System Using DFIG Controlled by Backstepping and Sliding Mode Strategies.International Journal of Renewable Energy Research-IJRER,2(3):421-430, 2012. https://doi.org/10.20508/ijrer.v2i3.249.g6040

[15] Soufi Y, Kahla S, Bechouat M. Feedback linearization control based particle swarm optimization for maximum power point tracking of wind turbine equipped by PMSG connected to the grid. International journal of hydrogen energy. 2016 Dec 7; 41(45): 20950-5.

[16] Benakcha M, Benalia L, Ammar A, Bourek A. Wind energy conversion system based on dual stator induction generator controlled by nonlinear backstepping and pi controllers. International Journal of System Assurance Engineering and Management. 2019 Aug; 10(4):499-509.

[17] Sahbi A, Moez A, Mohamed C. A New Robust Control Strategy for a Wind Energy Conversion System Based on a T-S Fuzzy Model. International Journal of Smart Grid-IJSMARTGRID, 2020, 4(2): 88-99. https://doi.org/10.20508/ijsmartgrid.v4i2.103.g87.

[18] Errami Y, Ouassaid M, Maaroufi M. A performance comparison of a nonlinear and a linear control for grid connected PMSG wind energy conversion system. International Journal of Electrical Power & Energy Systems. 2015 Jun 1;68:180-94.

[19] Errami Y, Obbadi A, Sahnoun S, Ouassaid M, Maaroufi M. Proposal of a backstepping control strategy for dynamic performance improvement of PMSG Wind Farm with common DC bus. In2016 International Renewable and Sustainable Energy Conference (IRSEC) 2016 Nov 14 (pp. 397-404). IEEE.

[20] Abdelhakim B, Ilhami C, Korhan K, Ramazan B. Modeling of a Permanent Magnet Synchronous Generator in a Power Wind Generation System with an Electrochemical Energy Storage. International Journal of Smart Grid-IJSMARTGRID, 2018, 2(4):197-202. https://doi.org/10.20508/ijsmartgrid.v2i4.26.g25.

[21] Moez A, Sahbi A, Habib B Z, Mohamed C. A Novel fuzzy Control Strategy for Maximum Power Point Tracking of Wind Energy Conversion System. International Journal of Smart Grid-IJSMARTGRID, 2019, 3(3): 120-127. https://doi.org/10.20508/ijsmartgrid.v3i3.63.g58.

[22] Mai N A, Ahmed A D, Medhat H E. A Novel Model Predictive Speed Controller for PMSG in Wind Energy Systems. International Journal of Renewable Energy Research-IJRER, 2022, 12(1): 170-180. https://doi.org/10.20508/ijrer.v12i1.12750.g8385.

[23] Peng X, Liu Z, Jiang D. A review of multiphase energy conversion in wind power generation. Renewable and Sustainable Energy Reviews. 2021 Sep 1;147:111172.

[24] Bounadja E, Boudjema Z, Djahbar A. A New DPC-SVM for Matrix Converter Used in Wind Energy Conversion System Based on Multiphase Permanent Magnet Synchronous Generator. Iranian Journal of Electrical & Electronic Engineering. 2019 Sep 1;15(3).

[25] Marwa G, Jihen A, Mohamed W N. Modelling of a PMSG based wind turbine system with diode rectifier based generator side converter. International Journal of Renewable Energy Research-IJRER, 2022, 12(3):1532-1539. https://doi.org/10.20508/ijrer.v12i3.13044.g8538.

[26] Habib B. Comparative Study Between Direct Vector Control and Fuzzy Sliding Mode Controller in Three-Level Space Vector Modulation Inverter of Reactive and Active Power Command of DFIG-Based Wind Turbine Systems. International Journal of Smart Grid-IJSMARTGRID, 2018, 2(4): 188-196. https://doi.org/10.20508/ijsmartgrid.v2i4.24.g24.

[27] Abdulrahman I A. The Integration of Intermittent Renewable Energy Sources to Smart Grid: A Comprehensive View. International Journal of Renewable Energy Research-IJRER, 2022, 12(3): 1614-1627. https://doi.org/10.20508/ijrer.v12i3.13110.g8556.

[28] Faridha Banu M R, Jayapragash R. A Qualitative Investigation on Multiport Converters for Renewable Energy Sourced DC Loads. International Journal of Renewable Energy Research-IJRER, 2022, 12(2): 1117-1130. https://doi.org/10.20508/ijrer.v12i2.12926.g8499.

[29] Hoa M N. A Comparative Study of Different Sliding Mode Control Strategies for PMSG-Based Standalone WECS. International Journal of Renewable Energy Research-IJRER, 2021, 11(4): 1977-1986. https://doi.org/10.20508/ijrer.v11i4.12170.g8354.

[30] Kominami T, Fujimoto Y. Inverter with reduced switching-device count for independent ac motor control. InIECON 2007-33rd Annual Conference of the IEEE Industrial Electronics Society 2007 Nov 5 (pp. 1559-1564). IEEE.

[31] Kominami T, Fujimoto Y. A novel nine-switch inverter for independent control of two three-phase loads. In2007 IEEE Industry applications annual meeting 2007 Sep 23 (pp. 2346-2350). IEEE.

[32] Oka K, Matsuse K. A nine-switch inverter for driving two AC motors independently. IEEJ Transactions on Electrical and Electronic Engineering. 2007 Jan;2(1):94-6.

[33] Dos Santos EC, Jacobina CB, Da Silva OI. Six-phase machine drive system with nine-switch converter. InIECON 2011-37th Annual Conference of the IEEE Industrial Electronics Society 2011 Nov 7 (pp. 4204-4209). IEEE.

[34] Reusser CA. Full-electric ship propulsion, based on a dual nine-switch inverter topology for dual three-phase induction motor drive. In2016 IEEE Transportation Electrification Conference and Expo (ITEC) 2016 Jun 27 (pp. 1-6). IEEE.

[35] Goyal GN, Aware MV. Speed sensorless control of multiple induction motor drives with single nine switch inverter. In2017 International Conference on Energy, Communication, Data Analytics and Soft Computing (ICECDS) 2017 Aug 1 (pp. 3639-3644). IEEE.

[36] Abbache MA, Tabbache B, Douida S, Benbouzid M. Direct torque control scheme for nine switches inverter fed two induction motors-based more electric vehicle powertrains. International Transactions on Electrical Energy Systems. 2021 Dec;31(12):e13175.

[37] Gulbudak O, Gokdag M. Dual-hysteresis band control of nine-switch inverter to control two induction motors. IEEE Transactions on Energy Conversion. 2021 Nov 30;37(2):788-99.

[38] Gulbudak O, Gokdag M. Finite control set model predictive control approach of nine switch inverter-based drive systems: Design, analysis, and validation. ISA transactions. 2021 Apr 1;110:283-304.

[39] Gokdag M. Modulated predictive control to improve the steady-state performance of NSI-based electrification systems. Energies. 2022 Mar 10;15(6):2043.

[40] Gulbudak O, Gokdag M, Komurcugil H. Lyapunov-based model predictive control of dual-induction motors fed by a nine-switch inverter to improve the closed-loop stability. International Journal of Electrical Power & Energy Systems. 2023 Mar 1;146:108718.

[41] Gulbudak O, Gokdag M, Komurcugil H. Sliding Mode Current Control Strategy for Nine-Switch Converter. In2021 IEEE 2nd International Conference on Smart Technologies for Power, Energy and Control (STPEC) 2021 Dec 19 (pp. 1-5). IEEE.

[42] Mousa HH, Youssef AR, Mohamed EE. Optimal power extraction control schemes for five-phase PMSG based wind generation systems. Engineering science and technology, an international journal. 2020 Feb 1;23(1):144-55.

[43] NEDJARI, H. Daaou, HADDOUCHE, S. Kheder, BALEHOUANE, A., et al. Optimal windy sites in Algeria: Potential and perspectives. Energy, 2018, vol. 147, p. 1240-1255.

[44] VAN HAAREN, Rob et FTHENAKIS, Vasilis. GIS-based wind farm site selection using spatial multi-criteria analysis (SMCA): Evaluating the case for New York State. Renewable and sustainable energy reviews, 2011, vol. 15, no 7, p. 3332-3340.

[45] MERZOUK, N. Kasbadji. Evaluation du gisement énergétique éolien contribution à la détermination du profil vertical de la vitesse du vent en Algérie. 2006. Thèse de doctorat. Thèse de doctorat d'état en physique énergétique, Université de Tlemcen.

[46] OUALI, Salima, KHELLAF, Abdallah, et BADDARI, Kamel. Etude des ressources géothermique du Sud de l'Algérie. Journal of Renewable Energies, 2006, vol. 9, no 4, p. 297-306.

[47] MASSOUM, Sarra. Contrôle avec les techniques de l'intelligence artificielle d'une source d'énergie éolienne à base d'une machine asynchrone à double alimentation avec système de stockage. 2018. Thèse de doctorat. Université El Djillali Liabès de Sidi Bel Abbès, Départemen.

[48] Renewable Energy Bulletin - No. 21, 2011, Center for the Development of Renewable Energies, Ministry of Higher Education and Scientific Research, pages 1 to 4.

[49] MERZOUK, N. Kasbadji, MERZOUK, M., BENYOUCEF, B., et al. Perspectives du pompage éolien dans le sud Algérien. Projet National de Recherche, domicilié au Centre de Développement des Énergies Renouvelables, Laboratoire d'Énergie Éolienne, Alger, 2007.

[50] Renewable Energy Bulletin - Wind Energy - Environment and Energy Management Agency, 2022.

[51] BELAKEHAL, Soltane. Conception & commande des machines à aimants permanents dédiées aux énergies renouvelables. universite costantine, 2010.

[52] world wind energy association,Half-year Report 2022: Worldwide Windpower Boom Continues in 2022,November 15, 2022 Press Releases, Statistics.

[53] Visual Capitalist. (n.d.). The largest producers of wind power by country. Retrieved March 3, 2025, from https://www.visualcapitalist.com/the-largest-producers-of-wind-power-by-country/

[54] YOUCEF, Djeriri, et al. Commande directe du couple et des puissances d'une MADA associée à un système éolien par les techniques de l'intelligence artificielle. 2015. Thèse de doctorat.

[55] BILLEL, Meghni. Contribution à l'amélioration des performances d'une chaine énergétique éolienne. 1955. Thèse de doctorat. These Doctorat, université Badji Mokhtar Annaba 2015.[4] Wikipedia.

[56] DOUADI, Tarek. Modélisation et stratégie de Commande de la Génératrice Asynchrone intégrée à un Système Eolien. 2020. Thèse de doctorat. Université de Batna 2.

[57] TRAORÉ, Moussa. Développement d'un simulateur numérique de rotors d'éoliennes Application à une chaîne de conversion éolienne utilisant une machine synchrone à aimants permanents. Universite du Quebec a Rimouski (Canada), 2016.

[58] DE ALEGRÍA, Iñigo Martinez, ANDREU, Jon, MARTÍN, José Luis, et al. Connection requirements for wind farms: A survey on technical requierements and regulation. Renewable and Sustainable Energy Reviews, 2007, vol. 11, no 8, p. 1858-1872.

[59] SAID, Chikha. Contribution à l'optimisation de la commande prédictive des convertisseurs statiques intégrés dans les chaines de conversion d'énergie éolienne. 2017. Thèse de doctorat. Université de Annaba.

[60] EL AIMANI, Salma. Modélisation des différentes technologies d'éoliennes intégrées dans un réseau de moyenne tension. 2004. Thèse de doctorat. Ecole Centrale de Lille.

[61] Desalegn B, Gebeyehu D, Tamrat B, Tadiwose T, Lata A. Onshore versus offshore wind power trends and recent study practices in modeling of wind turbines' life-cycle impact assessments. Cleaner Engineering and Technology. 2023 Dec 1;17:100691.

[62] Tumse S, Bilgili M, Yildirim A, Sahin B. Comparative Analysis of Global Onshore and Offshore Wind Energy Characteristics and Potentials. Sustainability. 2024 Aug 2;16(15):6614.

[63] Perera SM, Putrus G, Conlon M, Narayana M, Sunderland K. Wind energy harvesting and conversion systems: A technical review. Energies. 2022 Dec 8;15(24):9299.

[64] LOPEZ, Miguel. Contribution à l'optimisation d'un système de conversion éolien pour une unité de production isolée. 2008. Thèse de doctorat. Université Paris Sud-Paris XI.

[65] BELGACEM, Kheira et MEZOUAR, Abdelkader. Optimisation des performances des systèmes énergétique dans la production d'énergie éolienne à vitesse variable. 2015. Thèse de doctorat.

[66] Desalegn B, Gebeyehu D, Tamrat B, Tadiwose T. Wind energy-harvesting technologies and recent research progresses in wind farm control models. Frontiers in Energy Research. 2023 Feb 15;11:1124203.

[67] ABAD, Gonzalo, LOPEZ, Jesus, RODRIGUEZ, Miguel, et al. Doubly fed induction machine: modeling and control for wind energy generation. John Wiley & Sons, 2011.

[68] POITIERS, Frédéric. Etude et commande de génératrices asynchrones pour l'utilisation de l'énergie éolienne-machine asynchrone a cage autonome-machine asynchrone a double alimentation reliée au réseau. 2003. Thèse de doctorat. Université de Nantes.

[69] BELTRAN, Brice. contribution à la commande robuste des éoliennes à base de génératrices asynchrones double alimentation: du mode glissant classique au mode glissant d'ordre supérieur. 2010. Thèse de doctorat. Université de Bretagne occidentale-Brest.

[70] AHMIDI, Amir. Participation de parcs de production éolienne au réglage de la tension et de la puissance réactive dans les réseaux électriques. 2010. Thèse de doctorat. Ecole Centrale de Lille.

[71] BENSAADI, HACENE. contribution à la commande d'un aérogénérateur basé sur un GSAP. 2020. Thèse de doctorat. Université de Batna 2.

[72] CISSE, Koua Malick, HLIOUI, Sami, CHENG, Yuan, et al. Etat de l'art des topologies de machines électriques utilisées dans les véhicules électriques et hybrides. In : 3ème Symposium de Génie Electrique (SGE 2018). 2018.

[73] ANNANA, Adel. Analyse du comportement du moteur synchrone dans les entrainements electrique à vitesse variable. 2010. Thèse de doctorat. Université de Annaba-Badji Mokhtar.

[74] BOUMARAF, Farid. Commande d'un aérogénérateur-Apport des techniques de l'intelligence artificielle. 2014. Thèse de doctorat. Université de Batna 2.

[75] MIRECKI, Adam. Étude comparative de chaînes de conversion d'énergie dédiées à une éolienne de petite puissance. 2005. Thèse de doctorat.

[76] GUENOUNE, Ibrahim. Commandes non linéaires robustes de systèmes éoliens. 2018. Thèse de doctorat. École centrale de Nantes; Université Abou Bekr Belkaid (Tlemcen, Algérie).

[77] SABRI, Borhaneddine. Modélisation d'une chaine de conversion d'énergie éolienne à base d'une génératrice synchrone/asynchrone. 2019. Thèse de doctorat. Directeur: Dr. Mama BOUCHAOUR/Co-directeur: Mr. Merad Laaredj.

[78] BELAKEHAL, Soltane. Conception & commande des machines à aimants permanents dédiées aux énergies renouvelables. universite costantine, 2010.

[79] TRAN, Duc-Hoan. Conception Optimale Intégrée d'une chaîne éolienne" passive": analyse de robustesse, validation expérimentale. 2010. Thèse de doctorat. Institut National Polytechnique de Toulouse-INPT.

Chapter 2

Modeling of Parallel multi-machine system

2.1 Introduction

This chapter addresses the modeling of the 5-phase PMSGs. The discussion initiates with a comprehensive examination of multiphase generators, including their definitions, different classifications, benefits, and drawbacks. This foundational understanding establishes a basis for a more in-depth examination of the 5-phase PMSG, characterized by a set of five electrical and magnetic equations, along with a mechanical equation. Working with these equations can present significant challenges, even when using digital simulation tools. To tackle this, implementing a transformation is crucial. The transformation matrix allows for the conversion of a five-phase system into an equivalent four-phase (d-q-x-y) system, simplifying the mathematical representation and making analysis more straightforward. This transformation streamlines the modeling process and enhances the ability to design and control these machines effectively, making them more applicable in modern energy systems, such as RE generation and electric vehicle propulsion. This approach offers a more manageable framework for analysis, leading to enhanced performance and efficiency in practical applications.

2.2 Multi-phase Machine

Multi-phase machines, especially those beyond three phases, have several benefits compared to conventional three-phase systems [1-3]. Multi-phase machines are becoming more pertinent in contemporary applications across diverse sectors, such as electric automobiles, renewable energy, and aerospace. Their efficiencies, durability, and performance provide them a compelling option for many high-tech applications. The following delineates the principal applications of multi-phase machines:

1. Wind Power Generation Systems (WPGSs)

Multi-phase PMSGs are employed in WTs to maximize energy capture and improve grid stability. The multi-phase structure contributes to the reduction of torque ripple and enhances efficiency [1-3].

2. Electric Vehicles

The compact design and high efficacy of multi-phase machinery have led to their the increasing application in electric and hybrid vehicles. They offer improved torque control and more efficient operation [2-4].

3. Industrial Drives

Multi-phase machines are used in numerous industrial applications where high productivity and dependability are essential, including robotics and automation systems. They provide superior fault tolerance compared to conventional systems [3, 5].

4. Aerospace Applications

In the field of aerospace, the utilization of multi-phase machines is noteworthy due to their lightweight and compact design. This characteristic contributes significantly to high power density and efficiency, which are essential factors in the operation of aircraft systems [3, 6].

5. High-Power Application

Multi-phase machines demonstrate a commendable suitability for high-power applications, as they facilitate a more equitable distribution of power. This characteristic not only mitigates the potential for overheating but also enhances the overall stability of the system [6, 7].

2.2.1 Type 1

The machines that are classified as "Type 1" are those that have a number of stator phases (q) that is a multiple of three. This allows them to be categorized as η (η = 2, 3, 4,...) star three-phase machines. However, when considering a certain number of phases, there are several alternative configurations that may be achieved by adjusting the angle α between the two phases that are next to each other. The features of a dual-star machine (q = 6) which contains stars that are moved by δ = 30 (asymmetrical) are distinct from those of a machine that has stars that are shifted by δ = 60 (symmetrical). It is feasible to introduce the definition by the figures in the following manner in order to distinguish the many potential configurations [8, 9]:

$$q = 3\eta \ (\eta = 2, 3, 4, \dots) \tag{2.1}$$

$$\delta = {}^{\pi}/_{q} \tag{2.2}$$

$$q_{\delta} = {}^{\pi}/_{\delta} \tag{2.3}$$

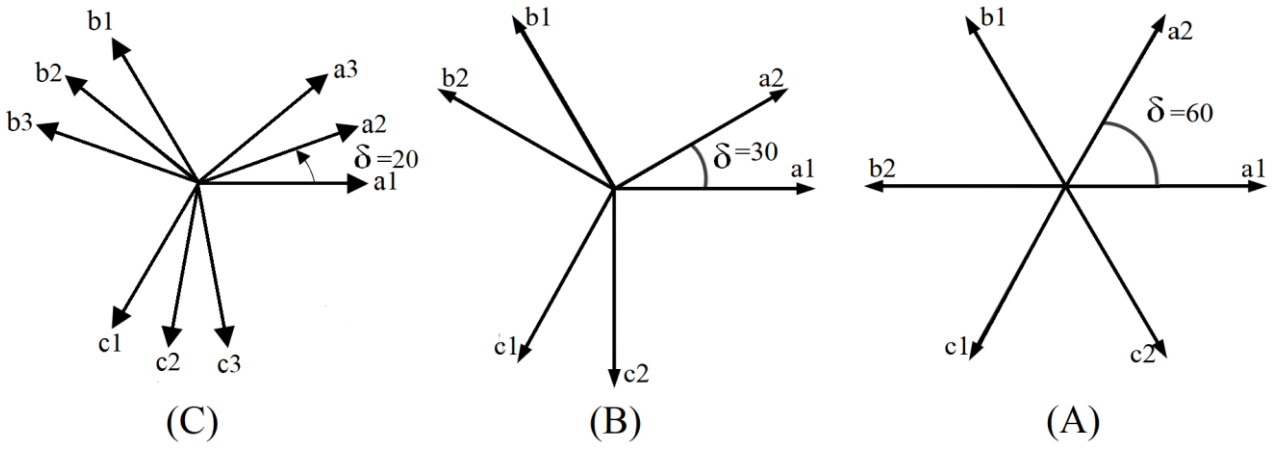

Fig. (2.1): Machines type1

2.2.2 Type 2

The multi-phase machines that are classified as "Type 2" are those that have an odd number of stator phases (q), as shown in Figure (2.2). The symbol α indicates the angular offset that exists between two adjacent phases. Therefore, the q phases are moved in a regular manner by an angle of 2π/q [8, 9].

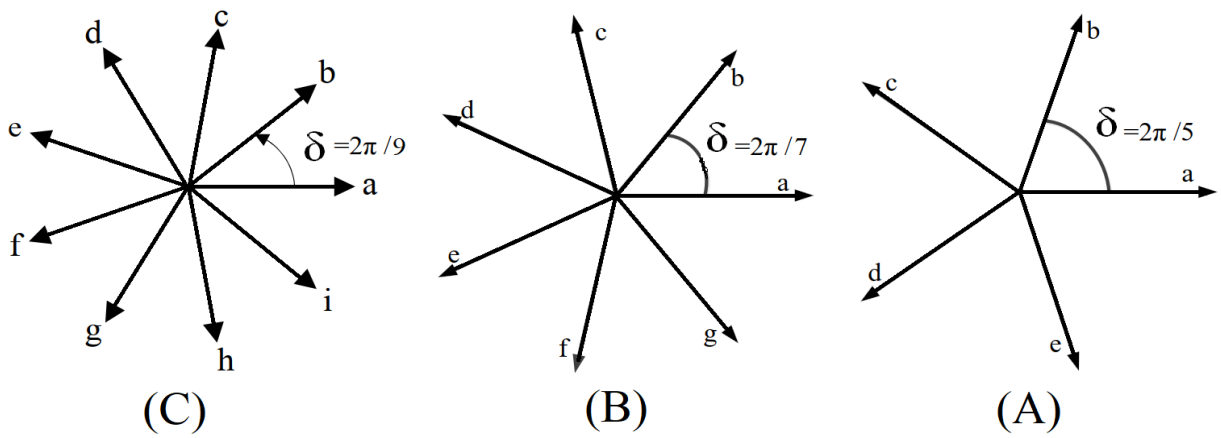

Fig. (2.2): Machines type 2

2.3 Multiple-Phase Machines: Pros and Cons

2.3.1 Advantages

Various benefits of multi-phase machines in comparison to three-phase machines have been highlighted in the many literature [6, 7, 10-15, 21]:

1. Reduced Torque Ripple

Utilizing additional phases contributes to a more refined torque generation, effectively reducing output fluctuations by increasing the frequency of torque pulsation while decreasing its amplitude. This leads to enhanced performance in applications that necessitate accurate controlling motion [10, 11].

2. Higher Power Density and its segmentation

Multi-phase machines offer the advantage of delivering greater power output while maintaining a more compact design in comparison to conventional machines. This proves to be especially advantageous in scenarios where spatial constraints are a consideration, such as in electric vehicles and aerospace applications [6, 7]. The addition of more phases to supply the machine leads to a decrease in the current for each phase, while maintaining the same voltage per phase. This ultimately results in a lower power output per phase when compared to a similar three-phase machine. This indicates that the requirement for parallel or series power switches in high power applications is eliminated, leading to a reduction in the number of components and a simplification of the inverter structure. This enhancement has

contributed positively to the reliability of high power applications [10, 12, 13].

3. Improved Fault Tolerance

Multi-phase machines are capable of maintaining effective operation even in the event of one or more phases experiencing failure. This redundancy contributes positively to system reliability, rendering them appropriate for critical applications, even in the absence of modifications to control system strategies, albeit with some degradation in operation and at a lower power level. This is a crucial necessity for applications where safety is paramount, such as in vehicle electric propulsion systems. Additionally, it is vital in situations where a drive trip and the resulting halt of the driven equipment could lead to significant economic repercussions due to interruptions in production [14].

4. Enhanced Efficiency

Multi-phase systems have the potential to enhance efficiency through improved current distribution and a decrease in harmonic distortion. This presents a favorable opportunity to minimize energy losses while enhancing the overall performance of the system [15].

2.3.2 Disadvantages

In light of the numerous advantages previously discussed. However, their use necessitates specific precautions and considerations that must be addressed to achieve optimal benefits, such as [9, 16]:

- The assembly (machine and converter) is more expensive than a 3-phase drive due to the increased number of components.
- The generation of significant stator current harmonics takes place when the machine operates with multi-leg converters, leading to increased losses that elevate both the size and expense of the machine-inverter.

2.4 Overview of Five-Phase PMSM

Synchronous machines encompass all machines where the rotor speed matches the speed of the rotating stator field. In the case of PMSM, the rotor excitation is supplied by permanent magnets (PM) [9]. The PMSM operates without requiring an additional DC power supply or field windings for rotor excitation. Consequently, the power losses associated with the field windings are removed in this type of machine. Furthermore, the magnets and redundant teeth in stators facilitate magnetic decoupling among the various groups of windings [9, 17].

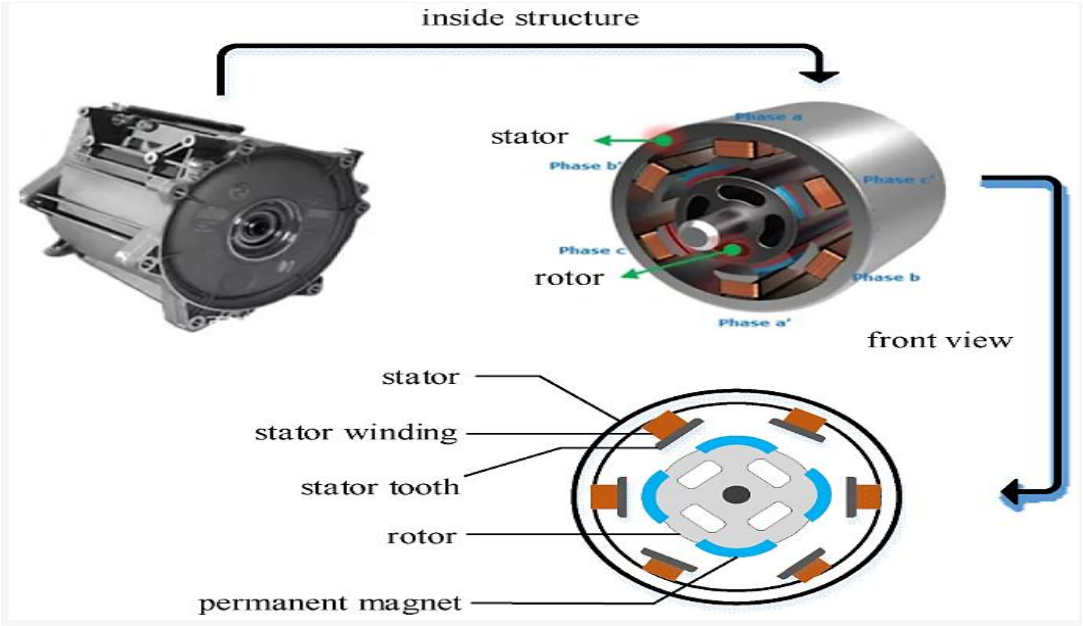

Fig. (2.3): Internal architecture of a PMSM

The makeup of this particular machine could be split into two fundamental components:

The stator: resembles that of an induction machine, featuring a five-phase winding supply. This configuration ensures that the electromotive forces produced by the rotor field's rotation are either sinusoidal or trapezoidal. This configuration is characterized by five axes (a, b, c, d, e), with a $\left(\frac{2\pi}{5}\right)$ phase shift between two adjacent phases.

The rotor: It is composed of PMs. The PMs offer the benefit of removing brushless rotor losses and eliminating the need for excitation current, thereby enhancing the machine's efficiency. Furthermore, there is no requirement to manage the amplitude of the rotor flux.

The PMSMs could be categorized in two primary ways: one based on the orientation of the field flux, which can be classified as a radial field, and the other based on the configuration of the magnets mounted in the rotor [18].

2.4.1 Based on the orientation of the field flux:

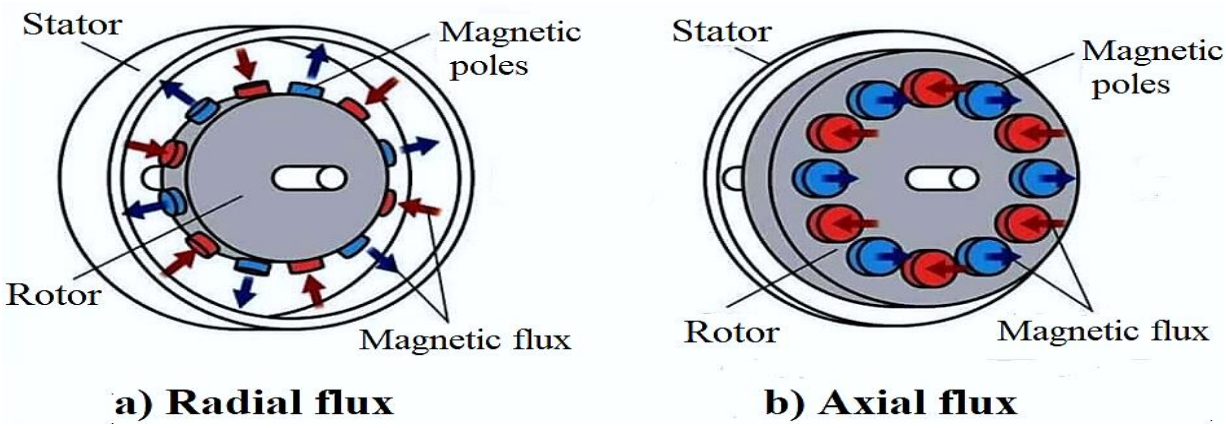

Fig. (2.4): Two different model of PM machine based on field flux

Axial Flux Permanent Magnet Generators (AFPMGs): In AF configurations, the magnetic flux traverses along the rotor's axis (see fig. 2.4.b). This kind is small and lightweight, making it appropriate for situations where space and weight are paramount considerations [18, 19].

In contrast to RF structures, these machines have substantial diameters and rather short axial lengths. The magnetic flux of a magnet is axial, whereas the current is radial. Various configurations exist for axial flux. The straightforward design features a rotor and stator (Fig. 2.5), while a double-gap arrangement includes a single stator situated between two rotors (Fig. 2.6 or mono rotor).In the third configuration, the rotor is positioned between two stators, as illustrated in Figure 2.7 [21, 22].

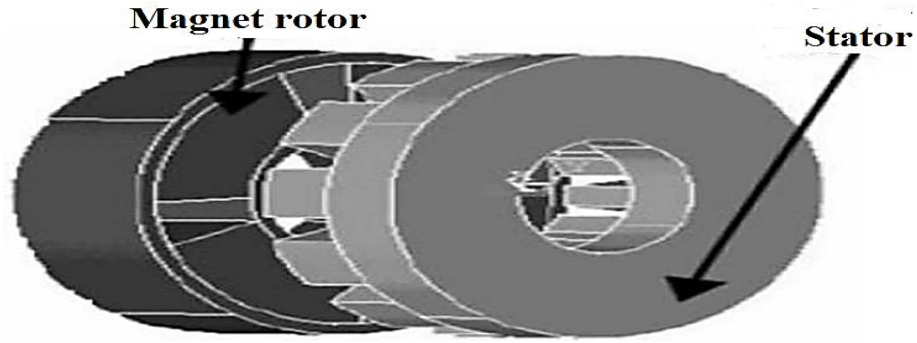

Fig. (2.5): Simple axial structure with a rotor and stator

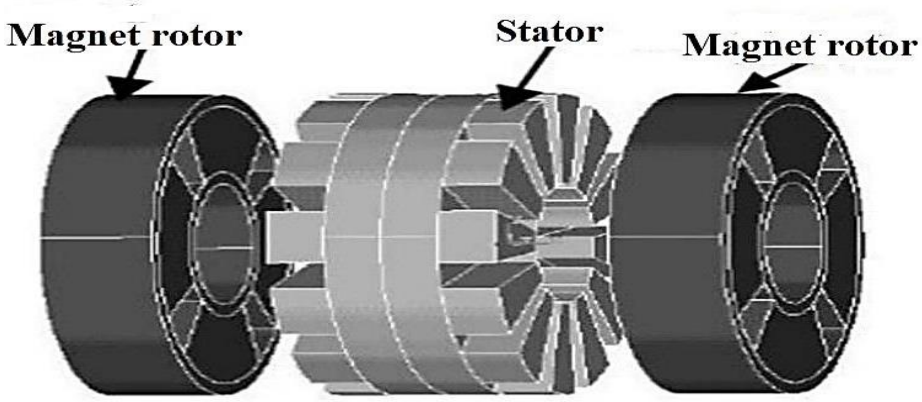

Fig. (2.6): Axial flux structure with double rotor and one stator

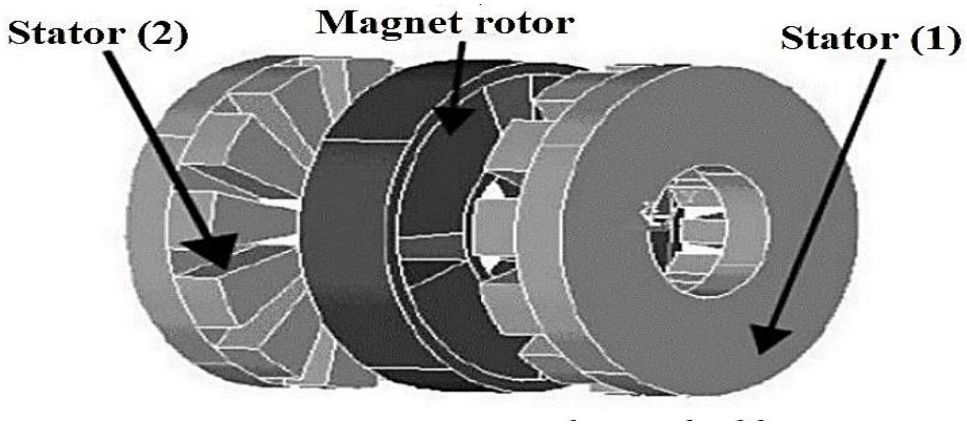

Fig. (2.7): Axial flux structure with double stator and rotor.

Radial Flux Permanent Magnet Generators (RFPMGs): This architecture features a radial magnetic flux path, with magnetic field lines the magnetic field lines extend radially from the rotor to the stator (see fig. 2.8.a). It is frequently utilized in applications involving wind power because of its straightforwardness and efficiency [9, 18]. The rotors of synchronous machines may be classified as exterior (Fig. 2.8.a) or internal (Fig. 2.8.b). Internal rotor machines are standard radial flux configuration (RFPM) machines. They are simple to execute and possess effective loss evacuation stators due to the peripheral placement of the stator. Typically, rotor losses are minimal owing to the use of permanent magnets. External rotor machines are often used in motor applications within the electric traction sector, generally designated as "wheel motors" [21, 23].

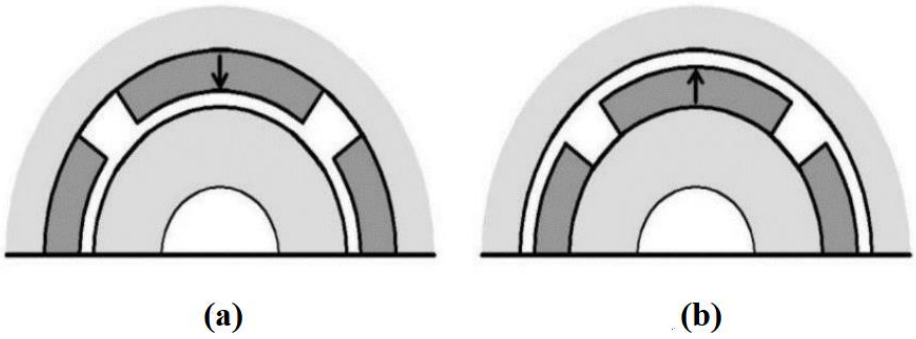

Fig. (2.8): Radial flux configuration: a) external rotor, b) internal rotor

2.4.2 based on the configuration of the magnets:

Surface-Mounted Permanent Magnet Generators (SMPMGs): This type (see Fig.2.9.a and b) is widely utilized due to its simplicity architecture and ease of manufacture, resulting in a consistent air-gap (the permeability of the permanent magnet is nearly equivalent to that of air, thereby making the magnetic material an extension of the air-gap $L_d = L_q$). However, at high speeds, there are certain risks associated with the magnets being affixed to the rotor surface, typically using an adhesive. This limitation results in reduced structural integrity and mechanical robustness. Furthermore, these magnets lack protection against the field generated by the stator [9, 20].

Interior Permanent Magnet Generators (IPMGs): In this configuration, the magnets are incorporated within the rotor iron (see Fig.2.9.c and d). The machine features salient poles, which contribute an additional torque, known as reluctance torque, alongside the synchronous torque, thereby enhancing the operational range of the machine. In this scenario, it is important to note that the magnetic circuit of the rotor exhibits anisotropic characteristics, leading to a significant dependence of the inductances on the rotor's position. This particular machine exhibits enhanced mechanical robustness and facilitates operation at elevated speeds. Conversely, it benefits from both mechanical and magnetic protection, which inherently contributes to a higher manufacturing cost [9, 20].

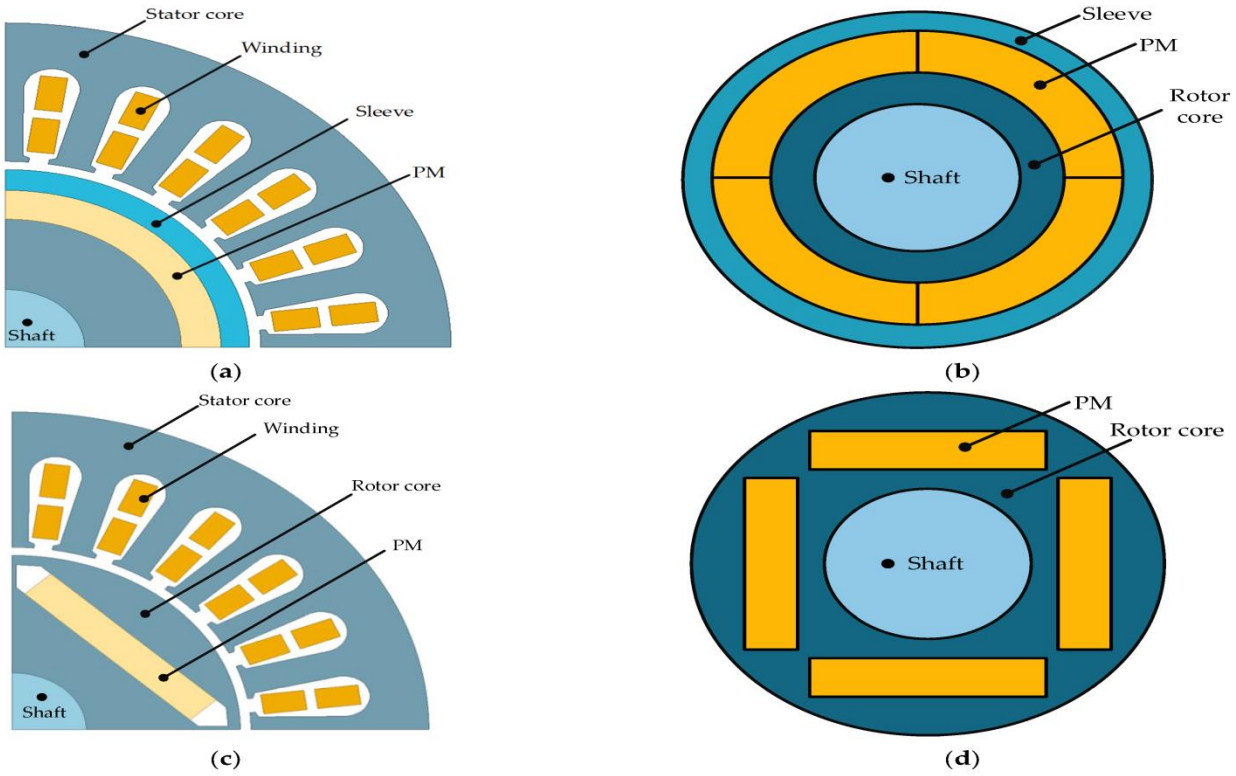

Fig. (2.9): The machine's model: (a) SPM machine model; (b) The SPM machine's rotor structure; (c) IPM machine model; (d) The IPM machine's rotor structure.

2.5 The operational principle of Permanent Magnet Synchronous Machines

In the permanent magnet synchronous machine, a stator coil creates power that produces an electromagnetic force revolving at an angular velocity (w_g). The rotor generates magnetic force induced by the excitation magnets and has an equal number of poles as the stator, which is supplied by a five-phase network. Consequently, the stator generates a field that induces rotation in the rotor. Increased torque on the shaft results in a larger angle of pole deflection. The rotor is disengaged from the rotational current once this angle surpasses 90 degrees. The timing speed is equivalent to the rotor rotation speed, so it is proportional to the stator supply frequency. The electrical torque angle characteristic is seen in Figure 2.10 [21, 22].

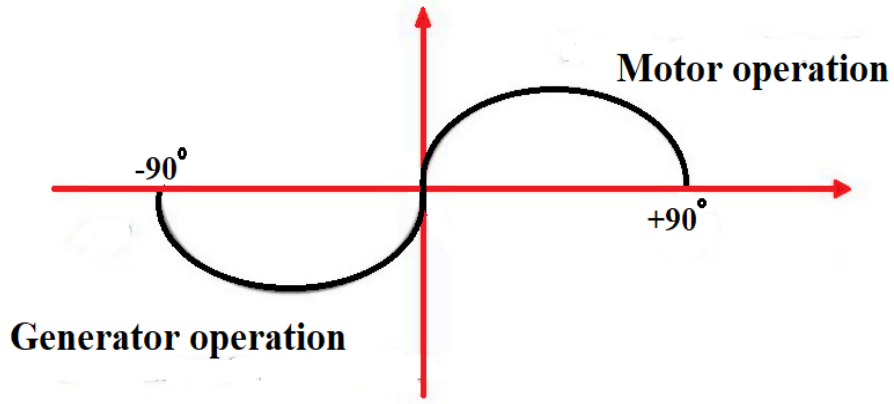

Fig. (2.10): Characteristic of the electric torque-angle

2.5.1 The operational concept in generator mode

The operating principle of PMSMs in generator mode entails the conversion of mechanical energy into EE via the interaction of the rotor's magnetic field with the stator's winding. The essential components of this operating mode are as follows:

The mechanical input, usually supplied by a prime mover (such as a wind turbine or water turbine), propels the rotor at a velocity above synchronous speed. This is crucial for the machine to operate as a generator.

The rotor velocity must be adequately elevated to surpass the back electromotive force (EMF), facilitating the extraction of electrical energy from the machine.

In generator mode, the PMSM functions by spinning the rotor, which contains permanent magnets. The rotor's rotation generates a rotating magnetic field that engages with the stator windings.

The interaction between the rotor's magnetic field and the stator generates an EMF in the stator windings, as per Faraday's law of electromagnetic induction.

In this mode, the PMSM generates an alternating current (AC) signal as its electrical output.

2.5.2 The operational concept in motor mode

The functioning of PMSMs in motor mode entails the transformation of electrical energy into mechanical energy. The interplay between the magnetic fields produced by the rotor and the stator facilitates this process. The essential elements of this operational concept are as follows:

In motor mode, the PMSM employs permanent magnets integrated inside the rotor to generate a magnetic field. When AC is applied to the stator windings, it produces a revolving magnetic field.

The interaction of the stator's spinning magnetic field with the rotor's magnetic field generates torque, resulting in the rotation of the rotor and the production of mechanical motion.

The rotor of the PMSM revolves in synchrony with the spinning magnetic field generated by the stator, indicating that the rotor speed corresponds to the frequency of the stator supply. The synchronous behavior is a defining trait of PMSMs.

The correlation between rotor speed (Ω_m) and stator supply frequency (F) is expressed by the equation:

$\Omega_m = \frac{2\pi F}{P}$, where P is the number of pole pairs.

The torque produced by the PMSM is directly proportional to the current in the stator windings and the intensity of the rotor's magnetic field. The torque may be regulated by modifying the current, facilitating exact control of motor performance.

2.6 Modeling of the Five-Phase PMSG

The five-phase PMSG comprises a stator with five-phase windings spatially displaced by $2\pi/5$ and a rotor equipped with permanent magnets. The models utilized by PMSG are predicated on the subsequent presumptions [8, 9]:

- Iron core losses, magnetic saturation, and eddy currents are not considered.
- Unsaturated magnetic circuits (proportionality between flow and current).
- It is assumed that the currents and voltages exhibit a sinusoidal nature.
- The thermal effect on the permanent magnets has been excluded from consideration.
- Consistent gap (absence of notch effect).

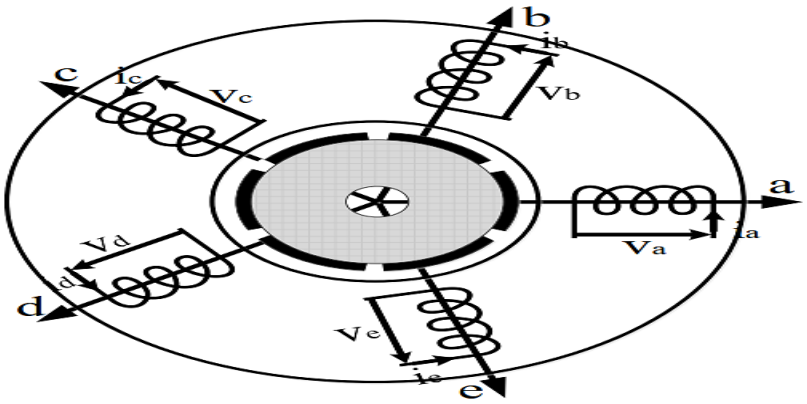

Fig. (2.11): Diagrammatic illustration of a five-phase PMSG

The five-phase PMSG might be formulated through the subsequent voltage and flux linkage equations presented in matrix form:

$$[V_{abcde}] = [R_s][I_{abcde}] + \frac{d[\Psi_{abcde}]}{dt}$$
$$[\Psi_{abcde}] = [L_s][I_{abcde}] + [\Psi_{fabcde}] \quad (2.4)$$

Where:

$$[V_{abcde}] = [V_{as} \quad V_{bs} \quad V_{cs} \quad V_{ds} \quad V_{es}]^t$$

$$[I_{abcde}] = [I_{as} \quad I_{bs} \quad I_{cs} \quad I_{ds} \quad I_{es}]^t$$

$$[\Psi_{abcde}] = [\Psi_{as} \quad \Psi_{bs} \quad \Psi_{cs} \quad \Psi_{ds} \quad \Psi_{es}]^t$$

$$[R_s] = diag[R_s \quad R_s \quad R_s \quad R_s \quad R_s]^t$$

The rotor flux is expressed by the following formula:

$$[\Phi_{fabcde}] = \Phi_f \begin{bmatrix} cos(\theta_m) \\ cos(\theta_m - 2\pi/5) \\ cos(\theta_m - 4\pi/5) \\ cos(\theta_m + 4\pi/5) \\ cos(\theta_m - 2\pi/5) \end{bmatrix} \quad (2.5)$$

The rotor position is denoted by θ_m, while Φ_f represents the fundamental amplitude of the permanent magnet flux linkages.

The stator inductances matrix, which encompasses both stator self and mutual inductances, is presented as follows:

$$[L_s] = \begin{bmatrix} L_{ls} + L_{ms} & L_{ms}\,cos(2\pi/5) & L_{ms}\,cos(4\pi/5) & L_{ms}\,cos(4\pi/5) & L_{ms}\,cos(2\pi/5) \\ L_{ms}\,cos(2\pi/5) & L_{ls} + L_{ms} & L_{ms}\,cos(2\pi/5) & L_{ms}\,cos(4\pi/5) & L_{ms}\,cos(4\pi/5) \\ L_{ms}\,cos(4\pi/5) & L_{ms}\,cos(2\pi/5) & L_{ls} + L_{ms} & L_{ms}\,cos(2\pi/5) & L_{ms}\,cos(4\pi/5) \\ L_{ms}\,cos(4\pi/5) & L_{ms}\,cos(4\pi/5) & L_{ms}\,cos(2\pi/5) & L_{ls} + L_{ms} & L_{ms}\,cos(2\pi/5) \\ L_{ms}\,cos(2\pi/5) & L_{ms}\,cos(4\pi/5) & L_{ms}\,cos(4\pi/5) & L_{ms}\,cos(2\pi/5) & L_{ls} + L_{ms} \end{bmatrix} \quad (2.6)$$

L_{ls} represents the leakage inductance. $L_{ls} + L_{ms}$ demonstrates the self-inductance of a phase, while $L_{ms}\cos(2\pi/5)$ and $L_{ms}\cos(4\pi/5)$ indicates the mutual inductance between phases.

2.6.1 Five-Phase PMSG Model in Stationary Frame

The stator's 5-phase winding is transformed utilizing the subsequent matrix [9, 25]:

$$[C] = \frac{2}{5}\begin{bmatrix} 1 & cos(\delta) & cos(2\delta) & cos(3\delta) & cos(4\delta) \\ 0 & sin(\delta) & sin(2\delta) & sin(3\delta) & sin(4\delta) \\ 1 & cos(2\delta) & cos(4\delta) & cos(6\delta) & cos(8\delta) \\ 0 & sin(2\delta) & sin(4\delta) & sin(6\delta) & sin(8\delta) \\ 1/2 & 1/2 & 1/2 & 1/2 & 1/2 \end{bmatrix} \quad (2.7)$$

Whereas: $\delta = {}^{2\pi}/_{5}$

The five-phase PMSG model in a stationary α-β -x-y frame is provided as follows:

$$\begin{aligned} V_{\alpha s} &= R_s I_{\alpha s} + L_s \frac{dI_{\alpha s}}{dt} - w_m \Psi_f \sin(\theta_g) \\ V_{\beta s} &= R_s I_{\beta s} + L_s \frac{dI_{\beta s}}{dt} + w_m \Psi_f \cos(\theta_g) \\ V_{xs} &= R_s I_{xs} + L_s \frac{dI_{xs}}{dt} \\ V_{ys} &= R_s I_{ys} + L_s \frac{dI_{ys}}{dt} \end{aligned} \tag{2.8}$$

The components of the flux can be formulated in the following manner:

$$\begin{aligned} \Psi_{\alpha s} &= L_s I_{\alpha s} + \Psi_f \cos(\theta_g) \\ \Psi_{\beta s} &= L_s I_{\beta s} + \Psi_f \sin(\theta_g) \\ \Psi_{xs} &= L_s I_{xs} \\ \Psi_{ys} &= L_s I_{ys} \end{aligned} \tag{2.9}$$

The mathematical formula for electromagnetic torque can be expressed in this manner:

$$T_{em} = \frac{5P}{2}\left(\Psi_{\alpha s} I_{\beta s} - \Psi_{\beta s} I_{\alpha s}\right) \tag{2.10}$$

2.6.2 Five-Phase PMSG Model in Synchronous Frame

The time-varying inductances must be removed from the model by applying a coordinate transformation, which simplifies the model. The variables of the five-phase machine are transformed into a reference frame (d-q-x-y) using the coordinate transformation. Therefore, the stator's five-phase winding is transformed using the following matrix [9, 25]:

$$[P] = \frac{2}{5}\begin{bmatrix} \cos(\theta_m) & \cos\left(\theta_m - \frac{2\pi}{5}\right) & \cos\left(\theta_m - \frac{4\pi}{5}\right) & \cos\left(\theta_m + \frac{4\pi}{5}\right) & \cos\left(\theta_m + \frac{2\pi}{5}\right) \\ -\sin(\theta_m) & -\sin\left(\theta_m - \frac{2\pi}{5}\right) & -\sin\left(\theta_m - \frac{4\pi}{5}\right) & -\sin\left(\theta_m + \frac{4\pi}{5}\right) & -\sin\left(\theta_m + \frac{2\pi}{5}\right) \\ 1 & \cos\left(\frac{4\pi}{5}\right) & \cos\left(\frac{8\pi}{5}\right) & \cos\left(\frac{12\pi}{5}\right) & \cos\left(\frac{16\pi}{5}\right) \\ 0 & \sin\left(\frac{4\pi}{5}\right) & \sin\left(\frac{8\pi}{5}\right) & \sin\left(\frac{12\pi}{5}\right) & \sin\left(\frac{16\pi}{5}\right) \\ \frac{1}{2} & \frac{1}{2} & \frac{1}{2} & \frac{1}{2} & \frac{1}{2} \end{bmatrix} \tag{2.11}$$

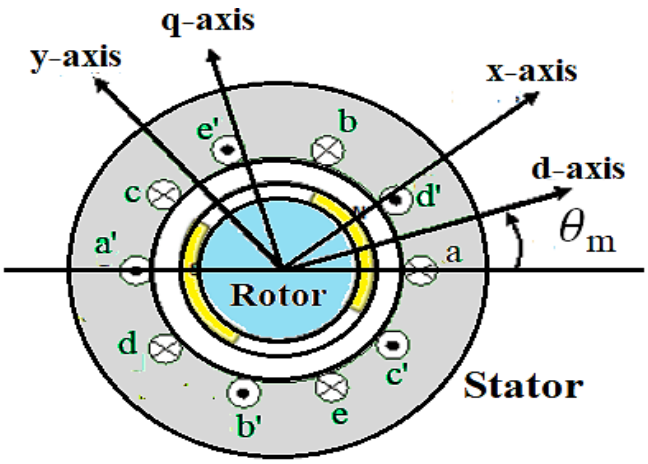

Fig. (2.12): d-q-x-y frame

Through the application of the aforementioned transformation to the equations showing the stator voltages and stator flux linkages, one can articulate the model of the five-phase PMSG within a rotating d-q-x-y frame as follows:

$$\begin{aligned} V_{ds} &= R_s I_{ds} + L_d \frac{dI_{ds}}{dt} - w_m L_q I_{qs} \\ V_{qs} &= R_s I_{qs} + L_q \frac{dI_{qs}}{dt} + w_m L_d I_{ds} + w_m \Psi_f \\ V_{xs} &= R_s I_{xs} + L_s \frac{dI_{xs}}{dt} \\ V_{ys} &= R_s I_{ys} + L_s \frac{dI_{ys}}{dt} \end{aligned} \tag{2.12}$$

The variables V_{ds}, V_{qs}, V_{xs}, and V_{ys} represent the stator voltages along the d-q-x-y axes. The stator currents in the d-q-x-y axes are represented by I_{ds}, I_{qs}, I_{xs}, and I_{ys}, respectively. L_d, L_q, and L_s represent the inductances within the context of the rotating frames. R_s represents the resistance of the stator.

The formula for flux linkages is offered in the following format:

$$\begin{cases} \Psi_{ds} = L_d I_{ds} + \Psi_f \\ \Psi_{qs} = L_q I_{qs} \\ \Psi_{xs} = L_s I_{xs} \\ \Psi_{ys} = L_s I_{ys} \end{cases} \tag{2.13}$$

Where Ψ_{ds}, Ψ_{qs}, Ψ_{xs} , Ψ_{ys} indicate the flux linkage within the d-q-x-y frame.

The relationship between electromagnetic torque, flux, and currents is expressed in the following way:

$$T_{em} = \frac{5}{2} P\left(\Psi_{ds} I_{qs} - \Psi_{qs} I_{ds}\right) \tag{2.14}$$

$$T_{em} = \frac{5}{2} P\left(\Psi_f I_{qs} + \left(L_d - L_q\right) I_{ds} I_{qs}\right) \tag{2.15}$$

Should the machine feature a Surface-mounted type where L_d equals L_q, the expression $\left(\left(L_d - L_q\right) I_{ds} I_{qs}\right)$ will yield a zero value, indicating the absence of reluctance torque.

Therefore, the torque formulation could be stated as:

$$T_{em} = \frac{5}{2} P\left(\Psi_f I_{qs}\right) \tag{2.16}$$

The mechanical equation might be expressed in the following form:

$$T_m - T_{em} = K_f \Omega_m + J \frac{d\Omega_m}{dt} \tag{2.17}$$

Consequently, using the modeling of 5-Ph PMSG (Eqs. (2.12), (2.13), (2.16), and (2.17)), we could formulate the state representation in the following way:

$$\begin{cases} \frac{dI_{ds}}{dt} = \frac{-R_s}{L_d} I_{ds} + \frac{P L_q}{L_d} I_q \Omega_m + \frac{1}{L_d} V_{ds} \\ \frac{dI_{qs}}{dt} = \frac{-R_s}{L_q} I_{qs} - \frac{P L_d}{L_q} I_d \Omega_m - \frac{P \Psi_f}{L_q} \Omega_m + \frac{1}{L_q} V_{qs} \\ \frac{dI_{xs}}{dt} = \frac{-R_s}{L_d} I_{xs} + \frac{1}{L_d} V_{xs} \\ \frac{dI_{ys}}{dt} = \frac{-R_s}{L_q} I_{ys} + \frac{1}{L_q} V_{ys} \\ \frac{d\Omega_m}{dt} = \frac{T_m}{J} - \frac{5}{2J} P\left(L_d - L_q\right) I_{ds} I_{qs} - \frac{5}{2J} P\, \Psi_f I_{qs} - \frac{K_f}{J} \Omega_m \end{cases} \tag{2.18}$$

2.7 Configuration of multi-machine wind system

Multi-machine WE systems are widely recognized for their utilization of the PMSG. Individual generators within the system can be independently controlled, which is one of its primary benefits. This feature has exhibited substantial performance stability and efficacy, particularly in the areas of energy capture optimization and grid reliability.

The independent control allows real-time modifications according to fluctuating wind conditions, guaranteeing that each generator functions efficiently. The control methods enhance fault tolerance and system design flexibility, enabling superior integration with other renewable energy sources and conventional power networks. With the rising need for RE solutions, the significance of PMSGs in multi-machine setups is expected to grow, providing improved efficiency and sustainability in energy production [26, 27].

The Figures depict the configuration of the multi-machine WE system, with Figs. (2.13) and (2.14)

highlighting the systems created by the researchers. This system is designed to boost energy generation by integrating multiple wind turbines, leading to an improved amount of energy produced.

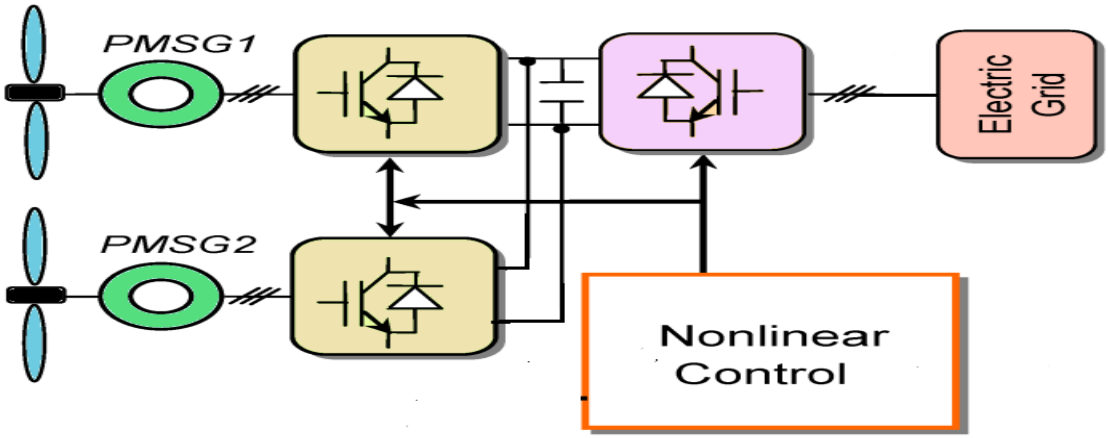

Fig. (2.13): Configuration of a WS utilizing two parallel PMSGs [26]

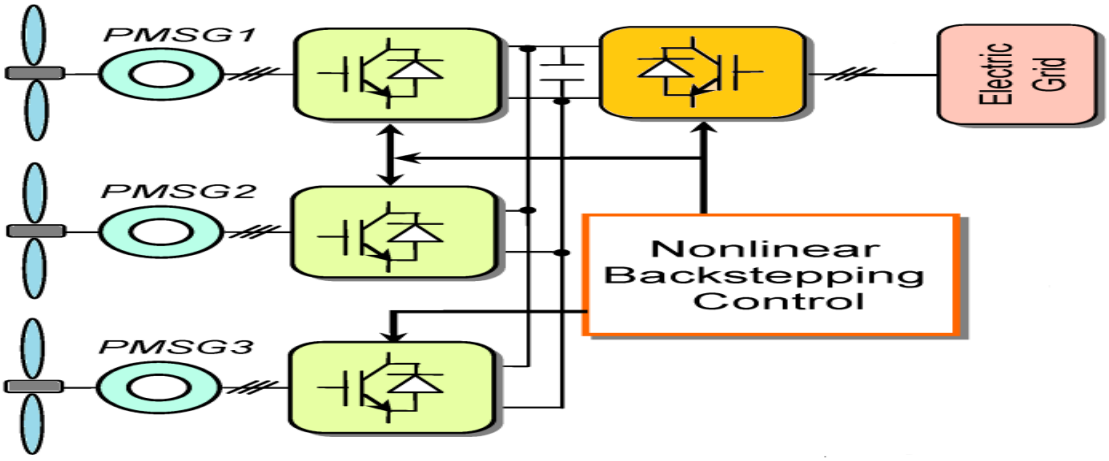

Fig. (2.14): Configuration of a WS utilizing three parallel PMSGs [27]

2.8 The novel configuration of multi-machine wind system

A unique configuration has been devised that uses a new kind of converter to concurrently link two generators, building on the previously described WPGSs. This novel design maintains the simplicity of the overall system and avoids introducing extra variables or complications in the modeling of the generators, similar to systems functioning with a single generator. This method facilitates a simple control design, eliminating superfluous complexities while also improving system performance. The capability to integrate multiple generators without altering the control framework represents a significant improvement in the efficiency and feasibility of WE systems. We could formulate the state representation for two 5-ph PMSGs in the following way:

$$\begin{cases} \frac{dI_{dsj}}{dt} = \frac{-R_{sj}}{L_{dj}} I_{dsj} + \frac{P_j L_{qj}}{L_{dj}} I_{qj} \Omega_{mj} + \frac{1}{L_{dj}} V_{dsj} \\ \frac{dI_{qsj}}{dt} = \frac{-R_{sj}}{L_{qj}} I_{qs} - \frac{P_j L_{dj}}{L_{qj}} I_{dj} \Omega_{mj} - \frac{P_j \Psi_{fj}}{L_{qj}} \Omega_{mj} + \frac{1}{L_{qj}} V_{qsj} \\ \frac{dI_{xsj}}{dt} = \frac{-R_{sj}}{L_{dj}} I_{xsj} + \frac{1}{L_{dj}} V_{xsj} \\ \frac{dI_{ysj}}{dt} = \frac{-R_{sj}}{L_{qj}} I_{ysj} + \frac{1}{L_{qj}} V_{ysj} \\ \frac{d\Omega_{mj}}{dt} = \frac{T_{mj}}{J_j} - \frac{5}{2J_j} P_j \left(L_{dj} - L_{qj}\right) I_{dsj} I_{qsj} - \frac{5}{2J} P_j \, \Psi_{fj} I_{qsj} - \frac{K_{fj}}{J_j} \Omega_{mj} \end{cases} \quad (2.19)$$

In this case, we will work with a multi-machine system setup consisting of two PMSGs, where (j=1, 2) denotes the machine number.

The table and figure below demonstrate how generators are connected using this specific type of transformer. One of the main advantages of this system is its simple connectivity, which does not require specialized laws or complex equations. This simplicity makes it easier to implement and integrate the generators, making the system more user-friendly for practical applications. By removing the need for intricate calculations, operators can concentrate on optimizing performance and reliability, ultimately enhancing the overall efficiency of the WPGS.

Table (2.1): The connection method of the 5-phase machines to the FSR.

	A	**B**	**C**	**D**	**E**
G1	A	B	c	d	E
G2	A	B	c	d	E

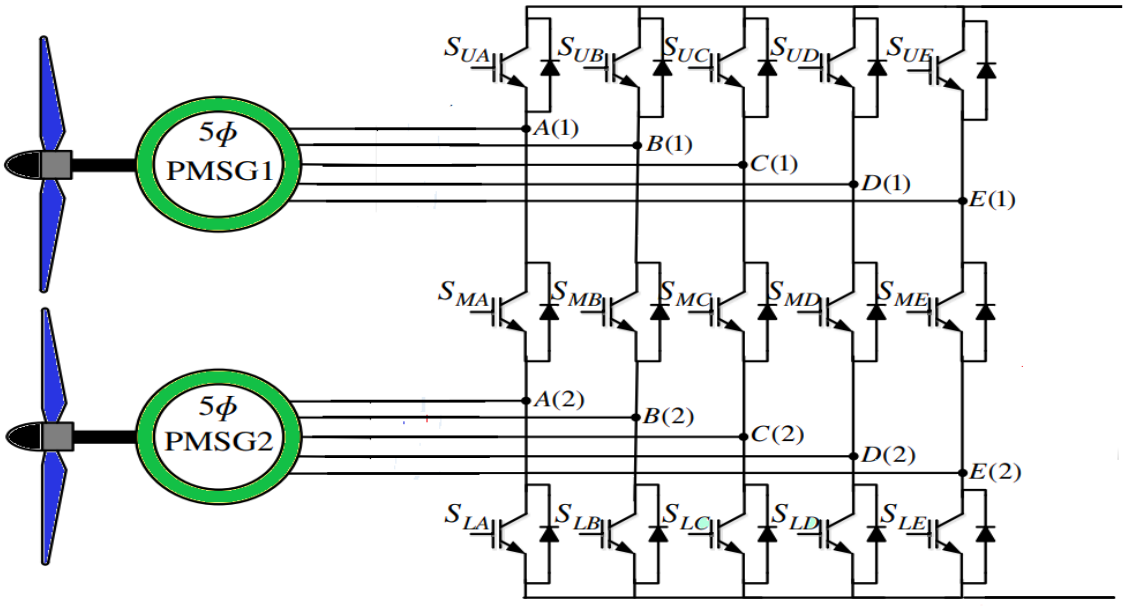

Fig. (2.15): The connection of 2 machines to the FSR.

2.9 Conclusion

This chapter delves into the modeling of PMSGs, emphasizing the theoretical foundations and practical applications crucial for grasping their operation. We explored different varieties of this machine, examining their features, benefits, and drawbacks.

The modeling process was comprehensive, involving the formulation of mathematical equations that characterize the electrical and mechanical dynamics of the motor. We highlighted the significance of precise modeling as it is the primary part of control design.

In summary, a comprehensive grasp of PMSGs modeling is crucial for engineers and practitioners within the field, as it establishes a foundation for progress in machine technology and its diverse applications. Within the diverse applications of these machines, power electronics converters are recognized as crucial components that facilitate their utilization across multiple sectors. The subsequent chapter will offer a detailed description and operational analysis of the converter implemented in this research while also drawing comparisons with other transformers that have been developed for similar applications across industries such as electric vehicles and renewable energy systems.

References

[1] Peng X, Liu Z, Jiang D. A review of multiphase energy conversion in wind power generation. Renewable and Sustainable Energy Reviews. 2021 Sep 1;147:111172.

[2] Barrero F, Duran MJ. Recent advances in the design, modeling, and control of multiphase machines—Part I. IEEE Transactions on Industrial Electronics. 2015 Jun 19;63(1):449-58.

[3] Duran MJ, Barrero F. Recent advances in the design, modeling, and control of multiphase machines—Part II. IEEE Transactions on Industrial Electronics. 2015 Jun 22;63(1):459-68.

[4] Frikha MA, Croonen J, Deepak K, Benômar Y, El Baghdadi M, Hegazy O. Multiphase motors and drive systems for electric vehicle powertrains: State of the art analysis and future trends. Energies. 2023 Jan 9;16(2):768.

[5] Tian B, Mirzaeva G, An QT, Sun L, Semenov D. Fault-tolerant control of a five-phase permanent magnet synchronous motor for industry applications. IEEE Transactions on Industry Applications. 2018 Mar 27;54(4):3943-52.

[6] Onambele C, Elsied M, Mpanda Mabwe A, El Hajjaji A. Multi-phase modular drive system: A case study in electrical aircraft applications. Energies. 2017 Dec 21;11(1):5.

[7] Kalaivani C, Rajambal K. Modeling of an efficient high power wind energy conversion system using self-excited multi-phase machines. Microprocessors and Microsystems. 2020 Apr 1;74:103020.

[8] Djahbar A. "Contribution à la commande multimachines connectés en série", Doctoral dissertation, Ph. D. thesis, USTO-MB University, Oran, Algeria.

[9] TOUNSI K. "Decoupled control of AC machines connected in parallel", Ph. D. thesis, University Hassiba Benbouali, Chlef, Algeria.

[10] Djafar HADIOUCHE "Contribution À L'étude de la Machine Asynchrone Double Étoile: Modélisation, Alimentation et Structure", Ph.D. Thesis, Nancy University, France, 2001.

[11] Fabrice Locment, "Conception et Modélisation d'une Machine Synchrone À 7 Phases À Aimants Permanents et Flux Axial : Commande Vectorielle En Modes Normal et Dégradé", Ph.D. Thesis, lille University, France, 2006.

[12] Martin Jones, "A Novel Concept of Series Connected Multi-Phase, Multi-Motor Drive Systems", Ph.D. Thesis, Liverpool John Moores University, UK, 2005.

[13] Samuli Kallio, "Modeling and Parameter Estimation of Double-Star Permanent Magnet Synchronous Machines ", Ph.D. Thesis, Lappeenranta University, Finland, 2014.

[14] Alberto Tessarolo, "Modeling and Analysis of Multiphase Electric Machines For HighPower Application", Ph.D. Thesis, Trieste University, Italy 2011.

[15] Xue Z, Niu S, Chau AM, Luo Y, Lin H, Li X. Recent Advances in Multi-Phase Electric Drives Model Predictive Control in Renewable Energy Application: A State-of-the-Art Review. World Electric Vehicle Journal. 2023 Feb 6;14(2):44.

[16] Antoine Bruyere "Modelisation et Commande d'un Alterno-Demarreur Heptaphase Pour Application Automobile Micro-Hybride", Ph.D. Thesis, Lille University, France, 2009.

[17] Loganayaki A, Kumar RB. Permanent magnet synchronous motor for electric vehicle applications. In2019 5th international conference on advanced computing & communication systems (ICACCS) 2019 Mar 15 (pp. 1064-1069). IEEE.

[18] Parsa L. Performance improvement of permanent magnet AC motors. Texas A&M University; 2005.

[19] Hao Z, Ma Y, Wang P, Luo G, Chen Y. A Review of Axial-Flux Permanent-Magnet Motors: Topological Structures, Design, Optimization and Control Techniques. Machines. 2022 Dec 7;10(12):1178.

[20] Du G, Li N, Zhou Q, Gao W, Wang L, Pu T. Multi-physics comparison of surface-mounted and interior permanent magnet synchronous motor for high-speed applications. Machines. 2022 Aug 17;10(8):700.

[21] BEKRAOUI F, HARROUZ A, DAHBI A. Etude et dimensionnement d'une éolien à vitesse variable basée sur une machine synchrone à aimant permanemment MSAP (Doctoral dissertation, UNIVERSITE AHMED DRAIA-ADRAR).

[22] S. Afsharnia, « Contrôle vectoriel des machines synchrones à aimants permanents : identification des paramètres et minimisation des ondulations de couple » thèse de Doctorat, Institut National Polytechnique de Lorraine, Mar 2018.

[23] G. P. NYOUMEA,« modèles d'identification et de commande d'un aérogénérateur à machine synchrone à aimants permanents »,Thèse de Doctorat, Univ du Québec, Avril 2018.

[24] A. Annane,« Analyse du comportement du moteur synchrone dans les entraînements électriques à vitesse variable » thèse de Magister, Université d'Annaba, 2010.

[25] Abu-Rub H, Iqbal A, Guzinski J. High performance control of AC drives with Matlab/Simulink. John Wiley & Sons; 2021 Apr 6.

[26] Errami Y, Ouassaid M, Maaroufi M. A performance comparison of a nonlinear and a linear control for grid connected PMSG wind energy conversion system. International Journal of Electrical Power & Energy Systems. 2015 Jun 1;68:180-94.

[27] Errami Y, Obbadi A, Sahnoun S, Ouassaid M, Maaroufi M. Proposal of a backstepping control strategy for dynamic performance improvement of PMSG Wind Farm with common DC bus. In2016 International Renewable and Sustainable Energy Conference (IRSEC) 2016 Nov 14 (pp. 397-404). IEEE.

Chapter 3

Fifteen-Switch Rectifier

3.1 Introduction

Power converters are regarded as vital elements in various electrical systems, fulfilling important roles in energy regulation and conversion. Different kinds of converters are employed in a range of applications, particularly in electric vehicles and the renewable energy sector [1]. Multi-machine systems, whether arranged in series or parallel, prominently utilize these transformers to enhance performance and efficiency.

The nine-switch (NSI) and fifteen-switch inverters (FSI) are among the most commonly utilized transformers in this context. These devices have shown remarkable abilities in the autonomous and efficient management of multiphase motors, improving operational reliability and accuracy across a range of applications [2-5].

Considering the benefits and performance traits of these inverters, a similar approach has been made to be used as rectifiers in systems that convert wind energy. This method lets two generators be connected in parallel at the same time, but each unit can be controlled separately. This new idea not only makes getting energy from the wind more efficient, but it also helps make the system more stable and quick to respond. Being able to handle multiple generators separately also makes it easier to connect them to the power grid. This makes sure that changes in wind energy production can be managed and optimized for grid needs. This flexibility is very important because the need for green energy sources keeps growing. This shows how important improved power converter technologies are in today's energy systems [6, 7].

This chapter demonstrates the operating concepts and design of the fifteen-switch rectifier. A computer simulation is then performed to verify the efficacy of this architecture.

3.2 Structure of fifteen-switch rectifier

Rectifiers are the predominant AC-DC power converters used in power conversion systems. The renowned two-level rectifier is applicable to a broad spectrum of applications, including generating systems and industrial motors. In the context of distributed generators, numerous rectifiers are required to regulate individual AC generators. While using a distinct rectifier for each generation ensures dependable functionality, it also escalates system complexity and size. In this context, a nine-switch rectifier (3-phase system) and a fifteen-switch rectifier (FSR) (5-phase system), as seen in Fig. (3.2), have been suggested to regulate two AC generators while using fewer semiconductors. Conceptually, FSR has emerged from the amalgamation of two rectifiers, with 10 independent input terminals (5-phase). This novel topology is attracting interest because to its benefits over conventional parallel

rectifier systems (see Fig. (3.1)) regarding dimensions, cost, and mass. FSR-based systems have been used in a broad spectrum of energy conversion systems [6, 7].

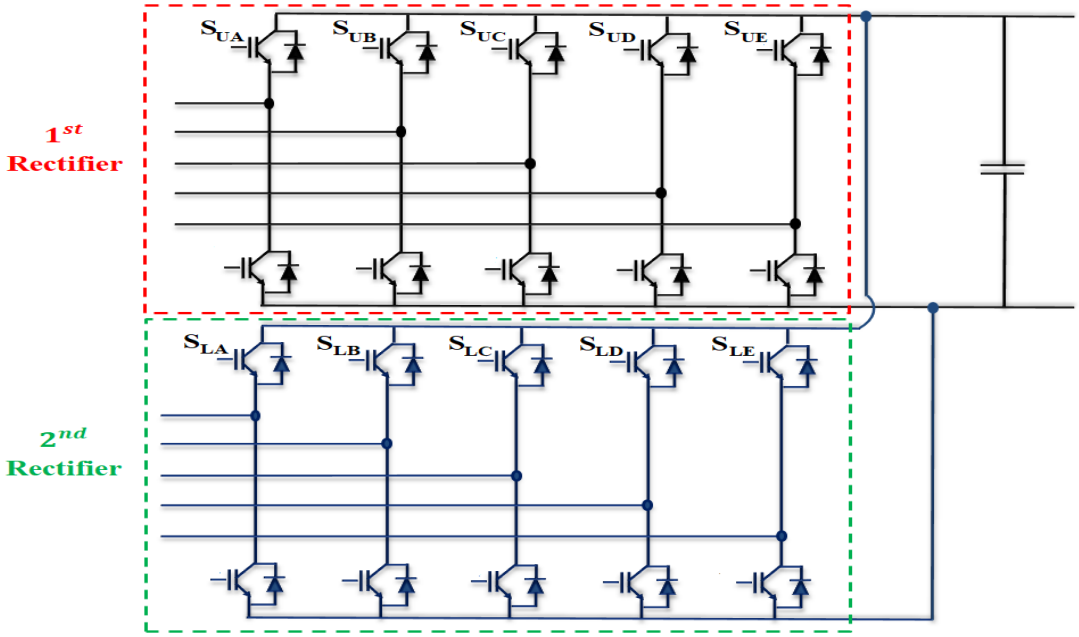

Fig. (3.1): Traditional multiphase rectifier based multi-machine system

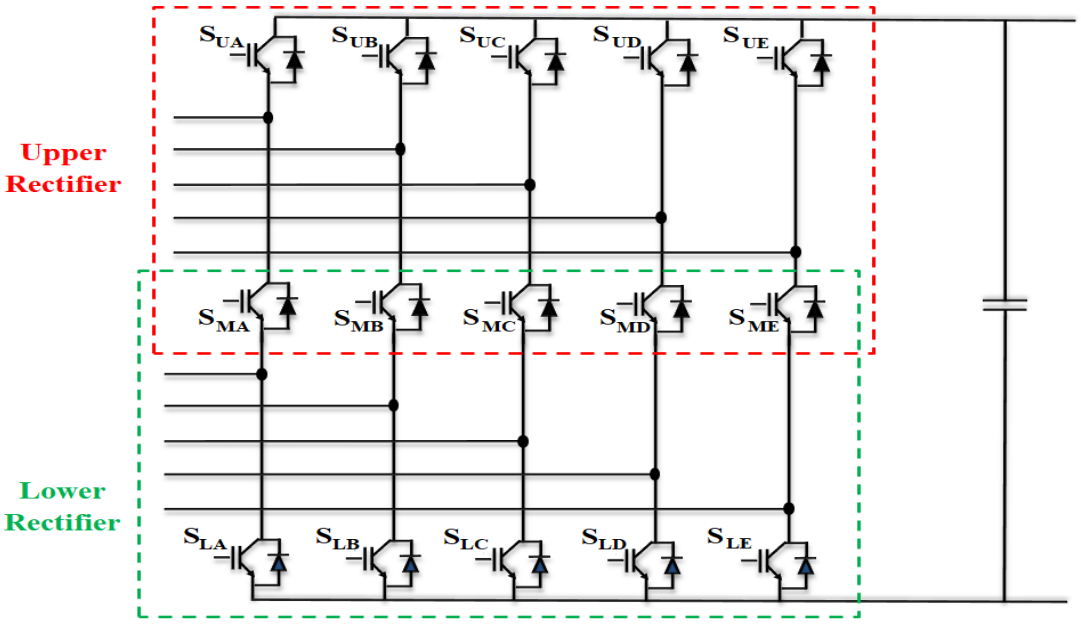

Fig. (3.2): The architecture of a fifteen-switch rectifier (FSR) based multi-machine system

3.3 Operating Principles of the fifteen-Switch Rectifier

The fifteen-switch rectifier architecture integrates two five-phase rectifiers with five common switches, enhancing its efficiency and functionality. The upper section is designated as rectifier1, while the lower section is referred to as rectfier2.The upper rectifier comprises switches labeled UA, UB, UC,

UD, UE, MA, MB, MC, MD and ME, whereas lower rectifier is composed of switches designated MA, MB, MC, MD, ME, LA, LB, LC, LD and LE. The switches MA, MB, MC, MD and ME are shared between the upper and lower rectifiers, facilitating coordinated operation and reducing component count.

The following formula defines the switch function of the S_{ij} switch in Fig. (3.3):

$$S_{ij} = \begin{cases} 1, S_{ij}\ closed \\ 0, S_{ij} open \end{cases} ; i=U, M, L; j=A,B,C,D,E \quad (3.1)$$

With:

$$S_{Uj} + S_{Mj} + S_{Lj} = 2 \quad (3.2)$$

3.4 Implementation of the PWM control technique

Figs. (3.3) and (3.4) depict the carrier-based pulse width modulation (PWM) control technique for the fifteen-switch rectifier. In this design, the upper and lower reference signals align with the upper and lower outputs, respectively. The gate signal for the upper switch of each leg is generated by comparing the carrier signal with the upper reference signal for the respective phase (designated as reference 1). The gate signal for the lower switch is similarly obtained by comparing the carrier signal with the lower reference signal for that phase (designated as reference 2).

Furthermore, the gate signal for the middle switch is produced by applying the logical XOR operation to the gate signals of the upper and lower switches. This distinctive method guarantees that a minimum of two switches are engaged in each leg simultaneously, thereby improving the inverter's performance and dependability.

Table (3.1): The switching state of the FSR and the voltage of its poles

	S_{Uj}	S_{Mj}	S_{Uj}	V_u	V_l
1	1	0	1	V_{dc}	0
0	0	1	1	0	0
-1	1	1	0	V_{dc}	V_{dc}

This PWM approach regulates the output voltage by varying the duty cycles of the switches, enabling exact waveform control. By guaranteeing that two switches are continuously activated, the system maintains a balanced load and mitigates the possibility of overloading any one switch.

Moreover, the carrier-based PWM control facilitates fast adaptation to fluctuations in load circumstances, rendering it appropriate for dynamic applications like renewable energy systems.

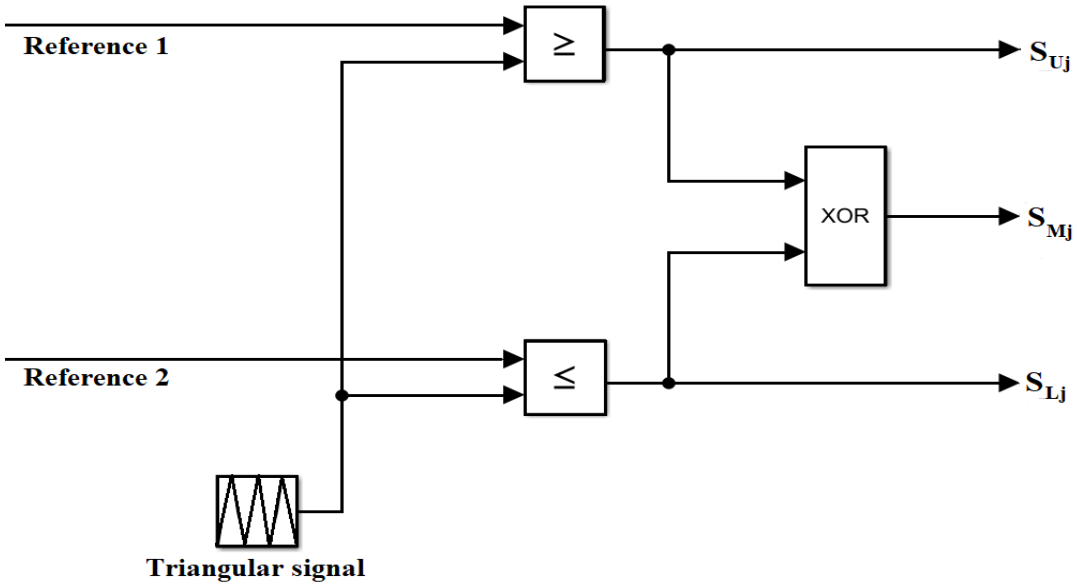

Fig. (3.3): Scheme for generating gate signals

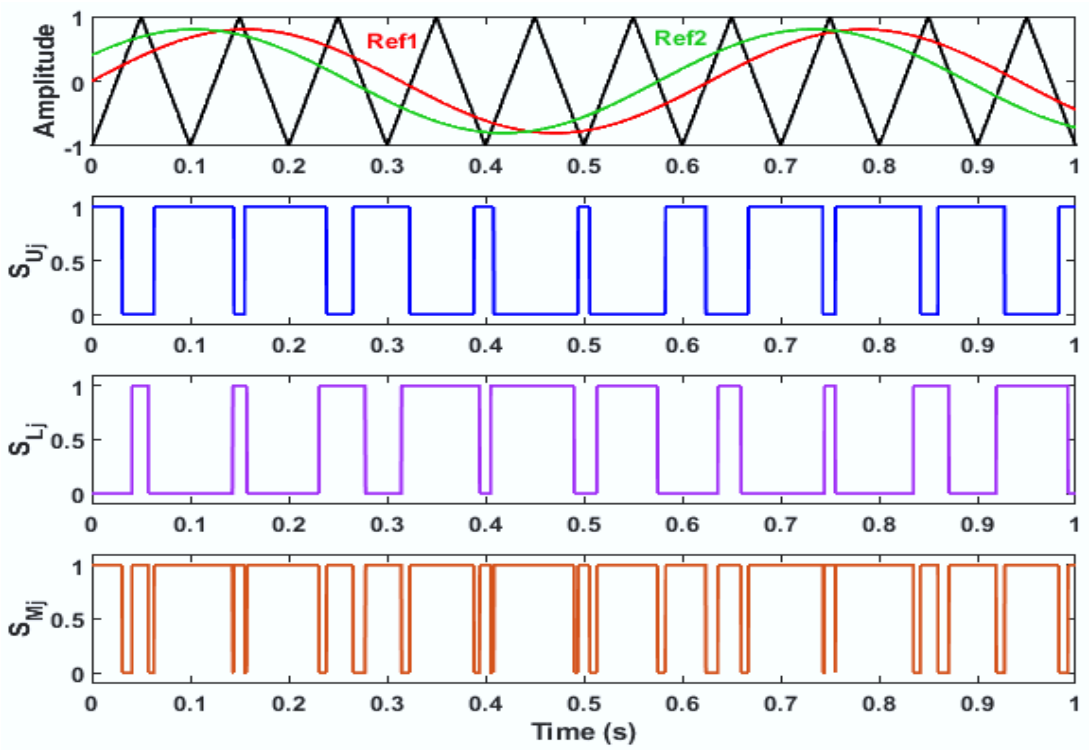

Fig. (3.4): Control signals for a FSR

3.5 The five-phase PWM rectifier's operational principle

The configuration of the power circuit for the two-level five-phase rectifier is depicted in Fig. (3.5).

This converter consists of five legs, each featuring insulated gate bipolar transistors (IGBTs) connected in parallel with anti-parallel diodes. The rectifier operates using a five-phase alternating current (AC) source, which can be produced by an appropriate generator.

This setup facilitates the effective transformation of the five-phase AC input into a matching DC output, rendering it especially beneficial for applications that demand high power levels and enhanced performance. The combination of IGBTs with anti-parallel diodes improves switching efficiency and minimizes conduction losses, leading to enhanced thermal management and increased overall system reliability.

Additionally, the five-phase rectifier topology presents multiple benefits compared to conventional three-phase systems, including diminished ripple in the output voltage. This presents an appealing option for a range of applications, particularly in renewable energy systems, where reliable and steady DC power is crucial for optimal performance.

The phase voltage for the five-phase source could be expressed as [8]:

$$
\begin{aligned}
V_a &= V_{max}\, sin(\omega t) \\
V_b &= V_{max}\, sin\left(\omega t - \tfrac{2\pi}{5}\right) \\
V_c &= V_{max}\, sin\left(\omega t - \tfrac{4\pi}{5}\right) \\
V_d &= V_{max}\, sin\left(\omega t - \tfrac{6\pi}{5}\right) \\
V_e &= V_{max}\, sin\left(\omega t - \tfrac{8\pi}{5}\right)
\end{aligned}
\tag{3.3}
$$

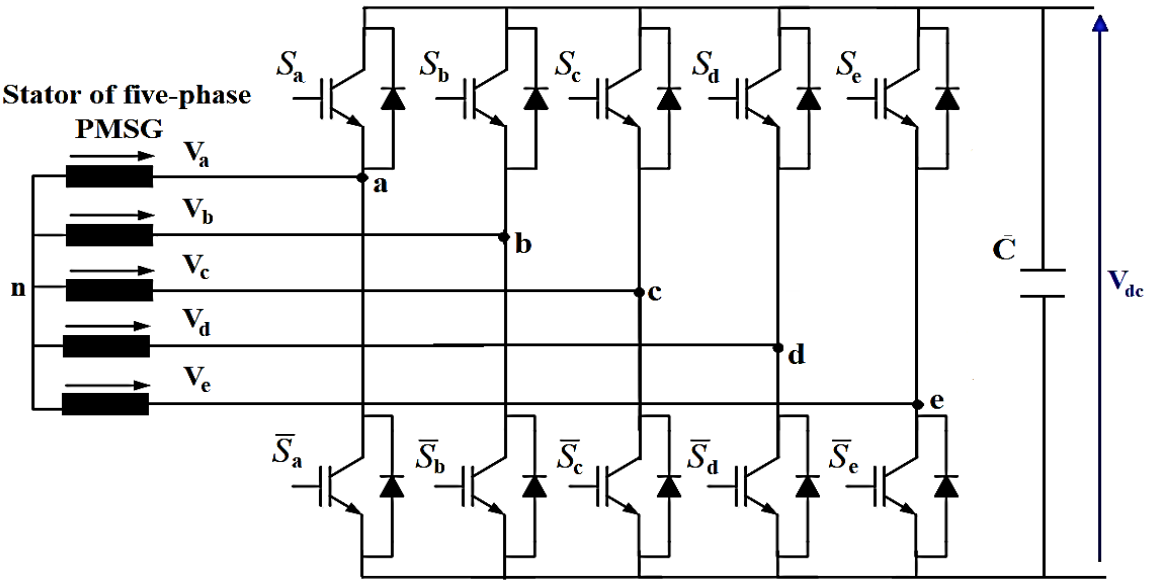

Fig. (3.5): Conventional 5-phase rectifier

The formulas of line-to-line voltage are provided as follows:

$$\begin{aligned} V_{ab} &= V_a - V_b \\ V_{bc} &= V_b - V_c \\ V_{cd} &= V_c - V_d \\ V_{de} &= V_d - V_e \\ V_{ea} &= V_e - V_a \end{aligned} \tag{3.4}$$

When the system is in equilibrium:

$$V_a + V_b + V_c + V_d + V_e = 0 \tag{3.5}$$

The subsequent equation expresses the average voltage across the terminals of this converter:

$$V_m = 1.87\, V_{max}\, cos(\gamma) \tag{3.6}$$

Where:

V_{max}: The maximum value of the line voltage.

γ: The firing angle.

The 5-phase rectifier demonstrates a total of thirty-two operational states, including thirty non-zero states and two zero states. The voltage vector corresponding to these states can be depicted in the α-β and x-y subspaces, as shown in Fig. (3.6) [9, 10]:

$$\begin{aligned} V_{\alpha\beta} &= V_\alpha + jV_\beta = \frac{2}{5}\left(V_a + V_b e^{j\gamma} + V_c e^{j2\gamma} + V_d e^{j3\gamma} + V_e e^{j4\gamma}\right) \\ V_{xy} &= V_x + jV_y = \frac{2}{5}\left(V_a + V_b e^{j2\gamma} + V_c e^{j4\gamma} + V_d e^{j6\gamma} + V_e e^{j8\gamma}\right) \end{aligned} \tag{3.7}$$

Where: $\gamma = \frac{2\pi}{5}$

The Clark-Concordia matrix could additionally be used for conversion to the same domain, as seen below: [11]:

$$\begin{bmatrix} V_\alpha \\ V_\beta \\ V_x \\ V_y \\ V_0 \end{bmatrix} = \sqrt{\frac{2}{5}} \begin{bmatrix} 1 & cos\left(\frac{2\pi}{5}\right) & cos\left(\frac{4\pi}{5}\right) & cos\left(\frac{6\pi}{5}\right) & cos\left(\frac{8\pi}{5}\right) \\ 0 & sin\left(\frac{2\pi}{5}\right) & sin\left(\frac{4\pi}{5}\right) & sin\left(\frac{6\pi}{5}\right) & sin\left(\frac{8\pi}{5}\right) \\ 1 & cos\left(\frac{4\pi}{5}\right) & cos\left(\frac{8\pi}{5}\right) & cos\left(\frac{12\pi}{5}\right) & cos\left(\frac{16\pi}{5}\right) \\ 0 & sin\left(\frac{4\pi}{5}\right) & sin\left(\frac{8\pi}{5}\right) & sin\left(\frac{12\pi}{5}\right) & sin\left(\frac{16\pi}{5}\right) \\ \frac{1}{\sqrt{2}} & \frac{1}{\sqrt{2}} & \frac{1}{\sqrt{2}} & \frac{1}{\sqrt{2}} & \frac{1}{\sqrt{2}} \end{bmatrix} \begin{bmatrix} V_a \\ V_b \\ V_c \\ V_d \\ V_e \end{bmatrix} \tag{3.8}$$

In these two planes, the 32 space vectors are strategically positioned at thirty-two different locations. Considering their magnitude, the space vectors can be thoughtfully classified into several different

categories: zero, small, medium, and large space vectors. It is evident from Fig (III.6) that medium length space vectors in the α-β plane correspond to medium length vectors in the x-y plane, while large vectors in the α-β plane are represented as small vectors in the x-y plane, and the reverse holds true as well [12, 13].

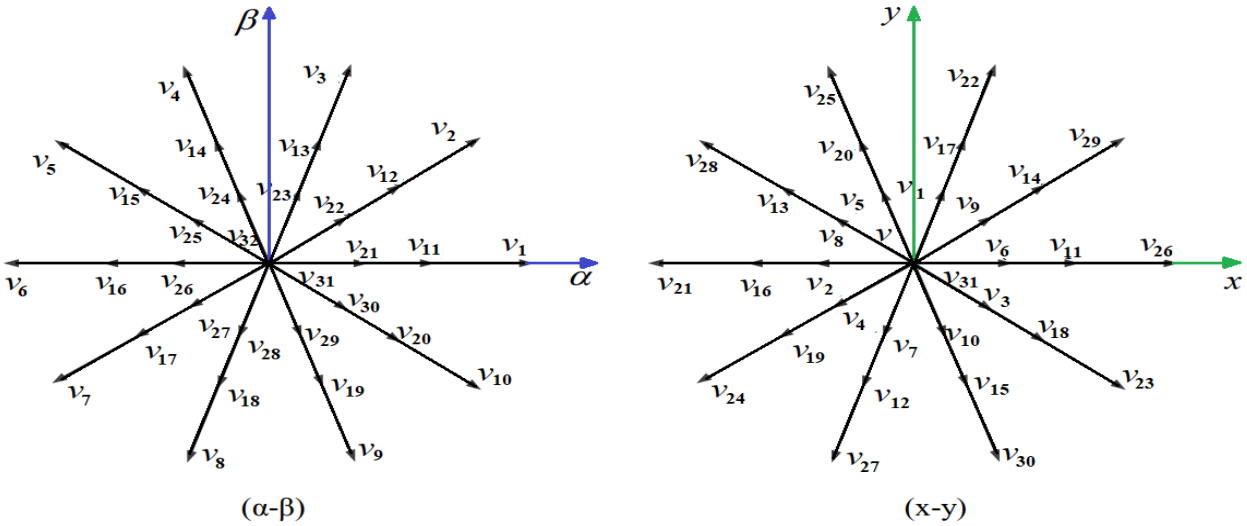

Fig. (3.6): The 5-phase rectifier space vectors in two two-dimensional subspaces.

This table displays all the operational states of the rectifier seen in the preceding illustration.

Table (3.2): The rectifier's switching states

K	S_a	S_b	S_c	S_d	S_e
1	1	1	0	0	1
2	1	1	0	0	0
3	1	1	1	0	0
4	0	1	1	0	0
5	0	1	1	1	0
6	0	0	1	1	0
7	0	0	1	1	1
8	0	0	0	1	1
9	1	0	0	0	1
10	1	0	0	0	1
11	1	0	0	0	0
12	1	1	1	0	1
13	0	1	0	0	0
14	1	1	1	1	0
15	0	0	1	0	0
16	0	1	1	1	1
17	0	0	0	1	0
18	1	0	1	1	1
19	0	0	0	0	1
20	1	1	0	1	1
21	0	1	0	0	1

22	1	1	0	1	0
23	1	0	1	0	0
24	0	1	1	0	1
25	0	1	0	1	0
26	1	0	1	1	0
27	0	0	1	0	1
28	0	1	0	1	1
29	1	0	0	1	0
30	1	0	1	0	1
31	0	0	0	0	0
32	1	1	1	1	1

3.6 The FSR's operational principle

The switching states of transformers vary based on their design, and the total number of potential switching states is often calculated using the formula 2^n, where n is the number of phases. Here, 2 denotes the quantity of switches in each leg. The previously mentioned transformer has 32 switching states, determined by the calculation $2^n = 32$.

Utilizing this technique for the FSR, the possible number of switching configurations is $3^5 = 243$. Nonetheless, as seen in Table (3.3), this table does not include all potential switching state possibilities, namely the states denoted by $\{1\}$, $\{0\}$, and $\{-1\}$ shown in Table (3.1). Significantly, the states $\{0\}$ and $\{-1\}$ cannot occur inside the same vector, since this would lead to a simultaneous connection of the load to both power sources. This requirement is essential for preserving the autonomy of each source, especially for their frequencies. Thus, vectors including both states $\{0\}$ and $\{-1\}$ are eschewed to maintain operational integrity and avert adverse interactions between the power sources.

The switching states are detailed in Table (3.3) Vectors 1 through 30 represent the upper active vectors, where the upper input is activated while the lower input remains at zero. Conversely, for vectors 31 through 60, the situation is reversed, with the lower input activated and the upper input at zero. Additionally, for vectors 61 to 63, both inputs are in a zero state.

Table (3.3): Switching state of FSR

Upper stage						Lower stage					
K	**Leg A**	**Leg B**	**Leg C**	**Leg D**	**Leg E**	**K**	**Leg A**	**Leg B**	**Leg C**	**Leg D**	**Leg E**
1	1	1	0	0	1	**31**	-1	-1	1	1	-1
2	1	1	0	0	0	**32**	-1	-1	1	1	1
3	1	1	1	0	0	**33**	-1	-1	-1	1	1
4	0	1	1	0	0	**34**	1	-1	-1	1	1
5	0	1	1	1	0	**35**	1	-1	-1	-1	1
6	0	0	1	1	0	**36**	1	1	-1	-1	-1
7	0	0	1	1	1	**37**	1	1	-1	-1	-1
8	0	0	0	1	1	**38**	1	1	1	-1	-1
9	1	0	0	0	1	**39**	-1	1	1	1	-1
10	1	0	0	0	1	**40**	-1	1	1	1	-1
11	1	0	0	0	0	**41**	-1	1	1	1	1
12	1	1	1	0	1	**42**	-1	-1	-1	1	-1
13	0	1	0	0	0	**43**	1	-1	1	1	1
14	1	1	1	1	0	**44**	-1	-1	-1	-1	1
15	0	0	1	0	0	**45**	1	1	-1	1	1
16	0	1	1	1	1	**46**	1	-1	-1	-1	-1
17	0	0	0	1	0	**47**	1	1	1	-1	1
18	1	0	1	1	1	**48**	-1	1	-1	-1	-1
19	0	0	0	0	1	**49**	1	1	1	1	-1
20	1	1	0	1	1	**50**	-1	-1	1	-1	-1
21	0	1	0	0	1	**51**	1	-1	1	1	-1
22	1	1	0	1	0	**52**	-1	-1	1	-1	1
23	1	0	1	0	0	**53**	-1	1	-1	1	1
24	0	1	1	0	1	**54**	1	-1	-1	1	-1
25	0	1	0	1	0	**55**	1	-1	1	-1	1
26	1	0	1	1	0	**56**	-1	1	-1	-1	1
27	0	0	1	0	1	**57**	1	1	-1	1	-1
28	0	1	0	1	1	**58**	1	-1	1	-1	-1
29	1	0	0	1	0	**59**	-1	1	1	-1	1
30	1	0	1	0	1	**60**	-1	1	-1	1	-1
Zero											
61	1	1	1	1	1						
62	0	0	0	0	0						
63	-1	-1	-1	-1	-1						

The subsequent figure illustrates the operational strategy of FSR.

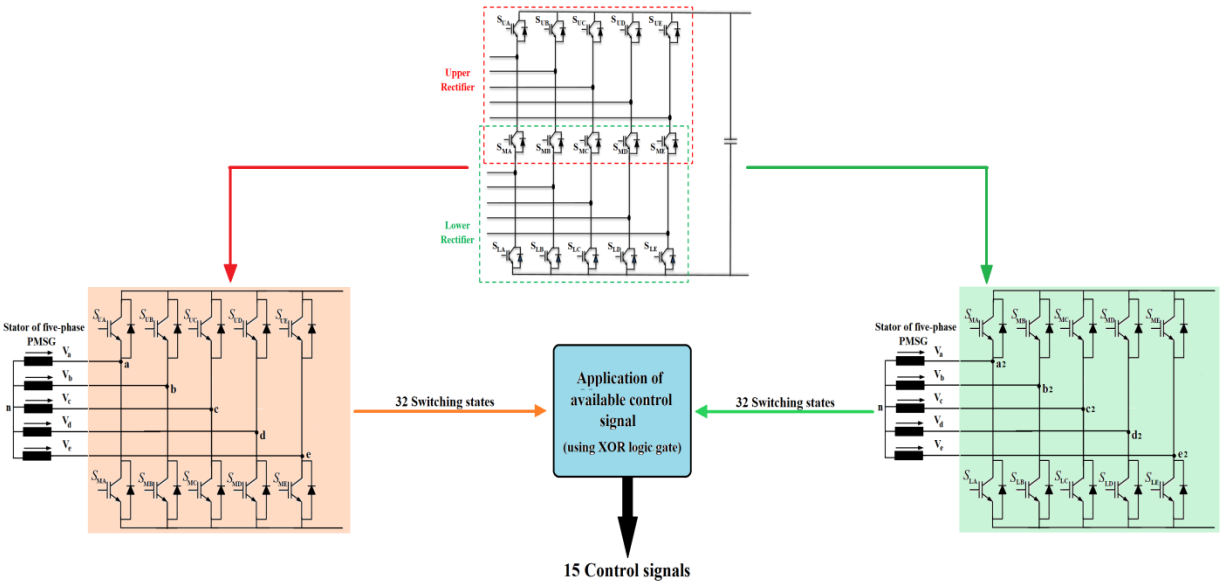

Fig. (3.7): FSR's Operational Strategy

Fig. (3.8) elucidates the operational principles of the FSR, employing vectors selected from Table (3.3). As highlighted in the previous discussion, it is clear that the two power sources are not connected simultaneously; at any given moment, either the first rectifier (upper power source) or the second rectifier (lower power source) is activated. This design ensures that the rectifier operates efficiently, maintaining the independence of each power source and preventing potential issues related to simultaneous connections, such as short circuits or interference between the sources. Such operational characteristics are crucial for optimizing performance in multi-phase systems.

	Lower Stage Deactivate	Lower Stage Active	Lower Stage Deactivate	Lower Stage Active	Lower Stage Deactivate	Lower Stage Active	.....
Lower Rectifier Vector	V_{32}	V_7	V_{32}	V_{15}	V_{32}	V_6	
Upper Rectifier Vector	V_2	V_{32}	V_8	V_{32}	V_{25}	V_{32}	.....
Corresponding FSR Signals	1 1 0 0 0 0 0 1 1 1 1 1 1 1 1	1 1 1 1 1 1 1 0 0 0 0 0 1 1 1	0 0 0 1 1 1 1 1 0 0 1 1 1 1 1	1 1 1 1 1 1 1 0 1 1 0 0 1 0 0	0 1 0 1 0 1 0 1 0 1 1 1 1 1 1	1 1 1 1 1 1 1 0 0 1 0 0 1 1 0	.....
	Upper Stage Active	Upper Stage Deactivate	Upper Stage Active	Upper Stage Deactivate	Upper Stage Active	Upper Stage Deactivate	

Fig. (3.8): Control inputs for the upper and lower stages are applied sequentially to the FSR

3.7 Dynamic Analysis of a fifteen-switch rectifier

A simulation of the FSR was conducted in MATLAB Simulink to validate the proposed configuration. Fig. (3.9) below illustrates the setup of the FSR connected to a resistive load, enabling

the assessment of the DC-link voltage output waveform. This simulation serves to confirm the operational effectiveness of the rectifier design and to analyze its performance characteristics under specified loading conditions. By examining the resulting waveform, insights can be gained into the rectifier's efficiency and stability in converting AC to DC.

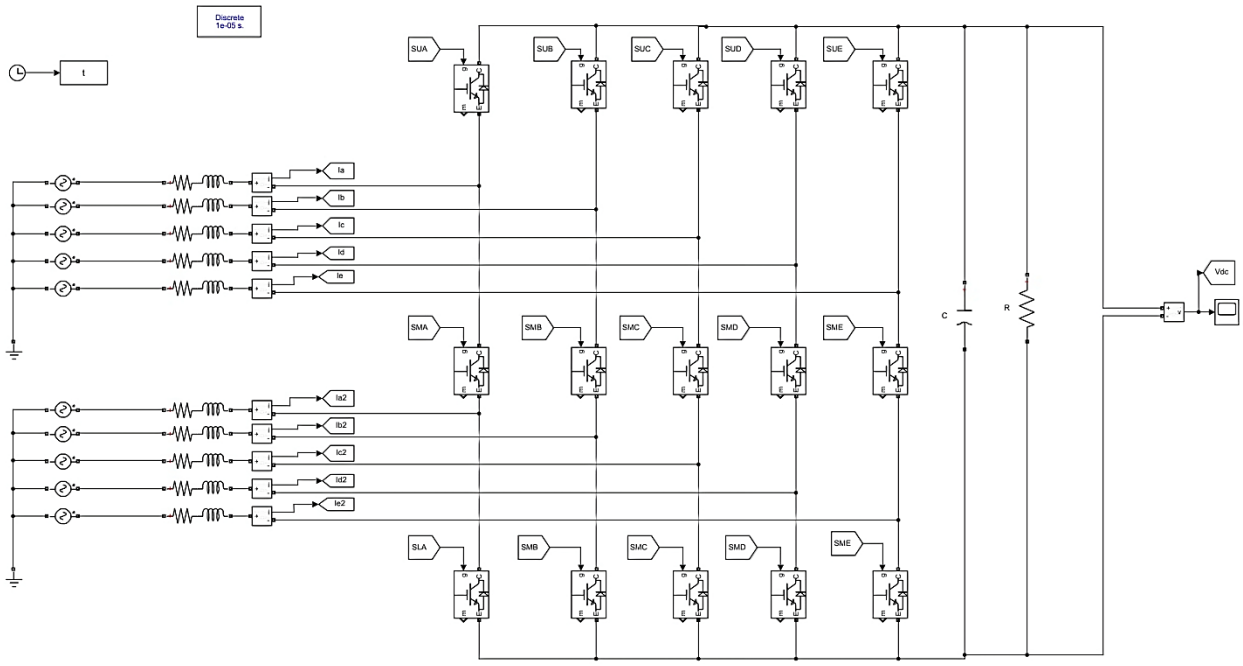

Fig. (3.9): The FSR's Simulink diagram

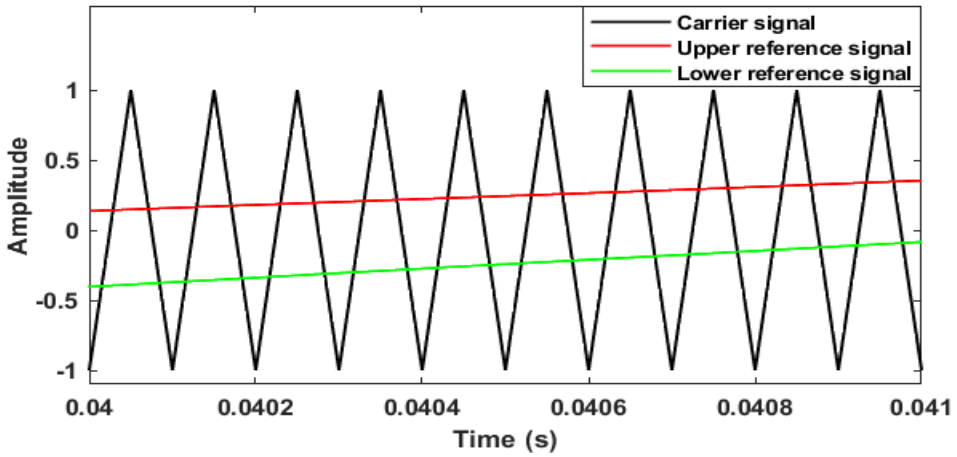

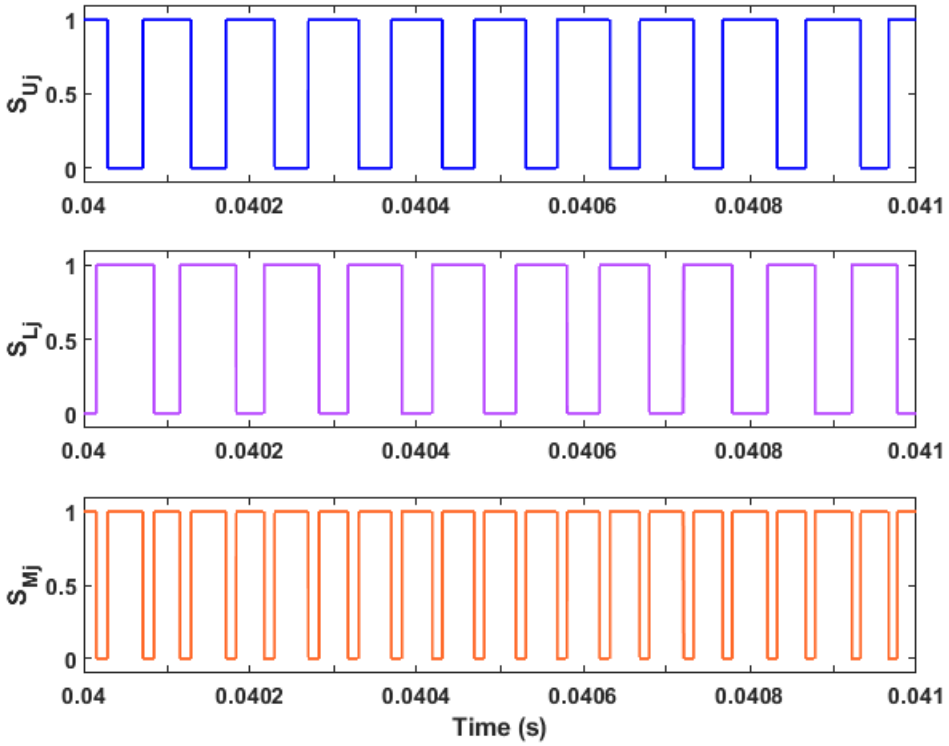

Fig. (3.10): The carrier and references control signals.

Fig. (3.10) demonstrates the sinusoidal PWM strategy applied to the 15-switch rectifier. Notably, the upper and lower pulses do not reach zero simultaneously, which is a critical feature of this configuration. This characteristic ensures the continuity of the three identified switching states, thereby enhancing the rectifier's operational stability and reducing the likelihood of undesirable outputs such as voltage dips or interruptions.

The fig. (3.11) displays the performance of the DC-link voltage in a 15-switch rectifier, demonstrating the actual voltage values mirroring the reference voltage quite well. This precise alignment implies good control and management of the DC-link voltage.

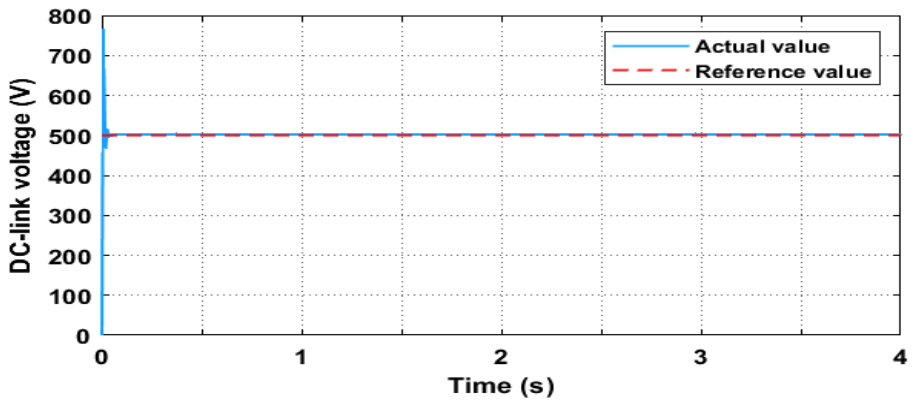

Fig. (3.11): The dc-bus voltages

3.8 Comparative analysis of the suggested and conventional converter

In the discussion of converters, it is essential to examine the key strengths and weaknesses associated with each type. This analysis serves to emphasize both the most significant advantages and the potential drawbacks, thereby aiding in the selection process based on the specific application requirements. Table (3.4) presents a detailed overview of the advantages and disadvantages of these converters, allowing for informed decision-making tailored to intended uses. Understanding these characteristics is crucial for optimizing performance and ensuring compatibility with desired operational conditions [7].

Table (3.4): Comparison between the suggested rectifier and the conventional one [7].

Advantages	
Two 5-phase rectifier	**15-switch rectifier**
• Smaller currents for equivalent power levels • Could provide improved performance under fault conditions. • Simple design • The design of control techniques, such as PWM or SVM, is uncomplicated.	• Decreased number of switching devices • Minimal cost, size, and weight • Reduced switching losses associated with this converter. • Uncomplicated design • keeping control simple • The experimental implementation necessitates only the use of a single digital signal processor (DSP).
Disadvantages	
• The experimental implementation necessitates only the use of 2 DSPs. • It requires 2 SVM blocks. • Issue of zero-sequence circulating currents.	• The output voltage amplitude is smaller in comparison to 2 separate rectifiers. • Switching devices with elevated current ratings.

3.9 Conclusion

This chapter performed an extensive examination and analysis of both a five-phase rectifier and a fifteen-switch rectifier, with a specific focus on the latter. All operational states of the fifteen-switch rectifier were thoroughly explained and illustrated, providing a clear understanding of its functionality. Additionally, the fundamental principles of the PWM strategy employed in this rectifier were discussed. An independent simulation was carried out to validate the performance of the newly proposed topology of the fifteen-switch rectifier and its independence in input control. The forthcoming chapter will also address the application of this converter within WPGSs, detailing various control strategies that can enhance its efficiency. The chapter aims to comprehensively understand how to maximize the converter's effectiveness in harnessing WE.

References

[1] Blaabjerg F, Liserre M, Ma K. Power electronics converters for wind turbine systems. IEEE Transactions on industry applications. 2011 Dec 23;48(2):708-19.

[2] Kominami T, Fujimoto Y. A novel nine-switch inverter for independent control of two three-phase loads. In2007 IEEE Industry applications annual meeting 2007 Sep 23 (pp. 2346-2350). IEEE.

[3] Dabour SM, Rashad EM, Abdel-Khalik A, Ahmed S, Massoud A. A new fifteen-switch inverter topology for two five-phase motors drive. In2016 Eighteenth International Middle East Power Systems Conference (MEPCON) 2016 Dec 27 (pp. 729-734). IEEE.

[4] Zhang J, Pang Y, Wang K, Xu D, Pan L. Modulation method for nine-switch converter based on equivalent mechanism between nine-switch converter and dual six-switch converters. IEEE Transactions on Industrial Electronics. 2020 Mar 16;68(4):2845-55.

[5] Rajambal K, Rajarajan B, Khan AU. Design analysis and implementation of nine switch inverter for the independent control of two AC motors. InIndia International Conference on Power Electronics 2010 (IICPE2010) 2011 Jan 28 (pp. 1-6). IEEE.

[6] Reusser CA, Kouro S, Cardenas R. Dual three-phase PMSG based wind energy conversion system using 9-switch dual converter. In2015 IEEE Energy Conversion Congress and Exposition (ECCE) 2015 Sep 20 (pp. 1021-1022). IEEE.

[7] Kamel T, Abdelkader D, Said B, Iqbal A. Sliding mode control of grid-connected wind energy system driven by 2 five-phase permanent magnet synchronous generators controlled by a new fifteen-switch converter. International Transactions on Electrical Energy Systems. 2020 Sep;30(9):e12480.

[8] Masoud MI. Fully controlled 5-phase, 10-pulse, line commutated rectifier. Alexandria Engineering Journal. 2015 Dec 1;54(4):1091-104.

[9] Dujic D, Grandi G, Jones M, Levi E. A space vector PWM scheme for multifrequency output voltage generation with multiphase voltage-source inverters. IEEE Transactions on Industrial Electronics. 2008 Apr 30;55(5):1943-55.

[10] Iqbal A, Levi E. Space vector modulation schemes for a five-phase voltage source inverter. In2005 European Conference on Power Electronics and Applications 2005 Sep 11 (pp. 12-pp). IEEE.

[11] Willems JL. Generalized Clarke components for polyphase networks. IEEE Transactions on Education. 1969 Mar;12(1):69-71.

[12] Rangari SC, Suryawanshi HM, Shah B. Implimentaion of large and medium vectors for SVPWM technique in five phase voltage source inverter. In2017 International Conference on Intelligent Computing and Control Systems (ICICCS) 2017 Jun 15 (pp. 751-756). IEEE.

[13] TOUNSI K. *Decoupled control of AC machines connected in parallel* (Doctoral dissertation, Abdelkader DJAHBAR/Said BARKAT).

Chapter 4

Fuzzy Backstepping Control of Multi-Machine Wind Power Generation System

4.1 Introduction

In nonlinear systems and those with changeable parameters, conventional control procedures often fail to satisfy essential performance criteria, including accuracy, robustness, response time, and other dynamic features intrinsic to various systems. Nonlinear control techniques are recognized as some of the most effective approaches in control theory; however, each methodology possesses unique strengths and weaknesses that differentiate it from others [1, 2].

Among these approaches, the Backstepping control (BC) approach is distinguished by its exceptional tracking precision, quick reaction time, and stability, mostly attributable to its reliance on the Lyapunov stability theory [3]. This method systematically designs the control law by decomposing the overall control problem into simpler sub-problems, which enhances its effectiveness. Despite its advantages, the BC approach has a significant limitation: its reliance on precise knowledge of system parameters. Variability or uncertainty in these parameters can adversely affect the controller's performance, potentially leading to instability or suboptimal operation [4].

To address this constraint, the Fuzzy Backstepping control (FBC) strategy was developed, which incorporates fuzzy logic (FL) to dynamically adjust the gains of the BC method. This adaptation enhances the control system's capability to accommodate disturbances and variations in system parameters while preserving tracking accuracy and response speed. By integrating FL, the approach offers a more robust framework for managing uncertainties, thereby improving the overall performance of the control system in dynamic environments.

In the present chapter, the fundamental principles of FL and the BC methodology will be elucidated. Subsequent to this introductory section, the BC strategy will be implemented within the system and integrated with FL in order to effectively manage the power conversion system. This integration aspires to augment the system's performance by capitalizing on the inherent strengths of both approaches.

4.2 Overview of Backstepping Control Techniques

Historically, the BC methodology was developed in the 1980s by Petar Kokotović for a specific class of systems designated as stringent feedback systems. Subsequently, extensive research and development have been conducted regarding this control approach [5].

4.2.1 Primary concepts

A lower triangular state structure characterizes these systems. The essence of the BC approach lies in decomposing the control challenge of the overall system into a series of subproblems associated with individual subsystems. This method involves using certain states as intermediate or "virtual commands"

in a recursive manner [6-8].

A series of Lyapunov functions (LFs) is used to formulate the control rules for these intermediary stages. Initially, a LF is selected for the first subsystem, which is progressively augmented as subsequent subsystems are stabilized. Ultimately, this process leads to the formulation of a global LF that ensures the stability of the entire system. This structured approach not only simplifies the control design process but also enhances the stability and performance of nonlinear systems [7, 8,10].

4.2.2 Affine form

In all nonlinear systems, it is essential to first express the system in an affine form. This transformation is crucial as it simplifies the analysis and control design processes. The affine form facilitates a clearer understanding of the system's dynamics by allowing for the separation of linear and nonlinear components [7].

$$\dot{x} = f(x) + g(x)u \tag{4.1}$$

With:

- $x \in R^n$: The vector of state variables;
- $u \in R^n$: The command input;
- $f: R^n \to R^n,\ g: R^n \to R^n$: Smooth nonlinear functions (infinitely derivable)

4.2.3 Lyapunov Function

The Lyapunov direct method, initially developed for the analysis of stability in nonlinear systems, has evolved into a robust technique for deriving control laws that ensure the stability of dynamic systems through state feedback. This method provides a structured approach to control design by utilizing LFs, which serve as indicators of system stability. By constructing suitable LFs, control engineers can establish that the closed-loop system will maintain stability despite disturbances or uncertainties.

The application of the Lyapunov method extends beyond the traditional analysis of stability; it is instrumental in the development of adaptive and robust control strategies. These strategies are of paramount importance for effectively managing systems that are subject to changing conditions and external disturbances, consequently enhancing the reliability and performance of dynamic systems in practical implementations [7, 9, 10]

The aim of state feedback control for the system (4.1) is to determine a state response:

$$u = \Phi(x) \tag{4.2}$$

Such that the closed-loop system:

$$\dot{x} = f\big(x, \Phi(x)\big) \tag{4.3}$$

The Lyapunov theorem delineates two characteristics for a LF $V(x)$ [11]:

- ✓ $V(x)$: is a Positive Definite Function (PDF): $(V(x=0)=0), V(x\neq 0)>0$
- ✓ $\dot{V}(x)$: is a Negative Definite Function (NDF):

$$\frac{dV(x)}{dt} = \dot{V}(x) = \frac{dV(x)}{dx}\dot{x} = \frac{dV(x)}{dx} f\big(x, \Phi(x)\big) \rightarrow \begin{cases} \dot{V}(x=0) = 0 \\ \dot{V}(x\neq 0) < 0 \end{cases}$$

The fundamental premise underlying these two properties is the concept of energy decrement in a dynamic system. This concept assumes that the energy in a dynamical system is represented by a continuous, non-negative function V(x), where the zero energy state is only attained at the equilibrium point (V(0) = 0). Accordingly, the decrement of energy signifies the progression towards the stable zero equilibrium state [11].

4.2.4 The Lower Triangular Shape

As previously mentioned, BC applies exclusively to nonlinear systems that have a state representation in lower triangular form. The dynamics of such a system is expressed by:

$$\begin{cases} \dot{x}_1 = f_1(x_1) + g_1(x_1)x_2 \\ \dot{x}_2 = f_2(x_1, x_2) + g_2(x_1, x_2)x_3 \\ \dot{x}_3 = f_3(x_1, x_2, x_3) + g_3(x_1, x_2, x_3)x_4 \\ \vdots \\ \dot{x}_{n-1} = f_{n-1}(x_1, x_2, \cdots, x_{n-1}) + g_{n-1}(x_1, x_2, \cdots, x_{n-1})x_n \\ \dot{x}_n = f_{n-1}(x_1, x_2, \cdots, x_n) + g_{n-1}(x_1, x_2, \cdots, x_n)u \end{cases} \tag{4.4}$$

4.3 Overview of Fuzzy Logic Techniques

Fuzzy logic represents a form of multi-valued logic that addresses reasoning of an approximate rather than definite and precise nature. In contrast to classical binary sets wherein variables may only assume true or false values, FL variables may possess truth values spanning the range between 0 and 1. This facilitates a more nuanced depiction of uncertainty and ambiguity, rendering it especially suitable for systems wherein human reasoning and decision-making processes are implicated.

FL is distinguished by the utilization of fuzzy sets, which are defined by membership functions (MF) that ascertain the extent to which an element is a member of a set. This methodology facilitates the modeling of intricate systems and processes that are arduous to describe employing conventional binary

logic. FL has been extensively applied in diverse domains, encompassing control systems [12].

To implement the FL technique in a real application, the following 3 steps are required [13]:

- ✓ Fuzzification - the conversion of classical or crisp data into fuzzy data or MFs.
- ✓ Fuzzy Inference Process - the combination of MFs with the control rules to derive the fuzzy output.
- ✓ Defuzzification - the utilization of various methods to calculate each associated output and compiles them into a lookup table. During the application, the output is selected from the lookup table based on the current input.

4.4 Implementation of Fuzzy backstepping Control

This section proposes a novel nonlinearity method using the BC technique to provide a resilient and highly efficient approach that addresses the limitations and challenges associated with the BC technique. The BC approach utilizes Lyapunov's stability theory to guarantee system stability. To maintain system stability, the FL method modifies the control gains of the BC. This adaptive method facilitates the enhancement of control efficacy and system stability under diverse operating situations [14, 15].

This system is divided into two primary sections: the machine side and the network side. The first section pertains to the components connected to the generators, while the second section refers to the components interfacing with the network. Accordingly, the control strategy is also divided into two main areas: control of the machines side converter (MSC) and control of the grid side converter (GSC).

4.4.1 MSC control

4.4.1.1 Backstepping control design

The suggested BC scheme for the parallel-connected two 5-phase PMSGs, powered by two turbines, is presented in Fig.(4.1). The reference speed and actual speed of each machine are utilized as inputs to the speed Backstepping controllers (BCs) to determine the q1-q2 axes reference current components. The remaining current components are maintained at zero. The measured currents are processed in the current BCs to obtain the d-q-x-y axes reference voltage components as outputs. These reference voltages are then transformed into the a-b-c-d-e frame, which serve as input signals to the PWM blocks. The PWM subsequently transmits the signals to the FSR to drive the two parallel-connected PMSGs.

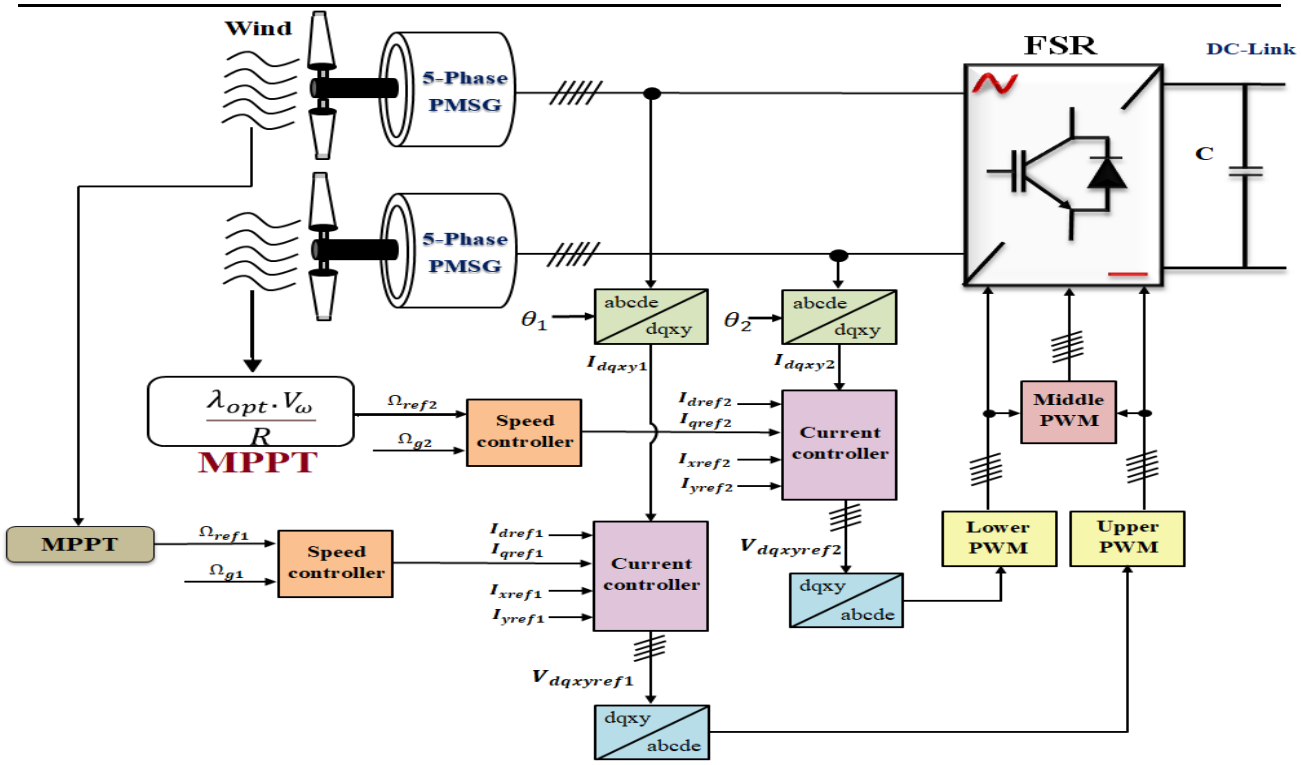

Fig. (4.1): The control design of FSR

The BC strategy is one of the most effective nonlinear strategies available in the field of control system design, owing to its high durability and exceptional performance characteristics. The application of this strategy in control system engineering is contingent upon the availability of the mathematical model (MM) describing the system dynamics. Furthermore, this method is predicated on the representation of the interconnected subsystems as first-order Lyapunov subsystems, which enhances the system's resilience against disturbances and overall stability. Additionally, the strategy employs a sequential step that generates virtual commands at each stage, ensuring the system's convergence to its equilibrium state [16-19].

Equation (4.5) delineates the MM of the machine used in this study, whereby the flux and voltage equations are specified. Additionally, add the 5-phase PMSG's mechanical equation to Equation (4.5) [20].

$$\begin{cases} \frac{dI_{dsj}}{dt} = \frac{-R_{sj}}{L_{dj}} I_{dsj} + \frac{P_j L_{qj}}{L_{dj}} I_{qj} \Omega_{mj} + \frac{1}{L_{dj}} V_{dsj} \\ \frac{dI_{qsj}}{dt} = \frac{-R_{sj}}{L_{qj}} I_{qsj} - \frac{P_j L_{dj}}{L_{qj}} I_{dj} \Omega_{mj} - \frac{P_j \Psi_{fj}}{L_{qj}} \Omega_{mj} + \frac{1}{L_{qj}} V_{qsj} \\ \frac{dI_{xsj}}{dt} = \frac{-R_{sj}}{L_{dj}} I_{xsj} + \frac{1}{L_{dj}} V_{xsj} \\ \frac{dI_{ysj}}{dt} = \frac{-R_{sj}}{L_{qj}} I_{ysj} + \frac{1}{L_{qj}} V_{ysj} \\ \frac{d\Omega_{mj}}{dt} = \frac{T_{mj}}{J_j} - \frac{5}{2J_j} P_j \left(L_{dj} - L_{qj}\right) I_{dsj} I_{qsj} - \frac{5}{2J} P_j \Psi_{fj} I_{qsj} - \frac{K_{fj}}{J_j} \Omega_{mj} \end{cases} \quad (4.5)$$

The control inputs vector is represented by $[u] = [V_{dsj} \quad V_{qsj} \quad V_{xsj} \quad V_{ysj}]^T = [u_{1j} \quad u_{2j} \quad u_{3j} \quad u_{4j}]^T$, whereas the state variables vector of the generator equations is represented by $[x] = [I_{dsj} \quad I_{qsj} \quad I_{xsj} \quad I_{ysj} \quad \Omega_{mj}]^T = [x_{1j} \quad x_{2j} \quad x_{3j} \quad x_{4j} \quad x_{5j}]^T$.

❖ Step 01:

The following formula could be utilized to identify the tracking error $\xi_{\Omega j}$:

$$\xi_{\Omega} = \Omega_{ref\_j} - \Omega_{mj} \tag{4.6}$$

The preceding equation's dynamic are expressed in this manner:

$$\dot{\xi}_{\Omega J} = \frac{d\dot{\xi}_{\Omega J}}{dt} = \dot{\Omega}_{ref\_j} - \dot{\Omega}_{mj}$$

$$\dot{\xi}_{\Omega j} = \frac{d\xi_{\Omega j}}{dt} = \dot{\Omega}_{ref\_j} - \frac{1}{J_j}\left[T_{tj} - \frac{5P_j}{2}\left(L_{dj} - L_{qj}\right).I_{dsj}.I_{qsj} - \frac{5P_j}{2}\Psi_{fj}.I_{qsj} - k_{fj}.\Omega_{mj}\right] \tag{4.7}$$

The main goal is to eliminate the mistake in speed error. To achieve this, we use the LF, which is described by the following formula:

$$V_{\Omega j} = \frac{1}{2}\xi_{\Omega j}^2 \tag{4.8}$$

The Lyapunov derivative is expressed as: [18]:

$$\dot{V}_{\Omega j} = \xi_{\Omega j}.\dot{\xi}_{\Omega j} = -k_{\Omega j}\xi_{\Omega j}^2 + \frac{\xi_{\Omega j}}{J_j}\left[J_j.\dot{\Omega}_{ref_j} - T_{tj} + k_{fj}.\Omega_m + \frac{5P_j}{2}.\Psi_{fj}.I_{qsj} + k_{\Omega j}J_j\xi_{\Omega j}\right]$$

$$+ \frac{5P_j}{2J_j}\left(L_{dj} - L_{qj}\right).I_{dsj}.I_{qsj}.\xi_{\Omega j} \tag{4.9}$$

The I_{qsj_ref} and I_{dsj_ref} the stator currents are chosen to provide the stabilising functions, referred to as virtual inputs.

$$\begin{cases} i_{dsj\_ref} = 0 \\ i_{qsj\_ref} = \frac{2}{5.P_j.\Psi_{fj}}\left[T_t - J_j.\dot{\Omega}_{ref\_j} - k_{fj}.\Omega_{mj} - k_{\Omega j}.J_j.\xi_{\Omega j}\right] \end{cases} \tag{4.10}$$

Substituting the values of I_{dsj_ref} , and I_{qsj_ref} into Equation (4.9) yields:

$$\dot{V}_{\Omega j} = -k_{\Omega j}.\xi_{\Omega j}^2 \leq 0 \tag{4.11}$$

❖ Step 02:

The purpose of this step, the determination of the MSC control voltages $\left(V_{dsj}, V_{qsj}, V_{xsj}, and\ V_{ysj}\right)$ is contingent upon the virtual inputs of the system, specifically the currents $\left(\ I_{dsj}, I_{qsj}, I_{xsj}, and\ I_{ysj}\right)$.

The following formulas serve as the foundation for determining the stator current errors [18]:

$$\begin{cases} \xi_{dj} = I_{dsj\_ref} - I_{dsj} \\ \xi_{qj} = I_{qsj\_ref} - I_{qsj} \\ \xi_{xj} = I_{xsj\_ref} - I_{xsj} \\ \xi_{yj} = I_{ysj\_ref} - I_{ysj} \end{cases} \tag{4.12}$$

Equation (4.12) could be employed to develop an updated form of the speed dynamics formula [19].

$$\dot{\xi}_{\Omega j} = \frac{d\xi_{\Omega j}}{dt} = \frac{1}{J_j}\left[-T_{tj} + \frac{5P_j}{2}\Psi_{fj}.i_{qsj} + \frac{5P_j}{2}\left(L_{dj} - L_{qj}\right).I_{dsj}.I_{qsj} + k_{fj}.\Omega_{mj}\right]$$

$$\dot{\xi}_{\Omega j} = \frac{1}{J_j}\left[-T_{tj} + \frac{5P_j}{2}\Psi_{fj}.\left(I_{qsj\_ref} - \xi_{qj}\right) - \frac{5P_j}{2}\left(L_{dj} - L_{qj}\right).I_{qsj}.\xi_{dj} + k_{fj}.\Omega_{mj}\right]$$

$$\dot{\xi}_{\Omega j} = \frac{1}{J_j}\left[-T_{tj} + \frac{5P_j}{2}\Psi_{fj}\left[\frac{2}{5.P_j.\Psi_{fj}}\left[T_t - k_{fj}.\Omega_{mj} - k_{\Omega j}.J_j.\xi_{\Omega j}\right]\right] - \frac{5P_j}{2}\Psi_{fj}.\xi_{qj} - \frac{5P_j}{2}\left(L_{dj} - L_{qj}\right).I_{qsj}.\xi_{dj} + k_{fj}.\Omega_{mj}\right]$$

$$\dot{\xi}_{\Omega j} = \frac{1}{J_j}\left[-k_{\Omega j}.J_j.\xi_{\Omega j} - \frac{5.P_j}{2}\Psi_{fj}.\xi_{qj} - \frac{5.P_j}{2}\left(L_{dj} - L_{qj}\right)I_{qsj}.\xi_{dj}\right] \tag{4.13}$$

The new dynamics of the present errors might be expressed using equations (4.5), (4.12), and (4.13) as follows [18, 19]:

$$\begin{cases} \dot{\xi}_{dj} = \dot{I}_{dsj\_ref} - \dot{I}_{dsj} \\ \dot{\xi}_{qj} = \dot{I}_{qsj\_ref} - \dot{I}_{qsj} \\ \dot{\xi}_{xj} = \dot{I}_{xsj\_ref} - \dot{I}_{xsj} \\ \dot{\xi}_{yj} = \dot{I}_{ysj\_ref} - \dot{I}_{ysj} \end{cases} \tag{4.14}$$

With:

$$\dot{\xi}_{dj} = \dot{I}_{dsj\_ref} - \dot{I}_{dsj} = \frac{R_{sj}}{L_{dj}}I_{dsj} - \frac{P_j.L_{qj}}{L_{dj}}I_{qsj}.\Omega_{mj} + \frac{1}{L_{dj}}V_{dsj} \tag{4.15}$$

$$\dot{\xi}_{qj} = \dot{I}_{qsj_{ref}} - \dot{I}_{qsj} = \frac{2}{5.P_j.\Psi_{fj}}\left[-k_{fj}.\dot{\Omega}_{mj} - k_{\Omega j}.J_j.\dot{\xi}_{\Omega j}\right] - \left(\frac{-R_{sj}}{L_{qj}}I_{qsj} - \frac{P_jL_{dj}}{L_{qj}}I_{dj}\Omega_{mj} - \frac{P_j\Psi_{fj}}{L_{qj}}\Omega_{mj} + \frac{1}{L_{qj}}V_{qsj}\right)$$

$$\dot{\xi}_{qj} = \frac{2}{5.P_J.J_j\Psi_{fj}}\left(\left(k_{\Omega j}.J_j - k_{fj}\right)\left[T_{tj} - \frac{5P_j}{2}\left(L_{dj} - L_{qj}\right).I_{dsj}.I_{qsj} - \frac{5P_j}{2}\Psi_{fj}.I_{qsj} - k_{fj}.\Omega_{mj}\right]\right)$$

$$+ \left(\frac{R_{sj}}{L_{qj}}I_{qsj} + \frac{P_jL_{dj}}{L_{qj}}I_{dj}\Omega_{mj} + \frac{P_j\Psi_{fj}}{L_{qj}}\Omega_{mj} - \frac{1}{L_{qj}}V_{qsj}\right) \tag{4.16}$$

$$\dot{\xi}_{xj} = \dot{I}_{xsj\_ref} - \dot{I}_{xsj} = 0 - \left[-\frac{R_{sj}}{L_{dj}} I_{xsj} + \frac{1}{L_{dj}} V_{xsj}\right] = \frac{R_{sj}}{L_{dj}} I_{xsj} - \frac{1}{L_{dj}} V_{xsj} \tag{4.17}$$

$$\dot{\xi}_{yj} = \dot{I}_{ysj\_ref} - \dot{I}_{ysj} = 0 - \left[-\frac{R_{sj}}{L_{qj}} I_{ysj} + \frac{1}{L_{qj}} V_{ysj}\right] = \frac{R_{sj}}{L_{qj}} I_{ysj} - \frac{1}{L_{qj}} V_{ysj} \tag{4.18}$$

The utilization of an alternate LF that incorporates the errors in each rotational speed and the stator current is essential to determine the appropriate reference voltages:

$$V_2 = \frac{1}{2}\left(\xi_{\Omega j}^2 + \xi_{dj}^2 + \xi_{qj}^2 + \xi_{xj}^2 + \xi_{yj}^2\right) \tag{4.19}$$

The new equation's time derivative in this manner:

$$\dot{V}_2 = \left(\xi_{\Omega j}.\dot{\xi}_{\Omega j} + \xi_{dj}.\dot{\xi}_{dj} + \xi_{qj}.\dot{\xi}_{qj} + \xi_{xj}.\dot{\xi}_{xj} + \xi_{yj}.\dot{\xi}_{yj}\right) \tag{4.20}$$

$$\dot{V}_2 = -k_{\Omega J}.\xi_{\Omega J}^2 - k_{dj}.\xi_{dj}^2 - k_{qj}.\xi_{qj}^2 - k_{xj}.\xi_{xj}^2 - k_{yj}.\xi_{yj}^2 + \xi_{\Omega j}\left[-\frac{5P_j}{2J_j}\Psi_{fj}.\xi_{qj} - \frac{5P_j}{2J_j}\left(L_{dj} - L_{qj}\right)I_{qsj}.\xi_{dj}\right] + \xi_{dj}\left[\frac{R_{sj}}{L_{dj}} I_{dsj} - \frac{P_j.L_{qj}}{L_{dj}} I_{qsj}.\Omega_{mj} + \frac{1}{L_{dj}} V_{dsj} + k_{dj}.\xi_{dj}\right] + \xi_{qj}\left[\frac{2}{5.P_J.J_j\Psi_{fj}}\left(\left(k_{\Omega j}.J_j - k_{fj}\right)\left[T_{tj} - \frac{5P_j}{2}\left(L_{dj} - L_{qj}\right).I_{dsj}.I_{qsj} - \frac{5P_j}{2}\Psi_{fj}.I_{qsj} - k_{fj}.\Omega_{mj}\right]\right) + \frac{R_{sj}}{L_{qj}} I_{qsj} + \frac{P_j L_{dj}}{L_{qj}} I_{dj}\Omega_{mj} + \frac{P_j\Psi_{fj}}{L_{qj}}\Omega_{mj} - \frac{1}{L_{qj}} V_{qsj} + k_{qj}.\xi_{qj}\right] + \xi_{xj}\left[\frac{R_{sj}}{L_{dj}} I_{xsj} - \frac{1}{L_{dj}} V_{xsj} + k_{xj}.\xi_{xj}\right] + \xi_{qj}\left[\frac{R_{sj}}{L_{qj}} I_{ysj} - \frac{1}{L_{qj}} V_{ysj} + k_{yj}.\xi_{yj}\right]$$

$$\dot{V}_2 = -k_{\Omega J}.\xi_{\Omega J}^2 - k_{dj}.\xi_{dj}^2 - k_{qj}.\xi_{qj}^2 - k_{xj}.\xi_{xj}^2 - k_{yj}.\xi_{yj}^2 + \xi_{dj}\left[\frac{R_{sj}}{L_{dj}} I_{dsj} - \frac{P_j.L_{qj}}{L_{dj}} I_{qsj}.\Omega_{mj} + \frac{1}{L_{dj}} V_{dsj} + k_{dj}.\xi_{dj} - \frac{5P_j}{2J_j}\left(L_{dj} - L_{qj}\right)I_{qsj}.\xi_{\Omega j}\right] + \xi_{qj}\left[\frac{2}{5.P_J.J_j\Psi_{fj}}\left(\left(k_{\Omega j}.J_j - k_{fj}\right)\left[T_{tj} - \frac{5P_j}{2}\left(L_{dj} - L_{qj}\right).I_{dsj}.I_{qsj} - \frac{5P_j}{2}\Psi_{fj}.I_{qsj} - k_{fj}.\Omega_{mj}\right]\right) + \frac{R_{sj}}{L_{qj}} I_{qsj} + \frac{P_j L_{dj}}{L_{qj}} I_{dj}\Omega_{mj} + \frac{P_j\Psi_{fj}}{L_{qj}}\Omega_{mj} - \frac{1}{L_{qj}} V_{qsj} + k_{qj}.\xi_{qj} - \frac{5P_j}{2J_j}\Psi_{fj}.\xi_{qj}\right] + \xi_{xj}\left[\frac{R_{sj}}{L_{dj}} I_{xsj} - \frac{1}{L_{dj}} V_{xsj} + k_{xj}.\xi_{xj}\right] + \xi_{qj}\left[\frac{R_{sj}}{L_{qj}} I_{ysj} - \frac{1}{L_{qj}} V_{ysj} + k_{yj}.\xi_{yj}\right] \tag{4.21}$$

Correspondingly, the subsequent voltages are utilized as reference voltages, and K_{dj}, K_{qj}, K_{xj} and K_{yj} are adjusted to positive values [18, 19]:

$$V_{dsj\_ref} = R_{sj}.I_{dsj} - P_j.L_{dj}.\Omega_{mj}.I_{qsj} - \frac{5P_j.L_{dj}}{2J_j}\left(L_{dj} - L_{qj}\right)I_{qsj}.\xi_{\Omega j} + k_{dj}.L_{dj}.\xi_{dj} \tag{4.22}$$

$$V_{qsj\_ref} = \frac{2}{5.P_J.J_j\Psi_{fj}}\left(\left(k_{\Omega j}.J_j - k_{fj}\right)\left[T_{tj} - \frac{5P_j}{2}\left(L_{dj} - L_{qj}\right).I_{dsj}.I_{qsj} - \frac{5P_j}{2}\Psi_{fj}.I_{qsj} - k_{fj}.\Omega_{mj}\right]\right) + \frac{R_{sj}}{L_{qj}} I_{qsj} + \frac{P_j L_{dj}}{L_{qj}} I_{dj}\Omega_{mj} + \frac{P_j\Psi_{fj}}{L_{qj}}\Omega_{mj} - \frac{1}{L_{qj}} V_{qsj} + k_{qj}.\xi_{qj} \tag{4.23}$$

$$V_{xsj\_ref} = R_{sj}.I_{xsj} + k_{xj}.L_{dj}.\xi_{xj} \quad (4.24)$$

$$V_{ysj\_ref} = R_{sj}.I_{ysj} + k_{yj}.L_{yqj}.\xi_{yj} \quad (4.25)$$

Substituting equations (4.22) to (4.25) into the $\dot{V}_2$ derivative formula, we get:

$$\dot{V}_2 = -k_{\Omega J}.\xi_{\Omega J}^2 - k_{dj}.\xi_{dj}^2 - k_{qj}.\xi_{qj}^2 - k_{xj}.\xi_{xj}^2 - k_{yj}.\xi_{yj}^2 \leq 0 \quad (4.26)$$

4.4.1.2 FBC approach

The new suggested FBC strategy is a development and modification based on the use of BC technique. The proposed topology consists of FL and BC, since the combination is formulated to get a precisely designed controller. Self-tuning FBC: this technique enhances its capacity by adjusting the control gains in FL each time during the control operation automatically. With the implementation of this adaptive tuning strategy, the controller can compensate for variability in system dynamics, uncertainties, and disturbances—leading to improved control performance while ensuring stability octave. In Fig. (4.2) The suggested method used to control capabilities is shown.

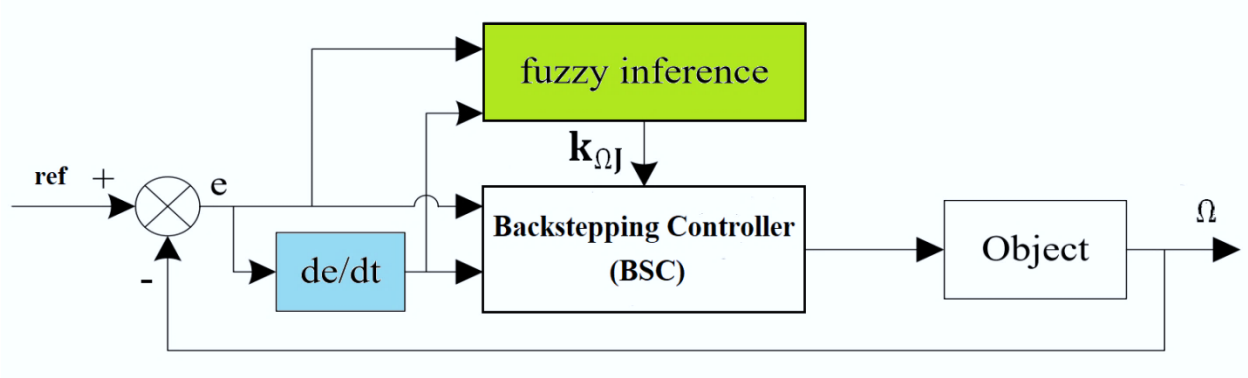

Fig. (4.2): Self-tuning structure of the FBC technique.

A two-dimensional FLC is employed, utilizing two inputs (the error(e), and error derivative$(\dot{e})$) and one output. The output, denoted as $K_{\Omega j}$, is utilized to modify the parameter of the BC responsible for adjusting the generator's speed. This parameter is considered crucial in the system. The adjustment process takes place in real-time, enabling the self-adaptation of different error and error rate of change in BC parameters to meet the system's requirements. In Fig. (4.3), the structure of the FL control used to improve the performance of the BC strategy is given, as it contains two inputs and only one output.

A two-dimensional FLC is used, which uses two inputs (error (e), and derivative of the error $(\dot{e})$) and one output. The output is denoted as $K_{\Omega j}$ and is used to change the parameters of the BC, which is responsible for regulating the generator speed. This parameter is considered critical in the system. The adjustment process is done in real time and allows self-adjustment of the various errors and error rates

of changing the BC parameters to meet the requirements of the system. Fig. (4.3) shows the structure of the FL controller used to improve the performance of the BC strategy, as it contains two inputs and only one output.

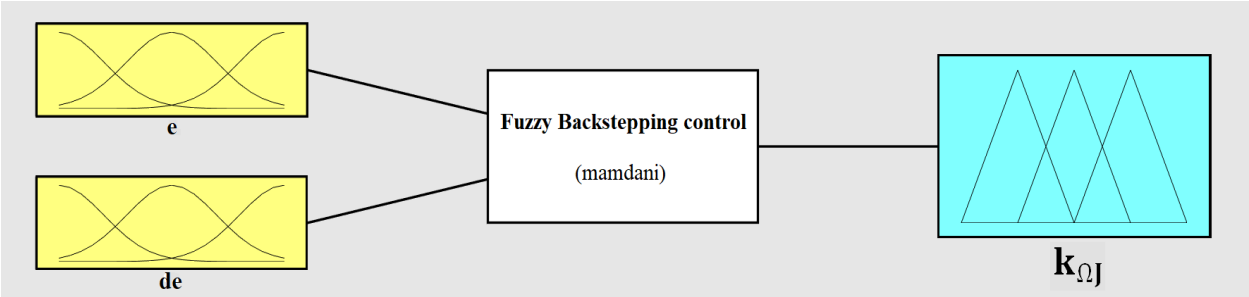

Fig. (4.3): Fuzzy controller's structural diagram.

The FLC rule involves mapping the linguistic input variables, namely e(t) and de(t), to the linguistic output variable K. The control method uses a set of nine membership functions: NVB (negative very big), NB (negative big), NM (negative medium), NS (negative small), Z (zero), PS (positive small), PM (positive medium), PB (positive big) and PVB (positive very big). These membership functions characterize the linguistic input variables, thereby ensuring the stability of the system. The membership functions of the two linguistic input variables, e(t) and ė(t), and the linguistic output variable K are shown in Figs. (4. 4) and (4.5). The membership functions are defined as VVS (very very small), VS (very small), S (small), M (medium), B (large), VB (very large, very large) and VVB (very very large). The details of the command method are shown in Table (4.1).

Table (4.1): Table containing FLC system rules.

$K_{\Omega j}$		e(t)								
		NVB	**NB**	**NM**	**NS**	**Z**	**PS**	**PM**	**PB**	**PVB**
$\dot{e}(t)$	**NVB**	VVB	VVB	VB	B	M	B	VB	VVB	VVB
	NB	VVB	VB	B	M	S	M	B	VB	VVB
	NM	VB	B	M	S	VS	S	M	B	VB
	NS	B	M	S	VS	VVS	VS	S	M	B
	Z	B	M	S	VS	VVS	VS	S	M	B
	PS	B	M	S	VS	VVS	VS	S	M	B
	PM	VB	B	M	S	VS	S	M	B	VB
	PB	VVB	VB	B	M	S	M	B	VB	VVB
	PVB	VVB	VVB	VB	B	M	B	VB	VVB	VVB

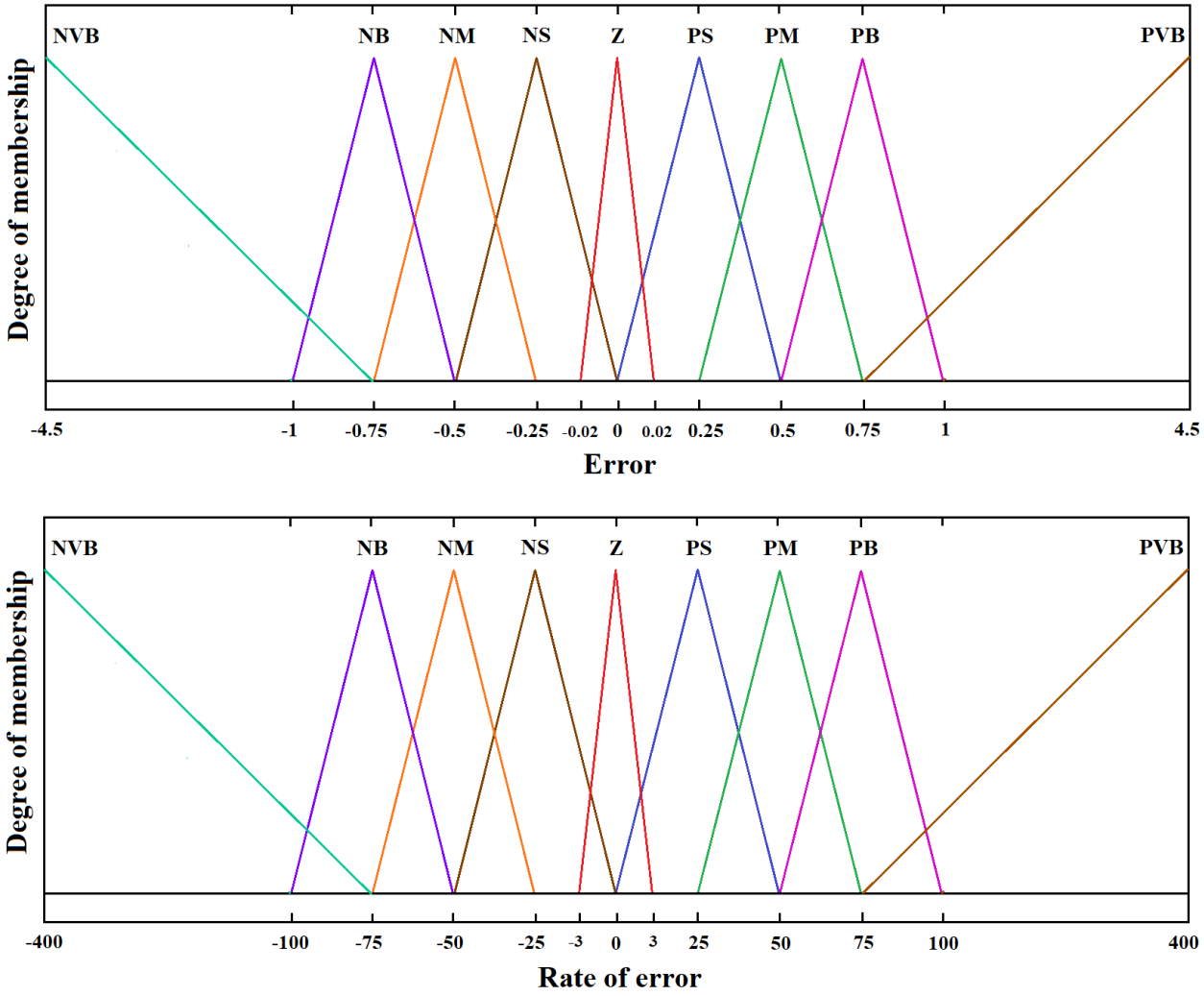

Fig. (4.4): MF of the error($\boldsymbol{e}$) and the rate of error ($\dot{\boldsymbol{e}}$).

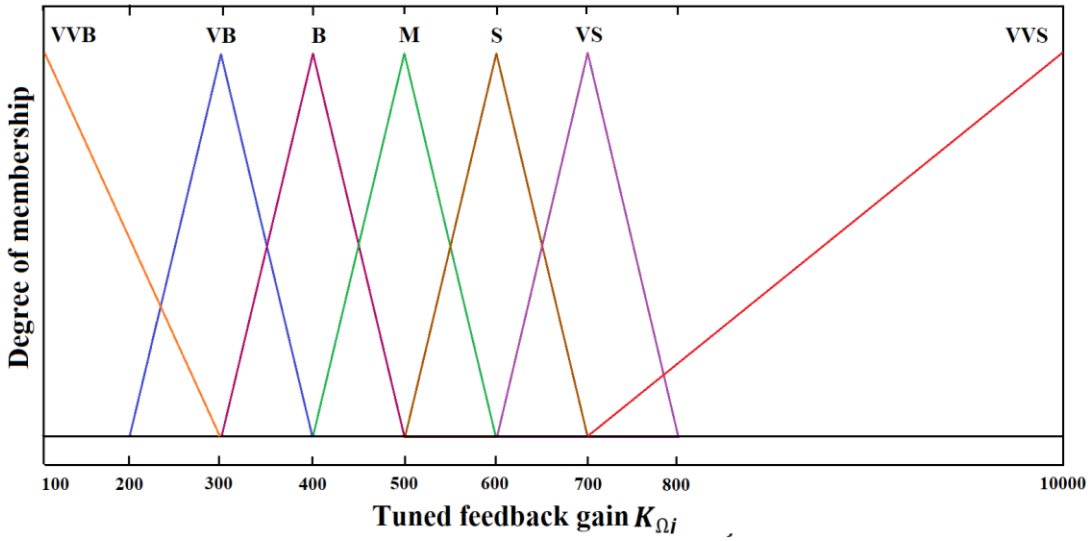

Fig. (4.5): The tuned $\boldsymbol{K_{\Omega J}}$ gains' MF.

4.4.2 GSC control

The grid voltages might be expressed concisely in the Park frame (d, q) in this way:

$$\begin{cases} V_{gd} = R_s I_{gd} + L_d \frac{dI_{gd}}{dt} - w_g L_q I_{gq} + V_{id} \\ V_{gq} = R_s I_{gq} + L_q \frac{dI_{gq}}{dt} - w_g L_d I_{gd} + V_{iq} \end{cases} \quad (4.27)$$

The following formulae indicate the injected P_g and Q_g:

$$\begin{cases} P_{grid} = \frac{3}{2}\left(V_{gd}.I_{gd} + V_{gq}.I_{gq}\right) \\ Q_{grid} = \frac{3}{2}\left(V_{gq}.I_{gd} - V_{gd}.I_{gq}\right) \end{cases} \quad (4.28)$$

GSC control involves setting $V_{qg} = 0$ and$V_{dg} = \|V_g\|$. The power mathematical equations are adjusted accordingly:

$$\begin{cases} P_{grid} = \frac{3}{2}\left(V_{gd}.I_{gd}\right) = \frac{3}{2}\left(\|V_g\|.I_{gd}\right) \\ Q_{grid} = \frac{3}{2}\left(-V_{gd}.I_{gq}\right) = -\frac{3}{2}\left(\|V_g\|.I_{gq}\right) \end{cases} \quad (4.29)$$

The DC-link connects the converter located on the MS and the converter located on the GS. By focusing on power balance and ignoring converter losses, the dynamic behavior of the DC-link voltage could be realistically described.

$$P_{gen} - P_g = \frac{1}{2}.C.\frac{dV_{dc}^2}{dt} \quad (4.30)$$

Equation (4.27) offers the state representation for both current and DC link voltage. The DC link voltage is correlated with the grid current, since a variation in the grid current immediately influences the DC link voltage value [20].

$$\begin{cases} \frac{dI_{gd}}{dt} = \frac{1}{L_g}V_{id} - \frac{R_g}{L_g}I_{gd} + W_g I_{gq} - \frac{1}{L_g}V_{gd} \\ \frac{dI_{gq}}{dt} = \frac{1}{L_g}V_{iq} - \frac{R_g}{L_g}I_{gq} - W_g I_{gd} - \frac{1}{L_g}V_{gq} \\ \frac{dV_{dc}^2}{dt} = \frac{2}{C}\left(-\frac{3}{2}V_{gd}.I_{gd} + P_{gen}\right) \end{cases} \quad (4.31)$$

The state variables are denoted as$[x] = \begin{bmatrix} I_{gd} & I_{gq} & V_{dc}^2 \end{bmatrix}^T = [x_1 \quad x_2 \quad x_3]^T$, while the controller inputs are represented by $[u] = [V_{id} \quad V_{iq}]^T$. The *Ps* generated through generators is indicated as P_{gen}, and the injected power is defined as P_{grid} [16, 17].

The suggested BC scheme for the 3-phase inverter fed by a wind system (WS) is depicted in Fig. (4.6). The reference DC-link voltage and the actual DC-link voltage are utilized as inputs to the voltage

Backstepping controller (BCs) to calculate the reference current component for the d-axis. The other current component (q) is maintained at zero. The measured currents are processed within the current BCs to produce the reference voltage components in the d-q axes as outputs. These reference voltages are converted into the a-b-c frame, which serves as input signals to the PWM blocks. The PWM then transmits these signals to the GSC to control the power injected into the grid.

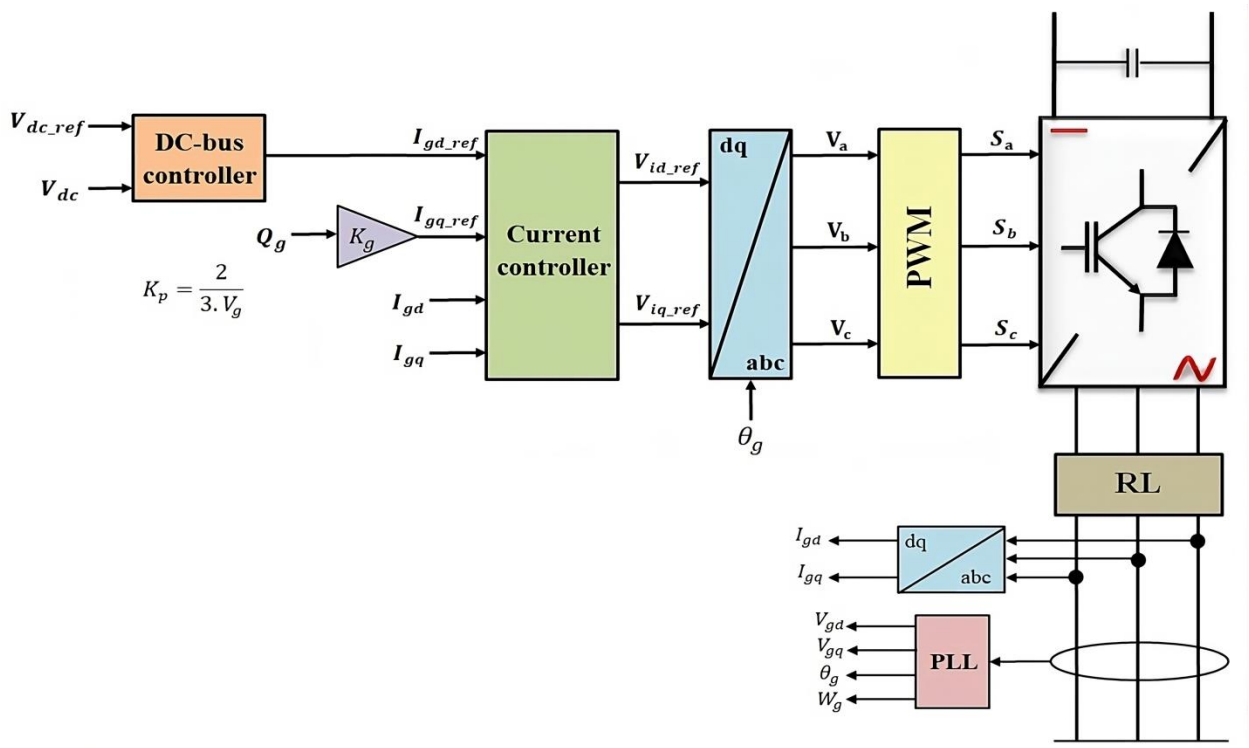

Fig. (4.6): The control design of GSC

- Step 01:

The error in DC-bus voltage (e_{dc}) might be calculated using the formula listed below [15, 18]:

$$e_{dc} = V_{dc\_ref}^2 - V_{dc}^2 \tag{4.32}$$

Since the present ingredient I_{gd} is classified as a virtual command component in order to lessen the amount of the error (e_{dc}), the LF is selected in the manner described below:

$$V_1 = \frac{1}{2} e_{dc}^2 \tag{4.33}$$

The LF's derivative is displayed as:

$$\dot{V}_1 = e_{dc}.\dot{e}_{dc} = e_{dc}\left(\dot{V}_{dc}^2 - \left[\frac{2}{C}\left(-\frac{3}{2}V_{gd}.I_{gd} + P_{gen}\right)\right]\right) \tag{4.34}$$

A key component of this approach is the generation of the virtual input, sometimes referred to as the

stabilizing equations, by selecting the network's current I_{gd} elements [18, 19].

$$I_{gd\_ref} = \frac{1}{V_{gd}}\left(\frac{2}{3}P_{gen} - \frac{C}{3}\left[\dot{V}_{dc}^2 + k_{dc}.e_{dc}\right]\right) \tag{4.35}$$

Following that, the formulae ($\dot{V}_1$) take on the following altered form:

$$\dot{V}_1 = -k_{dc}.e_{dc}^2 \leq 0 \tag{4.36}$$

- Step 02:

For monitoring P_g and Q_g, the BC is designed to generate voltage commands based on direct and quadrature current errors. As an outcome, the following error equations are utilized [19]:

$$\begin{cases} e_d = I_{gd\_ref} - I_{gd} \\ e_q = I_{gq\_ref} - I_{gq} \end{cases} \tag{4.37}$$

Based upon the Equation (4.35), the new form of $\dot{e}_{dc}$ is in below:

$$\dot{e}_{dc} = -k_{dc}.e_{dc}^2 - \frac{3}{C}V_{gd}.e_d \tag{4.38}$$

The derivative of Equation (4.37) is:

$$\begin{cases} \dot{e}_d = \dot{I}_{gd\_ref} - \left(\frac{1}{L_g}V_{id} - \frac{R_g}{L_g}I_{gd} + W_g I_{gq} - \frac{1}{L_g}V_{gd}\right) \\ \dot{e}_q = \dot{I}_{gq\_ref} - \left(\frac{1}{L_g}V_{iq} - \frac{R_g}{L_g}I_{gq} - W_g I_{gd} - \frac{1}{L_g}V_{gq}\right) \end{cases} \tag{4.39}$$

The new suggested LF is:

$$V_2 = \frac{1}{2}\left(e_{dc}^2 + e_d^2 + e_q^2\right) \tag{4.40}$$

The LF's derivative is offered as:

$$\dot{V}_2 = e_{dc}.\dot{e}_{dc} + e_d.\dot{e}_d + e_q.\dot{e}_q \tag{4.41}$$

$$\dot{V}_2 = -k_{dc}.e_{dc}^2 - k_d.e_d^2 - k_q.e_q^2 + e_d\left[\dot{I}_{gd\_ref} - \left(\frac{1}{L_g}V_{id} - \frac{R_g}{L_g}I_{gd} + W_g I_{gq} - \frac{1}{L_g}V_{gd}\right) + k_{dg}.e_d - \frac{3}{C}V_{gd}.e_{dc}\right] + e_q\left[\dot{I}_{gq\_ref} - \left(\frac{1}{L_g}V_{iq} - \frac{R_g}{L_g}I_{gq} - W_g I_{gd} - \frac{1}{L_g}V_{gq}\right) + k_{qg}.e_q\right] \tag{4.42}$$

The reference voltages were established via equation $\dot{V}_2$ in the manner described below [19]:

$$V_{id\_ref} = R_g.I_{gd} - W_g.L_g.I_{qg} + V_{gd} - \frac{3}{C}V_{gd}.L_g.e_{dc} + k_{dg}.L_g.e_d \tag{4.43}$$

$$V_{iq\_ref} = R_g.I_{gq} + W_g.L_g.I_{dg} + V_{gq} + k_{qg}.L_g.e_q \tag{4.44}$$

The Equation's demeanor (4.42) might be stated simply in this way:

$$\dot{V}_2 = -k_{dc}.e_{dc}^2 - k_{dg}.e_d^2 - k_{qg}.e_q^2 \leq 0 \tag{4.45}$$

where, k_{dc}, k_{dg}, and k_{qg} are constants with positive values.

The suggested approach at the level of two converters is shown in Fig. (4.7), which depicts the suggested energy system. Every WT in this suggested system makes use of a own MPPT. Additionally, estimate is done using the phase-locked loop (PLL) technique, which improves the stability and robustness of the suggested control.

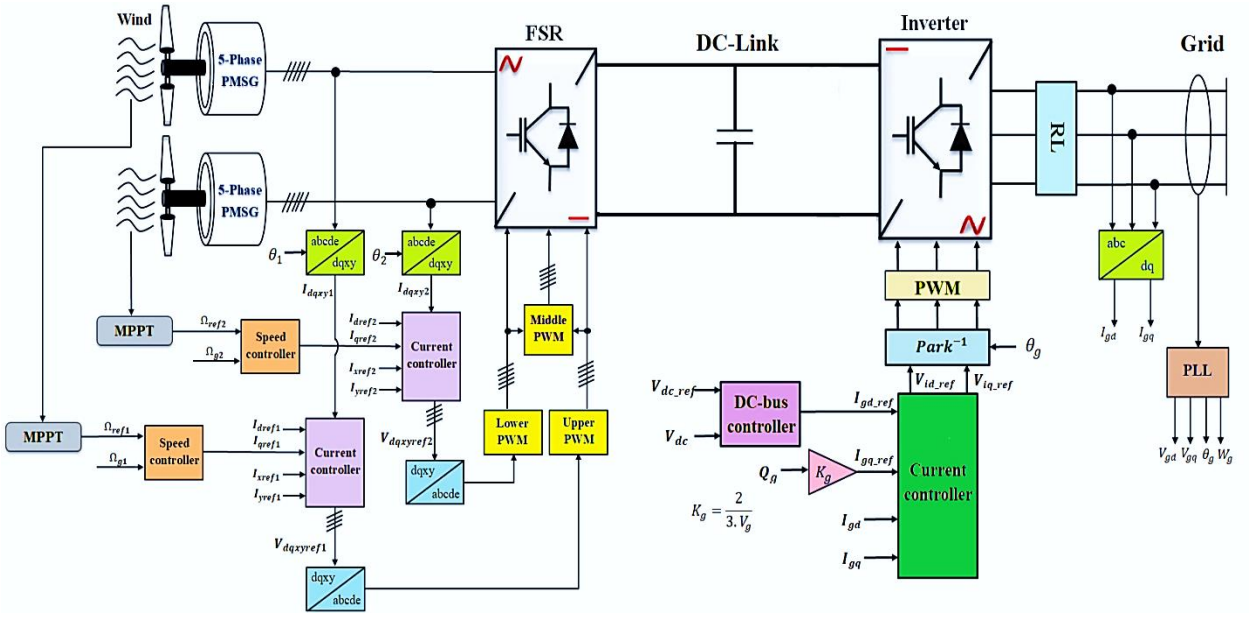

Fig. (4.7): WPGS's general command structure.

4.4.3 System stability study

There are many strategies that can be used to study stability, among which Lyapunov theory and Bode curve are the most commonly used strategies. It is well known that Lyapunov's complex strategy theory is derived based on complex algebraic methods, because it requires a lot of calculations, which increases the possibility of calculation errors. However, the Bode curve is a graphical method that is light and simple and does not require complex calculations. In this work, the Bode curve is used to prove the stability of the FBC technique. Fig. (4.8) shows the Bode curve of the conventional BC technique for two generators, and Fig. (4.9) shows the Bode curve of the FBC technique for two generators, where both the amplitude (dB) and the phase are extracted from one curve.

It is observed that the Bode curves of the two generators in the case of the two strategies are identical, which is a consequence of employing two generators with analogous characteristics.

As could be seen in Figs. (4.8) and (4.9), the values of the amplitude (dB) and phase take negative values, which confirms the stability of the two techniques used. You can also see that the amplitude (dB) and phase values decrease as the frequency increases when using both controls. In the BC technique, the amplitude (dB) range is from -80dB to -160dB and the phase range is from 0 degrees to -90 degrees. It should be noted that the phase variation range in the FBC technique is the same as the phase variation range in the BC technique. The amplitude (dB) variation range in the FBC technique is from -127 dB to -170 dB. Therefore, the FBC technique provides a various scope of changes in the magnitude's value (dB) compared to the BC topology.

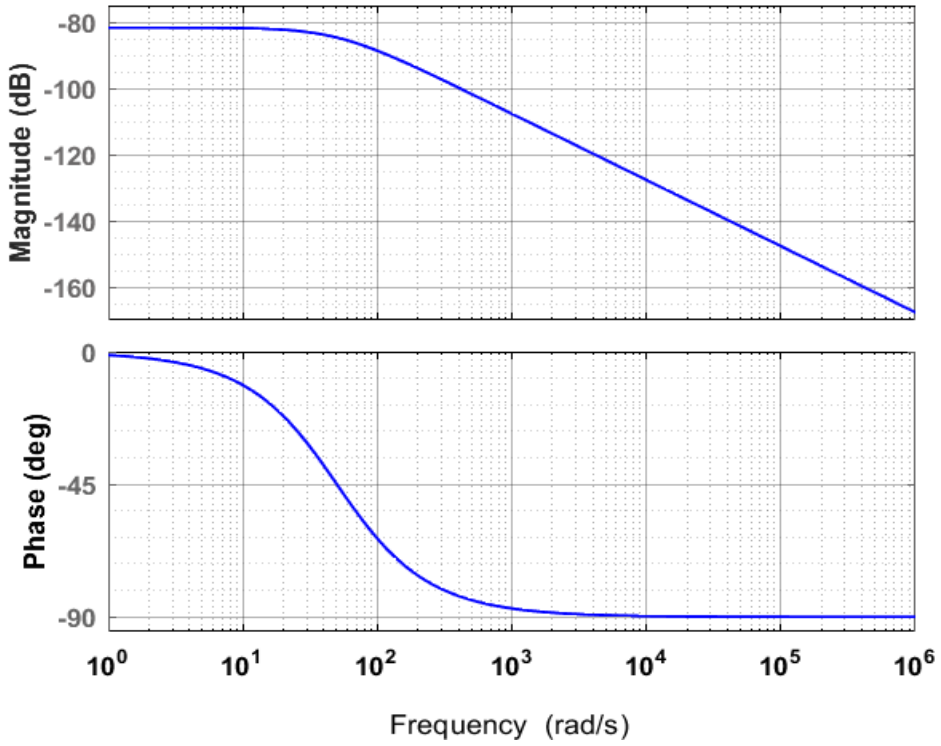

a) Five-phase PMSG 1

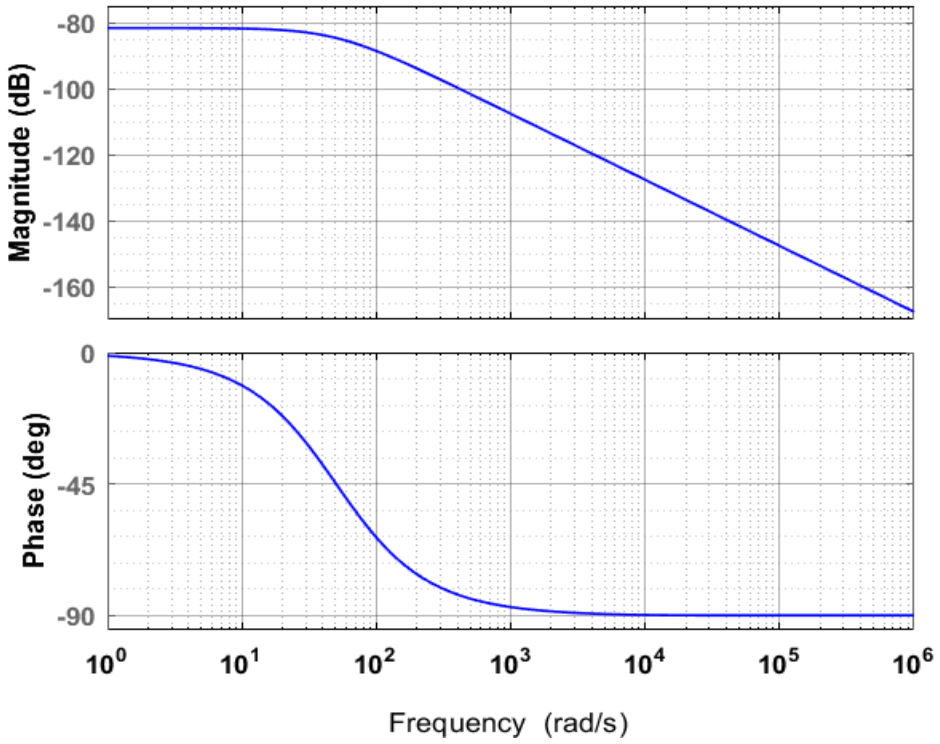

b) Five-phase PMSG 2

Fig. (4.8): Budd curve for BC technique.

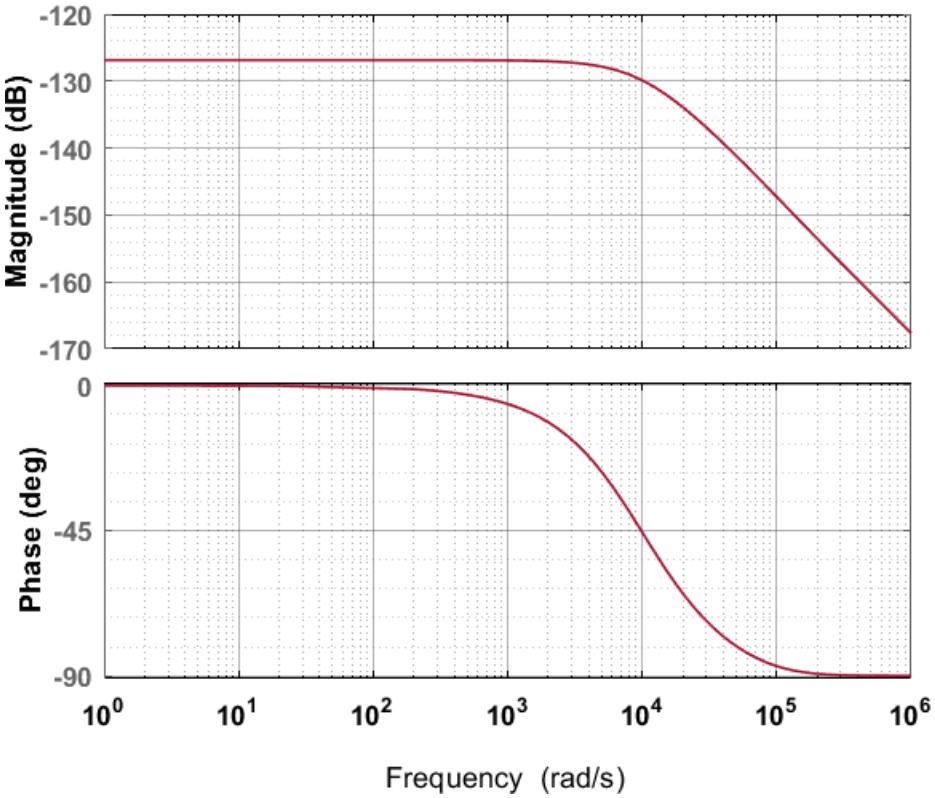

a) Five-phase PMSG 1

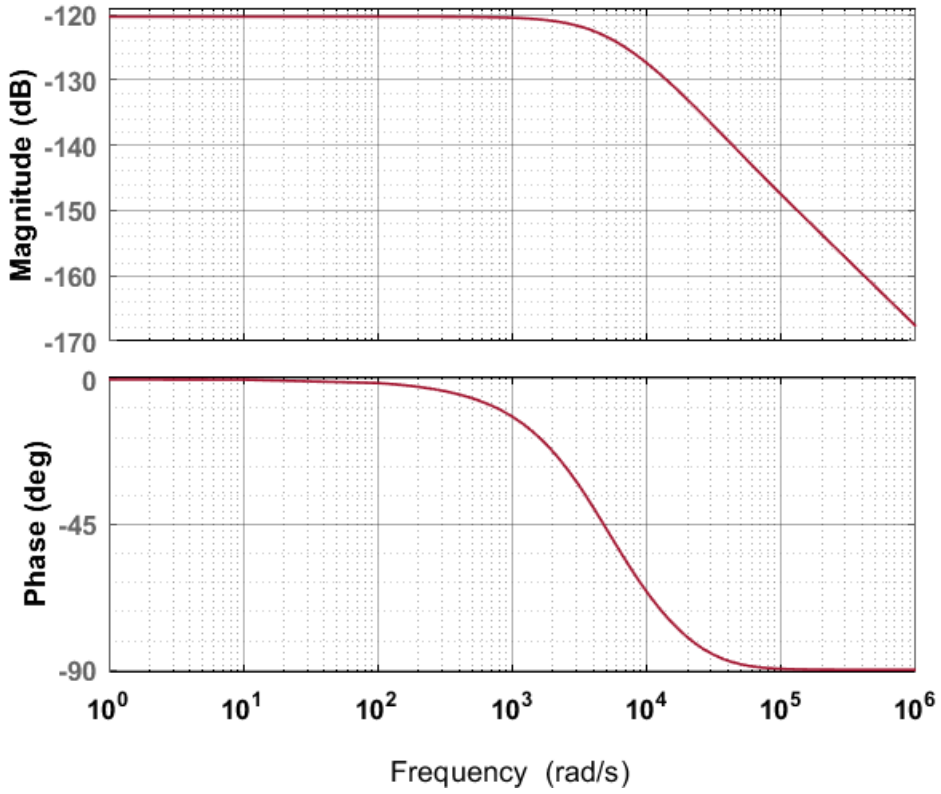

b) Five-phase PMSG 2

Fig. (4.9): Budd curve for FBC strategy.

4.5 Results

To validate the effectiveness of the recommended command approach for the WS with multiple generators as depicted in Fig. (4.7), MATLAB is utilized as the simulation platform. The resilience of the command system is assessed employing a wind profile generated to emulate real-world circumstances. The performance of the control in tracking set references and attaining energy efficiency is evaluated under the influence of a fluctuating wind profile. The system and generators parameters employed in the simulations are presented in Appendices A and B.

4.5.1 Steps WS test

The initial assessment is to examine the suggested FBC technique in comparison to the BC utilizing WS in steps, as this assessment intends to demonstrate the robustness of the FBC approach within the context of a WPGS. Although the wind profile employed (Fig. (4.10)) in this assessment may not accurately reflect real-world conditions, it serves as a mechanism to evaluate the performance of the selected command approach in response to abrupt changes in instructions. The same WS alteration is utilized for both WTs.

Fig. (4.11) illustrates the rotational speed of both generators when utilizing both the FBC and BC

controls. It is observed that the speed of the two generators exhibits a change in WS, accompanied by a rapid dynamic response from the two controllers. The proposed FBC strategy demonstrates an advantage over the BC strategy. Furthermore, the FBC strategy in the case of two generators yielded better results in terms of exceeding the speed limit value, compared to the BC strategy. However, regarding the speed response time, the FBC strategy provided less satisfactory results than the BC technique. This negative aspect can be attributed to the values of the proposed strategy's gains and the inherent characteristics of the FL, where the number of rules plays a pivotal role in enhancing the performance of the FBC technique.

Fig. (4.12) depicts the temporal variation of torque for the two control strategies (FBC and BC). This figure demonstrates that the changes in torque mirror the patterns observed in rotational speed and wind speed. As the wind speed increases, the torque value correspondingly rises, and vice versa. Additionally, it is noted that the level of fluctuations is more pronounced in the case of the BC strategy compared to the FBC technique. Furthermore, it is observed that both control methods exceed the limit value, although the proposed FBC approach is preferable as it reduces the extent of this exceedance.

Fig. (4.13) illustrates the change in I_d and I_q for the two generators when both controls are applied. Figs. (4.13-a) and (4.13-b) are for the first generator, whereas Figs. (4.13-c) and (4.13-d) are for the second generator. Figs 13a and 13c show that the current I_d of the two generators is constant and closely approximates the reference value. When the two controls are utilized in the presence of ripples, this current does not vary in response to WS changes. Even if the limit value is surpassed, the current value stays constant at (0) throughout the experiment. The FBC approach lowered the current's (I_d) ripple and overshoot values when compared to the BC technique.

The current I_q for the generators are displayed in Figs. (4.13-b) and (4.13-d) when both controls (FBC and BC) are applied. When both controls are utilized, this current closely matches the reference value while also surpassing the limit value. This current fluctuates in response to variations in WS, with its value increasing and decreasing as WS rises and falls. It is also worth noting that this current has negative values for the two generators, indicating that they are creating energy rather than consuming it, which is a positive thing. When compared to the BC approach, the FBC technique lowered the value of both the ripples and the current's marginal value.

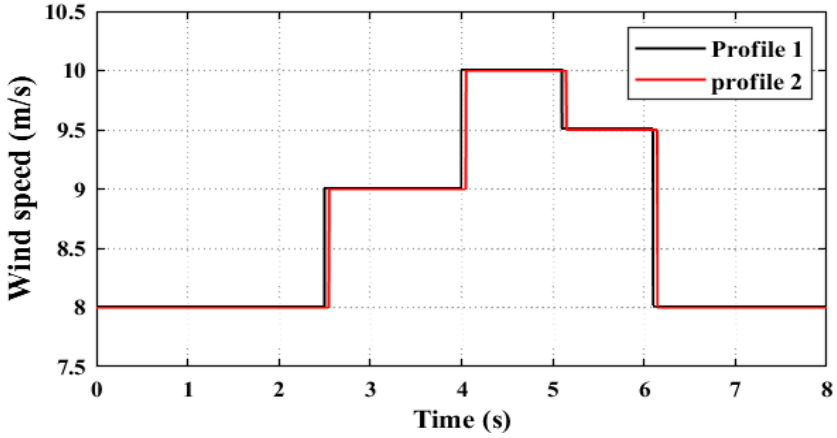

Fig. (4.10): Steps wind velocity profiles**.**

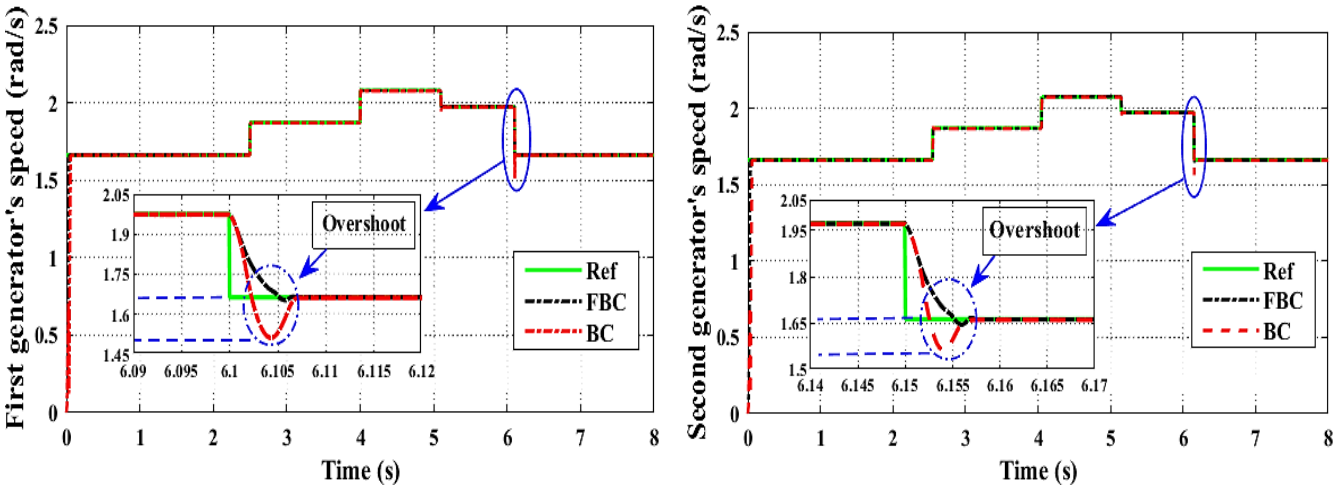

a) PMSG1 b) PMSG2

Fig. (4.11): Generators' mechanical speed

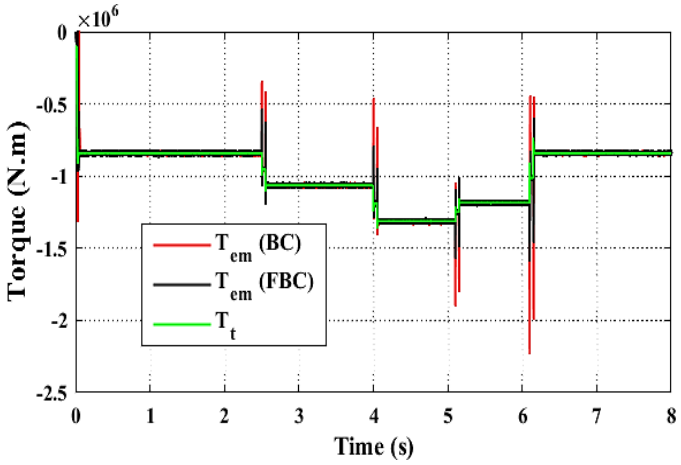

Fig. (4.12): PMSGs' electromagnetic torque.

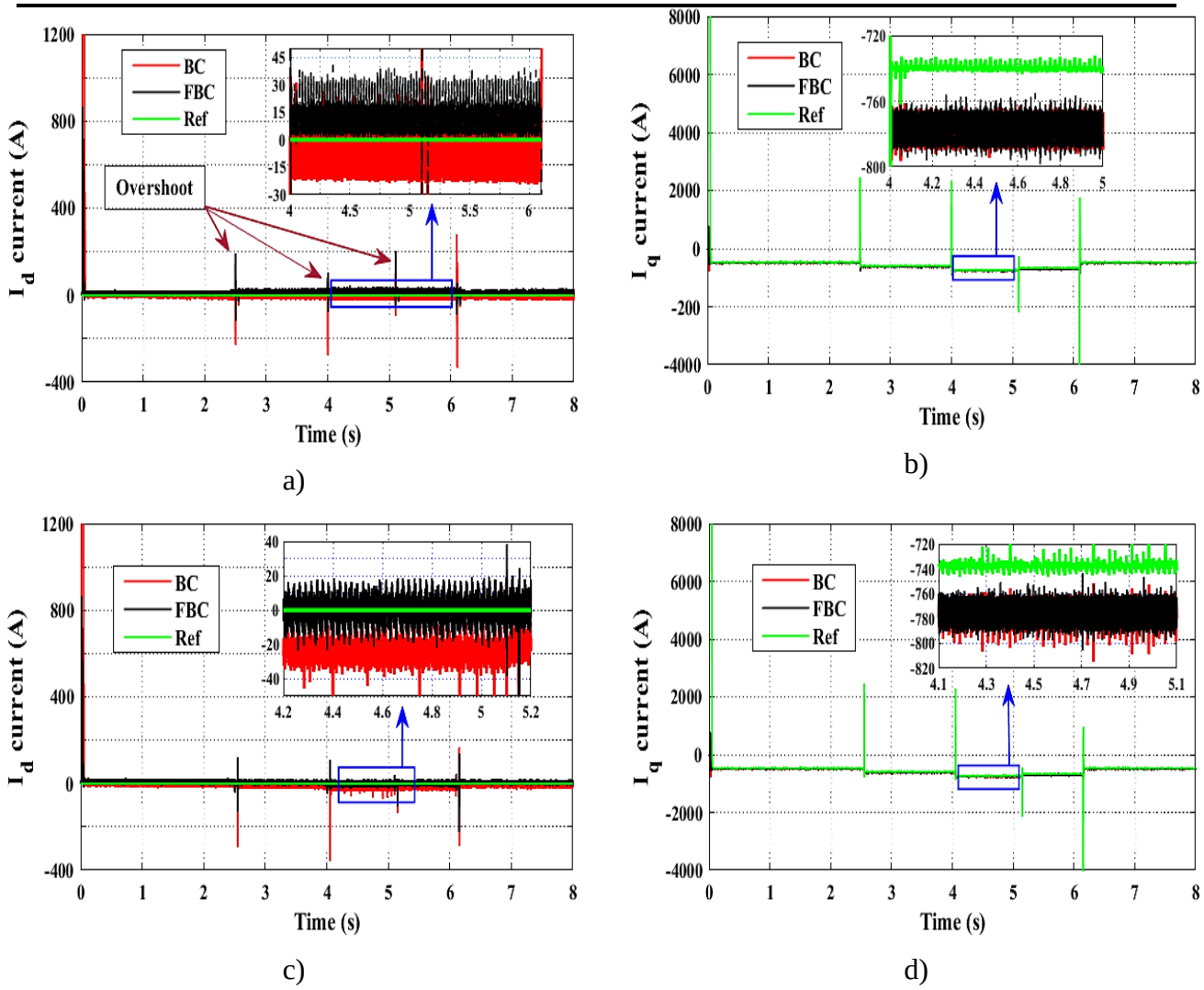

Fig. (4.13):I_d- I_q currents: (a, b) PMSG-1, (c, d) PMSG-2

Fig. (4.14) illustrates the power, grid voltage and current THD for both controllers in the case of generator 1. The grid voltage for the FBC and the BC approaches are shown in Figs (4.14-a) and (4.14-b), respectively. From both figures, it can be seen that the supply voltage follows the reference value very well and there are ripples. These ripples are larger when using the BC than when using the FBC. In addition, this voltage value is fixed for both controls and is 2500 volts, because this value does not vary with the change of WS.

Figs. (4.14-c) and (4.14-d) show P_g and Q_g for both controllers, respectively. P_g for both controllers follows the reference value very well and both controllers have a fast dynamic response, which gives the FBC technique an advantage in terms of response time. Also note that the P_g waves are lower when using the FBC technique compared to the BC strategy, which shows the high performance of the FBC technique and its efficiency in improving power quality. Q_g for both controllers remains constant and does not change with changes in WS, since its value follows the reference value very well in the

presence of waves. These waves are larger when using the BC technique compared to the FBC approach.

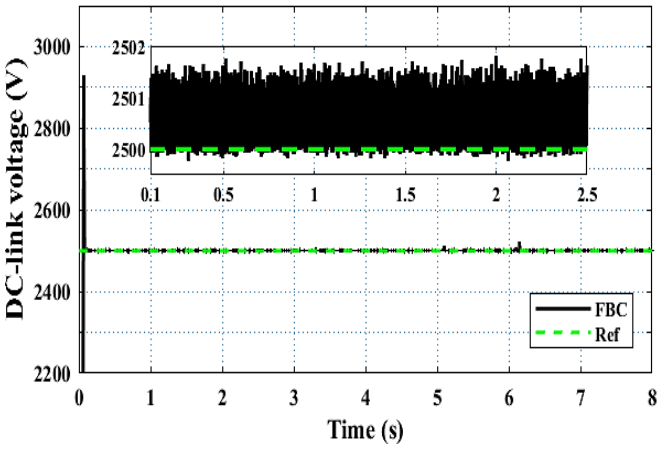

a)

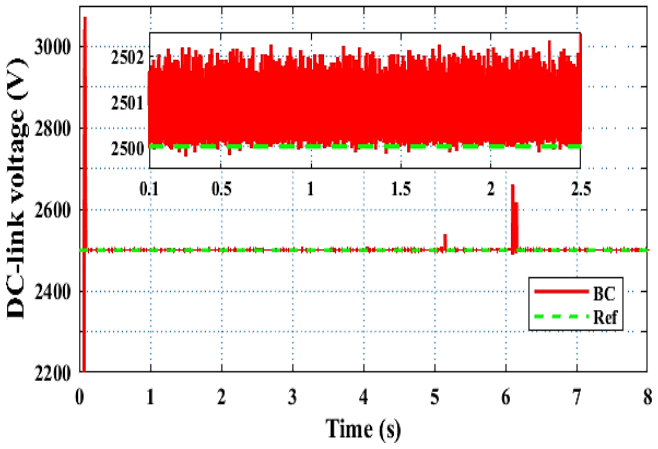

b)

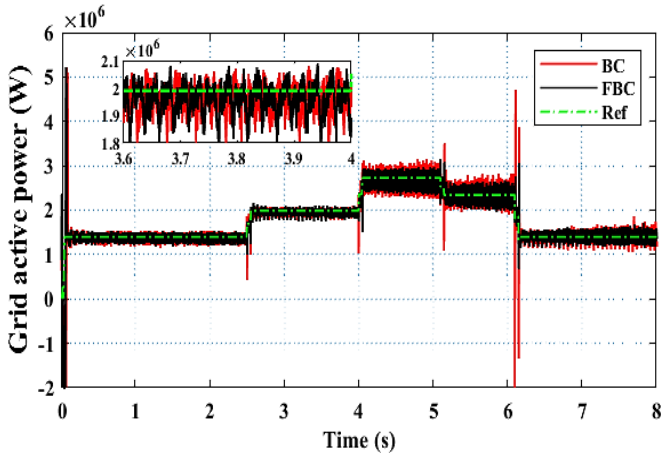

c)

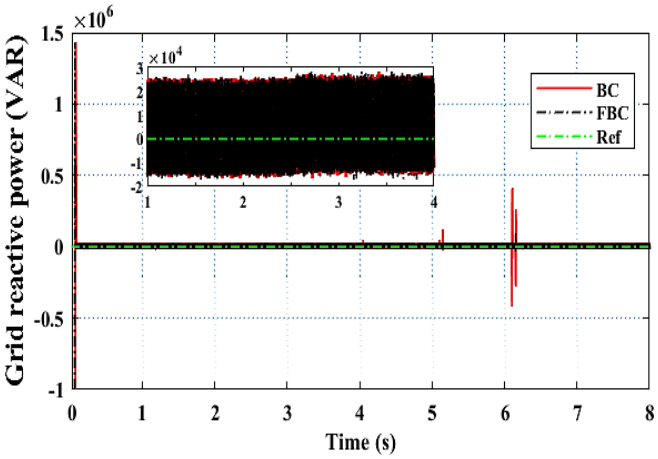

d)

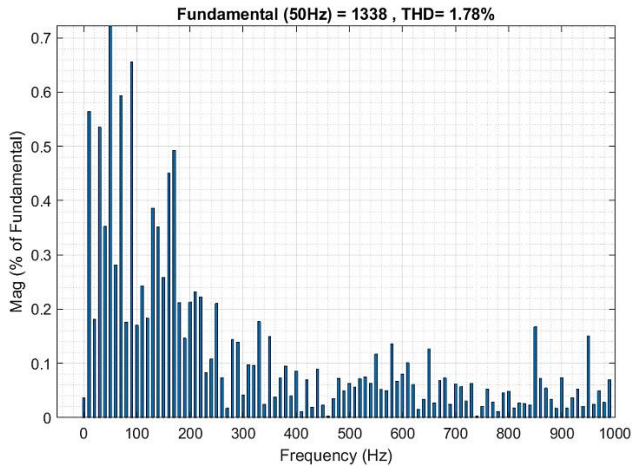

e) THD (FBC)

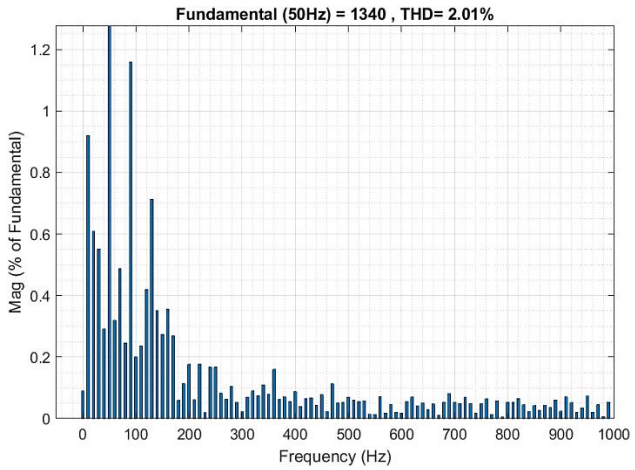

f)THD (BC)

Fig. (4.14): DC-link voltage, power, and THD of the suggested methods.

The THD values for both controls are shown in Figs. (4.14-e) and (4.14-f). This value is 1.78% and 2.01% for the FBC method and the BC strategy, respectively. Thus, the FBC method significantly reduces the THD value compared to the BC method, estimated at 11.44%. However, the FBC method provides unsatisfactory results in terms of the basic signal amplitude (50 Hz) compared to the BC strategy. The values of this amplitude are 1338A and 1340A for the FBC method and the BC method, respectively. This negativity could be attributed to the profit value of the FBC method, as it can be overcome in the future by using other strategies such as genetic algorithms to calculate the profit of the FBC method.

Table (4.2) provides the values and percentages of lessen for ripple, response time, SSE, power overshoot, and DC-link voltage. This table clearly shows the superiority of the FBC technique over the BC strategy in this test, as seen by the decrease percentages in Table (4.2). The FBC method decreased Q_g reaction time, ripples, SSE, and overshoot by an estimated 15.05%, 2.5%, 6.66%, and 0%, respectively. The P_g score was dropped by 14.28%, 16.66%, 16.66%, and 7.41%, respectively. The DC-link voltage ratios were estimated at 11.73%, 30.43%, 14.28%, and 24.43%, respectively.

Table (4.2): The response time, overshoot, ripples, and SSE ratios of the five-phase PMSG energy (test 1).

		***Pg* (W)**	***Qg* (VAR)**	**DC link voltage (V)**
BC	Ripples	300000	40000	2.3
	SSE	18000	15000	1.4
	Overshoot	2.7 M	1.43 M	570
	Response time (s)	0.098	0.093	0.0895
FBC	Ripples	250000	39000	1.6
	SSE	15000	14000	1.2
	Overshoot	2.5 M	1.43 M	425
	Response time (s)	0.084	0.079	0.075
Improvement Ratios	Ripples	16.66 %	2.5 %	30.43 %
	SSE	16.66 %	6.66 %	14.28
	Overshoot	7.41 %	0 %	24.43 %
	Response time	14.28 %	15.05 %	11.73 %

4.5.2 Variable wind velocity test

The wind velocity profile utilized varies between 9.5 m/s and 11.5 m/s over a period of 8 s (Fig. (4.15)). The simulations were performed with Q_g reference $Q_g = 0$, constant DC link reference voltage 2500 V, constant line voltage 690 V and frequency 50 Hz.

Fig. (4.16) displays the torque and P_g produced by the PMSGs, which are clearly aligned with the wind profile. Furthermore, it demonstrates a remarkable consistency between the torque of the WT and

the generator's torque, indicating a high level of consistency.

The generators speed response under varying WSs using two command approaches, namely BC and FBC, is presented in Fig. (4.17). Both approaches demonstrate satisfactory performance. However, a more thorough analysis of the detailed figures reveals that the FBC approach outperforms BC in several significant areas. These include a quicker response time, effective elimination of overshoot, and superior tracking of the desired values.

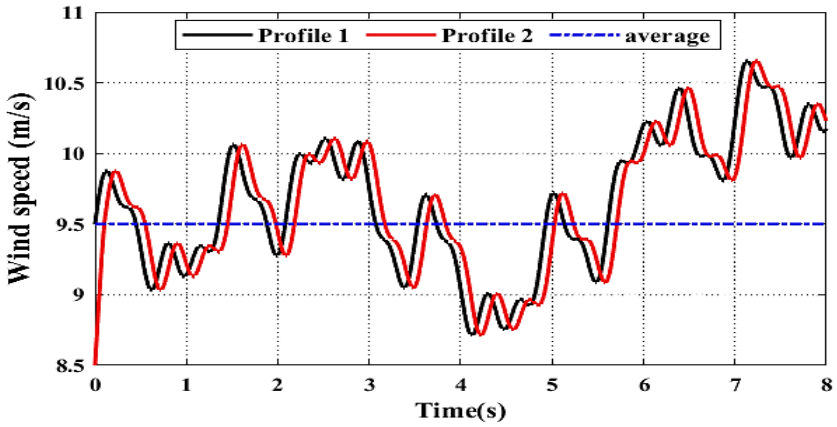

Fig. (4.15): Variable WS profile.

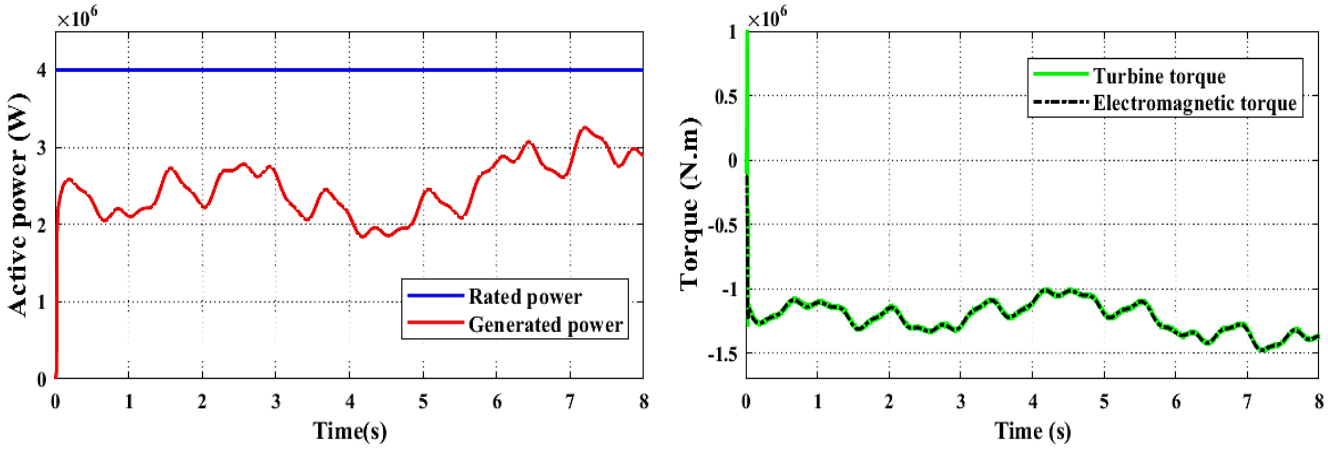

a) b)

Fig. (4.16): Simulation outcomes of WPGS controlled by FBC: a)Total mechanical power; b) Total torque

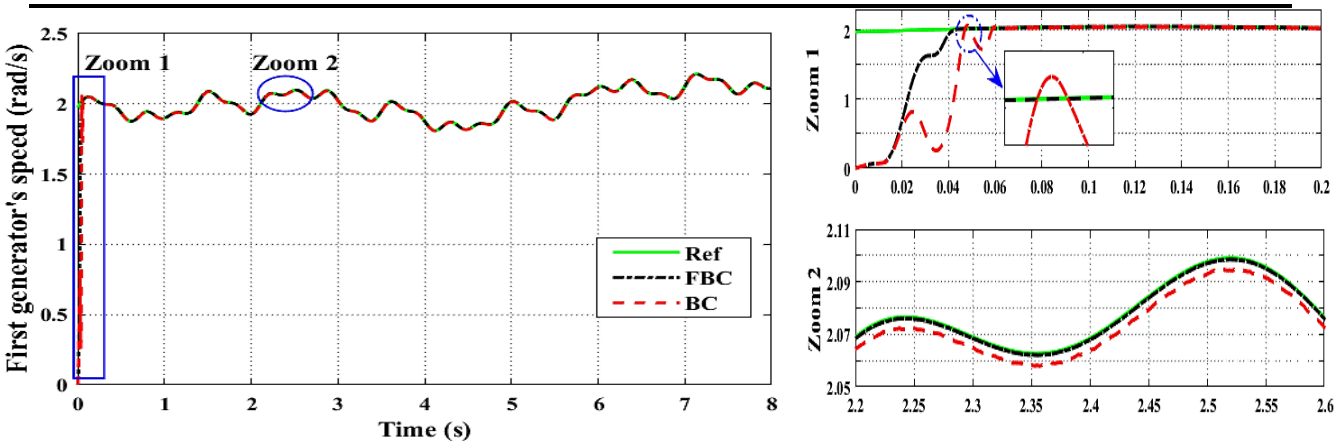

a)

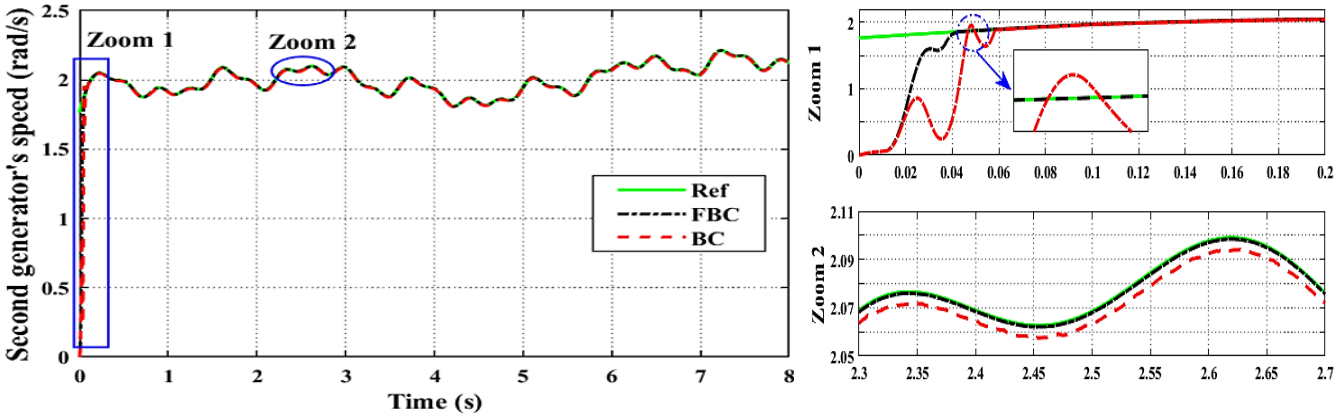

b)

Fig. (4.17): PMSGs' mechanical speed.

Fig. (4.18) depicts the outcomes of the power, current, THD, and DC-link voltage for both techniques when utilizing Generator 1. Figs (4.18-a) and (4.18-b) illustrate the line voltage for the two control methods. It is observed that this voltage maintains a constant value of 2500 volts, as the voltage value is not influenced by the shape of the WS variation in the presence of ripples. These ripples are more prominent in the case of the BC method compared to the FBC strategy.

Figs. (4.18-c) and (4.18-d) demonstrate P_g and Q_g, respectively. The Q_g value stays constant and is unaffected by the form of the WS modification, since it is equal to zero. It should also be noticed that employing the BC method results in more Q_g ripples than using the FBC technique. However, it is worth noting that the change in P_g is the same as the change in WS, since substantial undulations are detected when utilizing the BC method rather than the FBC method. This capacity closely follows the reference with a rapid dynamic reaction, as the FBC approach beats the BC strategy in terms of response time.

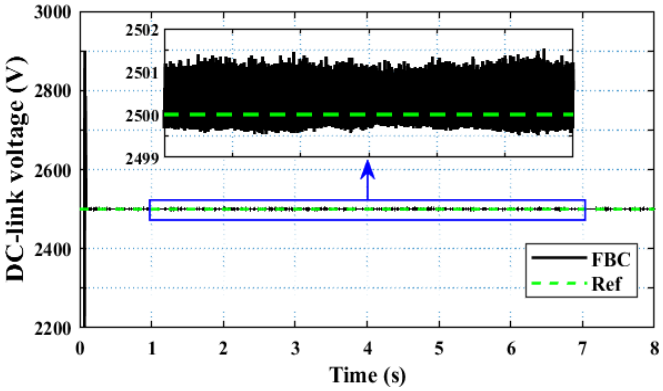

a)

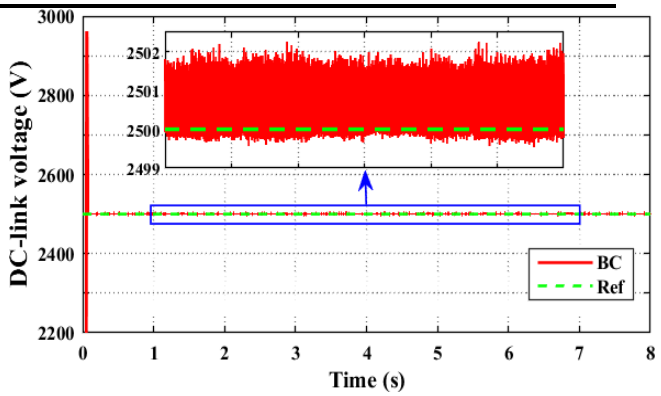

b)

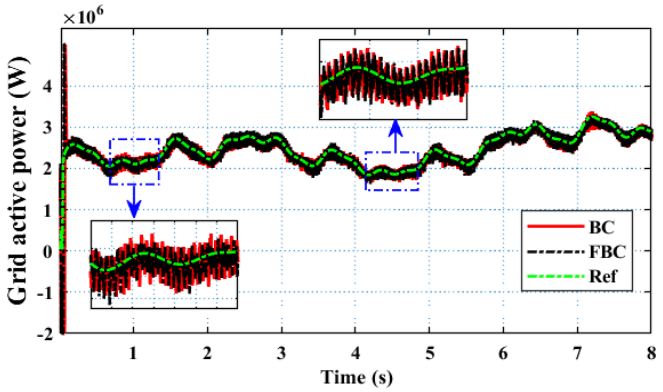

c)

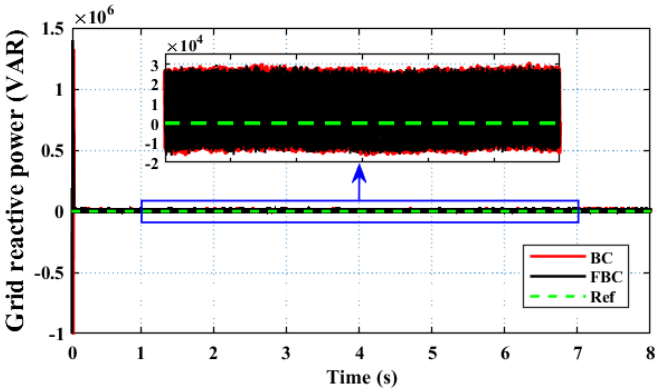

d)

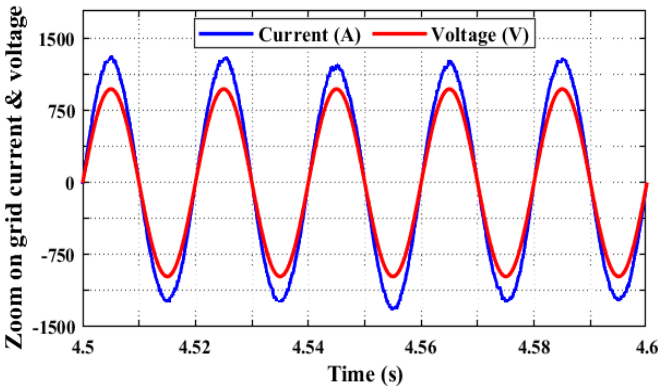

e) Stream and voltage (FBC)

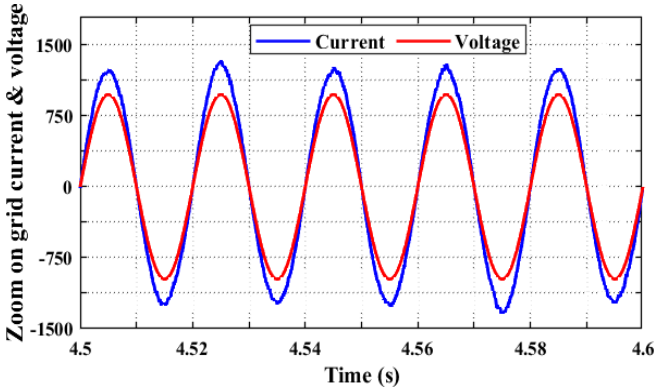

f) Stream and voltage (BC)

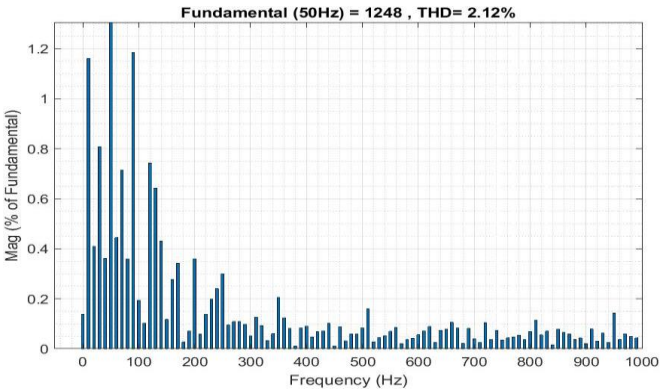

g) THD (FBC)

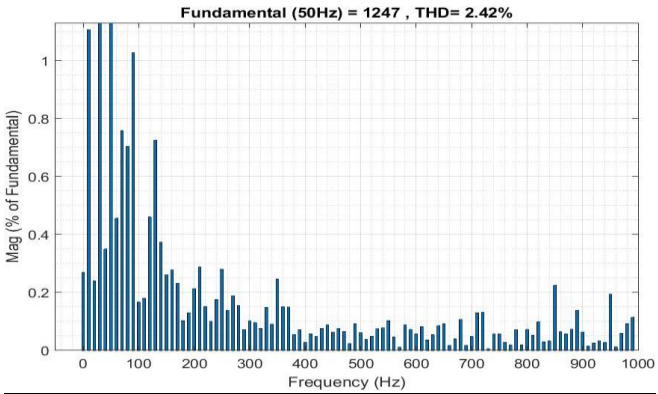

h) THD (BC)

Fig. (4.18): The simulation outcomes of test 2.

Figs. (4.18-e) and (4.18-f) show the current and voltage for both of these controllers. It is noticed that the current and voltage have a sinusoidal form, which gives the FBC methodology an edge in terms of quality over the BC method. Figs. (4.18-g) and (4.18-h) show the values for the amplitude of the basic signal (50 Hz) and the THD of current. The THD values for the FBC and BC techniques were 2.12% and 2.42%, respectively. As a result, the FBC greatly lowered the value of THD, with an estimated reduction rate of 12.40%. This percentage implies that the present quality is high when the FBC is employed, indicating the efficacy of this technique. The amplitude of the fundamental signal (50 Hz) in Figs. (4.18-g) and (4.18-h) was 1248 A and 1247 A for the FBC and BC strategies, respectively. These figures highlight the FBC technique's superiority over the BC approach, since they demonstrate the degree of the FBC technique's efficacy and capacity to enhance stream quality.

Table (4.3) presents the numerical findings obtained from the second experiment. It is observed that the FBC approach provided favorable results compared to the BC technique, as evidenced by the calculated reduction ratios, where the ripples, response time, SSE, and overshoot of DC-link voltage were reduced by approximately 20%, 15.85%, 33.33%, and 16.66%, respectively. The P_g approach exhibited reduction ratios of approximately 13.33%, 15.22%, 20%, and 4%, respectively. In the case of Q_g, the reduction percentages were estimated at 6.66%, 15.85%, 20%, and 0%, respectively.

Table (4.3): The response time, overshoot, ripples, and SSE ratios of the five-phase PMSG energy (Test 2).

		***Ps* (W)**	***Qs* (VAR)**	**DC link voltage (V)**
BC	Ripples	300000	45000	2.5
	SSE	20000	15000	1.5
	Overshoot	2.5 MW	1.4 M	480
	Response time (s)	0.092	0.085	0.082
FBC	Ripples	260000	42000	2
	SSE	16000	12000	1
	Overshoot	2.4 MW	1.4 M	400
	Response time (s)	0.078	0.072	0.069
Improvement Ratios	Ripples	13.33 %	6.66 %	20 %
	SSE	20 %	20 %	33.33 %
	Overshoot	4 %	0 %	16.66 %
	Response time	15.22 %	15.85 %	15.85 %

4.5.3 Robustness test

As part of this investigation, an additional test was conducted to furnish further evidence regarding the durability and reliability of the proposed method in comparison to the previous technique. This test, designated as the robustness test, entailed modifying the system parameters halfway through the

simulation process. By subjecting the system to parameter variations, the robustness test evaluates the capability of the FBC approach to sustain stable and consistent performance under dynamic conditions. This approach facilitates a comprehensive assessment of the strategy's ability to withstand and adapt to changes in the operational environment of the system.

Fig. (4.19) shows the generators' velocity characteristics. After analyzing the data, it is clear that the BC technique increases the error rate and causes ripples in the generator speed waveform after 6 seconds. This behavior could be attributed to the BC method's considerable dependence on system parameters. Because of the dynamic nature of system characteristics, the BC approach has difficulty successfully controlling generator speed, resulting in greater error rates and the appearance of undesirable ripples in the speed profile. In comparison, the FBC approach performs substantially better. The generator speed utilizing the FBC methodology continues to follow the reference value brilliantly and consistently, unaffected by variations in the system parameters.

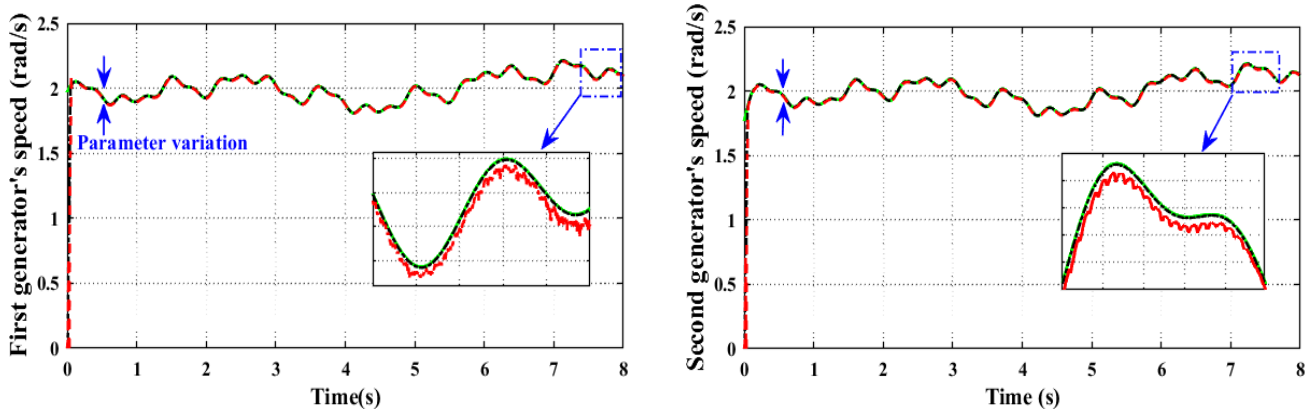

a) Speed (Generator 1) b) Speed (Generator 2)

Fig. (4.19): PMSGs' mechanical speed (Robust test)

Fig. (4.20) summarizes the important results on GS performance. Figs. (4.20-a) and (4.20-b) exhibit power profiles, one for P_g and the other for Q_g, demonstrating the FBC approach's stability and consistency in contrast to the BC method. The results show that the new test had a significant influence on the BC approach, with an apparent rise in power ripples for both P_g and Q_g. This shows a less constant and variable power injection into the grid under BC method. Figs. (4.20-c) and (4.20-d) support this observation by revealing a decrease in the quality of the current waveform and an increase in the proportion of THD when utilizing the BC technique.

The THD values were 2.36% and 4.56%, respectively, for the FBC and BC approaches. These results show that the FBC strategy surpasses the BC approach in this test in terms of THD value, which was decreased by an estimated 48.25 percent. This percentage implies that the present quality is much

greater than when employing the BC technique. It should also be highlighted that the FBC method outperforms the BC approach in terms of fundamental signal amplitude (50 Hz), with values of 1259 A and 1263 A for both the BC and FBC techniques, respectively. These findings illustrate the FBC technique's great performance and efficacy in enhancing the features of the analyzed system. In comparison, the FBC method had a very modest influence on system performance, remaining constant and consistent throughout the test. The FBC technique displays greater resilience and control capabilities, effectively minimizing the influence of test circumstances on grid-side performance.

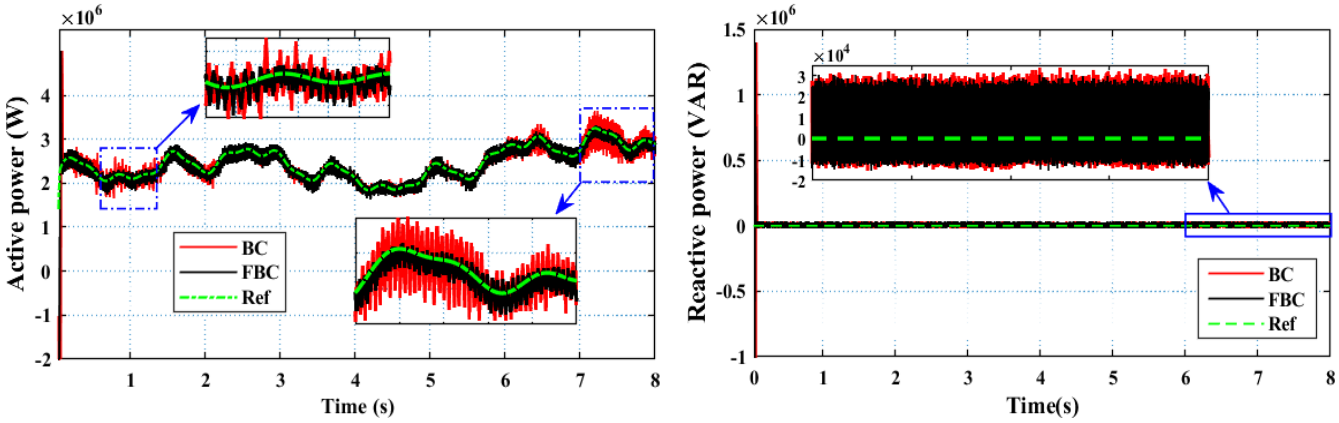

a) P_g

b) Q_g

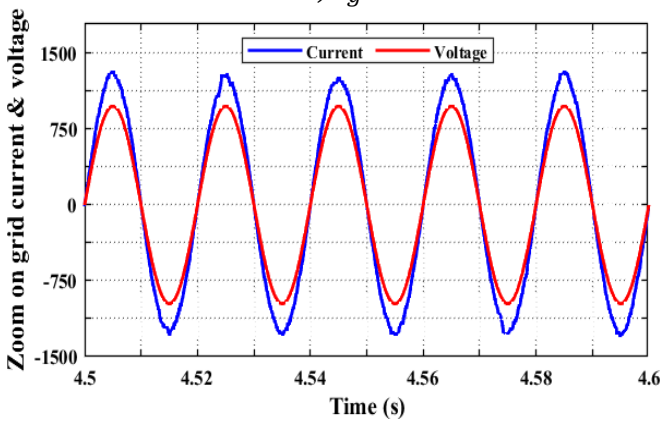

c) Stream and voltage (FBC)

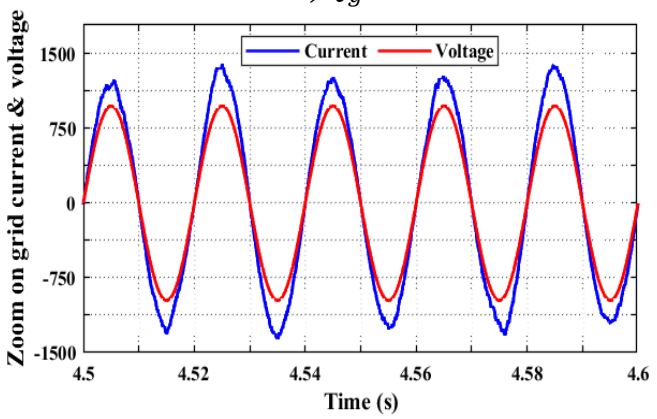

d) Stream and voltage (BC)

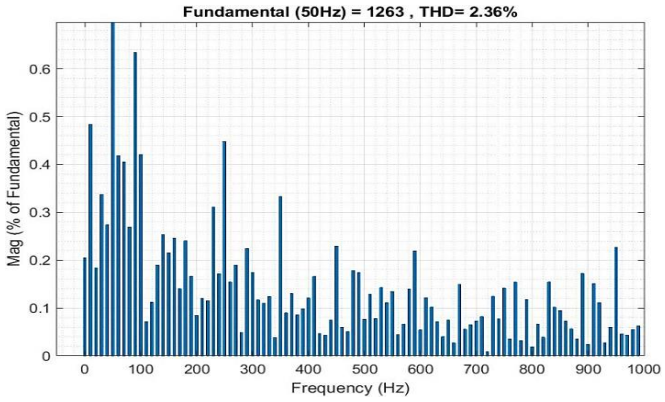

e)

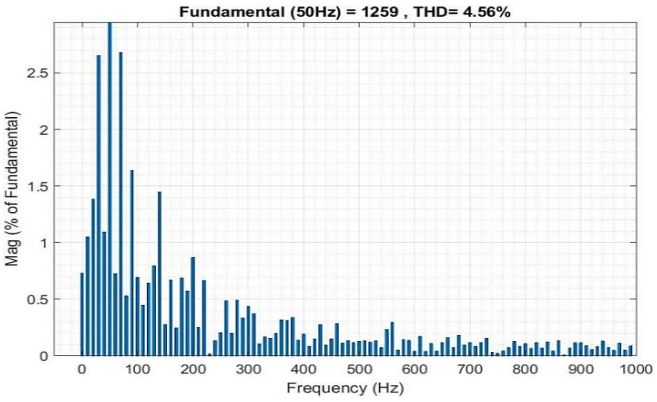

f)

Fig. (4.20): The results of test 3.

Table (4.4) presents the numerical data for the third control test. The table includes the values of response time, ripples, overshoot, and SSE of energy and DC-link voltage. Additionally, the necessary reduction ratios have been calculated to determine the extent of the performance and efficiency of the FBC technique compared to the traditional BC. The results indicate that the FBC technique outperformed the traditional BC strategy, as evidenced by the calculated reduction rates. Specifically, for the case of P_g, the FBC strategy reduced response time, ripples, overshoot, and SSE by 19.8%, 46%, 3.45%, and 82%, respectively. These findings demonstrate the superior performance of the FBC technique compared to the traditional BC method.

In the context of Q_g, the FBC technique has been observed to diminish the ripples, response time, SSE, and overshoot by approximately 10.42%, 21.05%, 23.53%, and 1.43%, respectively. These findings demonstrate the superior performance of the FBC in comparison to the traditional BC, rendering it a viable solution within the domain of control systems.

In terms of DC-link voltage, the FBC approach decreases ripples, overshoot, reaction time, and SSE by 26.09%, 17.95%, 22.82%, and 38.88%, respectively. These findings suggest that the FBC approach outperforms the conventional BC topology, making it a viable control option.

Table (4.4): The response time, ripples, overshoot, and SSE ratios of the five-phase PMSG energy (Test 3).

		***Pg* (W)**	***Qg* (VAR)**	**DC-link voltage (V)**
BC	Ripples	500000	48000	2.3
	SSE	100000	17000	1.8
	Overshoot	2.9 M	1.4 M	585
	Response time (s)	0.101	0.095	0.092
FBC	Ripples	270000	43000	1.7
	SSE	18000	13000	1.1
	Overshoot	2.8 M	1.38 M	480
	Response time (s)	0.081	0.075	0.071
Improvement Ratios	Ripples	46 %	10.42 %	26.09 %
	SSE	82 %	23.53 %	38.88
	Overshoot	3.45 %	1.43 %	17.95 %
	Response time	19.8 %	21.05 %	22.82 %

Table (4.5) provides a comparison of the finished work with other methodologies (References [17] and [20]) regarding the current's THD, simplicity, robustness, and stability. This table indicates that the implemented FBC approach yielded a much reduced THD value compared to other controls, including DPC and SMC. The suggested FBC technique presents complexity challenges for some current controls, such as DPC, which is a disadvantage. Besides its complexity, the FBC technique offers several advantages over other control methods like SMC. However, in terms of robustness, the FBC

approach outperforms certain current controls, which is a good thing since it makes the developed FBC technique a potential control option.

Table (4.5): Comparative analysis of performance among several control techniques.

References		Stability	Simplicity of implementation	Grid current THD (%)	Robustness
[17]	**DPC**	Medium	Simple	2.77	Weak
	SMC	Good	Simple	3.12	Strong
	BSC	Very good	Medium	1.91	Medium
	MPC	Good	Medium	1.25	Strong
[20]	**DPC**	Medium	Simple	107.75	Weak
	DPC-SVM	Medium	Simple	51.44	Weak
	Proposed FBC	Very good	Complicated	1.78	Strong

4.6 Conclusion

This chapter concentrates on applying a intelligent nonlinear command approach to a variable-speed WPGS employing 5-phase PMSGs. The chapter initially presents the concept of nonlinear command based on the Lyapunov stability technique. It emphasizes the continuous adjustment of command gains through the utilization of a FL approach to optimize the performance of the wind power generation system. The command algorithm described in this chapter ensures the speed regulation and precise tracking of setpoints. The 5-phase PMSGs modeling, wind power generation system, and intelligent command theory are thoroughly developed. A simulation is conducted utilizing the MATLAB tool. The research concludes with important findings, which are explained as follows:

- The suggested approach exhibits superior performance compared to the nonlinear command approach across various wind profile scenarios.
- The control algorithm's continuous adjustment of gains ensures robustness against wind profile variations.
- The control approach guarantees accurate speed regulation and effective tracking of different references with improved performance.
- This control demonstrates high energy efficiency and achieves a power factor close to unity, affirming its efficiency.

- Simulation results indicate that the intelligent command approach enhances both the static and dynamic performance of the WPGS.

General Conclusion

General Conclusion

Enhancements in the design and functionality of WPGSs are crucial to augment their competitiveness in electricity production. In this regard, the primary objective of the research presented in this thesis is to study and develop a control design for two parallel-connected 5-phase PMSGs. This design enables independent control of the two 5-phase PMSGs, which are supplied by a FSR. The research addresses the key aspects of each chapter as follows:

In the first chapter, we provided a comprehensive overview of WE production in Algeria, including a definition of wind energy and a classification of existing wind generators. We discussed the two primary types of WTs: fixed-speed and variable-speed, along with the various configurations of wind energy conversion systems. In the second place, we examined the key characteristics of both onshore and offshore WE, highlighting the energy output associated with each type and identifying the major global investors in this sector. This analysis underscores the increasing importance of wind energy in the global energy landscape. In the third place, we explored the different configurations of WTs, specifically focusing on asynchronous and synchronous generators. In last place, we concluded with a detailed explanation of modeling wind turbines. This structured approach aims to provide a thorough understanding of the current state and future potential of WE technologies.

Chapter two concentrated on the kind of generator used in this research. We began by defining multiphase machines and discussing their most significant applications, along with a detailed examination of their various types, advantages, and disadvantages. Following this, we provided an overview of five-phase PMSMs, identifying their key components and essential elements. A comprehensive explanation of the different types of five-phase PMSMs was also included, highlighting their specific applications in various industries. Furthermore, we elucidated the modeling procedure for the 5-phase PMSG, demonstrating the theoretical foundation essential for comprehending its functioning. This chapter also included a discussion on the modeling of two parallel PMSGs within the generation system. This thorough analysis aims to contribute to the understanding of multiphase technology and its relevance in modern energy systems.

Chapter three concentrated on the crucial component of this conversion system, namely the fifteen-switch rectifier. First, a simple definition was provided with an explanation of the general engineering of this transformer. After that, an explanation of how it works was explained, and the method of using the PWM unit on this type of converter was explained. To provide a comprehensive and good explanation of this converter, and based on traditional rectifiers, the method of operation of the

traditional five-phase rectifier was explained, with an explanation of all operating cases. After that, all operating cases were also explained and the FSR was explained, with work on a simple simulation that explains the operation of this converter. Ultimately, the key strengths and weaknesses of FSR were discussed in comparison to the use of two conventional rectifiers in parallel.

In the fourth chapter, the application of the FBC strategy to a multi-machine WPGS is discussed in detail. The chapter commences by defining the BC technology and elucidating its fundamental principles and salient characteristics. Subsequently, a comprehensive explication of FL is provided, highlighting its essential features and merits. Subsequently, the application of the BC strategy to the entire WPGS has been thoroughly examined, including a detailed description of how FL is integrated into the control framework. The chapter concludes with the presentation of simulation results obtained from multiple test scenarios designed to evaluate the efficacy of the suggested strategy. These results demonstrate that the FBC approach substantially outperforms traditional BC, showcasing its robust performance and potential for enhancing the efficiency and reliability of WPGS.

Future Works

Future work could explore a broad range of areas within this field to ensure continuity in research. Therefore, some potential suggestions and perspectives include:

- This work will be attempted experimentally using real equipment to prove these results obtained.
- Implementing diverse nonlinear control methodologies in conjunction with artificial intelligence control strategies.
- Addressing the most important weakness of the FSR, which is the output voltage amplitude.
- Working on multi-machine WPGSs that can accommodate more than two generators.

Appendices

APPENDIX A

TABLE A.1. Detailed WT specification

Coefficients	R	ρ	C_{pmax}	λ_{opt}
$C_1 = 0.5176, C_2 = 116, C_3 = 0.4, C_4 = 5, C_5 = 21, C_{6=}0.0068$	39 m	1.225 kg/m^3	0.48	8.1

TABLE A. 1. Detailed PMSGs parameters

Parameters	P_n	R_s	L_s	P	J	Ψ_f
Values	2 MW	0.821 mΩ	1.573 mH	26	6300 Kg/m^2	13.0282 Wb

TABLE A. 2. Detailed Grid filter and DC-link parameters

Parameters	C	F_g	R_g	L_g	V_{dc-ref}
Values	0.038 F	50 Hz	0.01 Ω	0.001 H	2500 V

APPENDIX B

Controllers Parameters

TABLE B. 1. BC parameters (MSC)

	Speed controller	**Currents controller**			
BC	$K_{\Omega j} = 2500$	$K_{dj} = 30000$	$K_{qj} = 30000$	$K_{xj} = 20$	$K_{yj} = 20$

TABLE B. 2. BC parameters (GSC)

	DC-link voltage controller	**Currents controller**	
BC	$K_{dc} = 10000$	$K_{dg} = 10000$	$K_{qg} = 100000$

References

References

[1] Rhaili SE, Abbou A, Marhraoui S, Moutchou R. Robust Sliding Mode Control with Five Sliding Surfaces of Five-Phase PMSG Based Variable Speed Wind Energy Conversion System. International Journal of Intelligent Engineering & Systems. 2020 Jul 1;13(4).

[2] Mousa HH, Youssef AR, Mohamed EE. Optimal power extraction control schemes for five-phase PMSG based wind generation systems. Engineering science and technology, an international journal. 2020 Feb 1;23(1):144-55.

[3] Bossoufi BA, Karim MO, Lagrioui AH, Taoussi M. FPGA-Based Implementation Sliding Mode Control and nonlinear Adaptive Backstepping control of a Permanent Magnet Synchronous Machine Drive. Wseas Trans. Syst. Control. 2014 Feb;9:86-100.

[4] Sakouchi A, Bounadja E, Djahbar A. Nonlinear control via Backstepping for five-phase permanent magnet synchronous generator-based wind generation system. In2023 2nd International Conference on Electronics, Energy and Measurement (IC2EM) 2023 Nov 28 (Vol. 1, pp. 1-6). IEEE.

[5] Ghaffar MK, Fadhel FS, Arif NE. Application of the generalized backstepping control method for lotka-volterra prey-predator system with constant time delay. InJournal of Physics: Conference Series 2022 Aug 1 (Vol. 2322, No. 1, p. 012012). IOP Publishing.

[6] Vaidyanathan S, Azar AT, editors. Backstepping control of nonlinear dynamical systems. Academic Press; 2020 Aug 15.

[7] Hassan KK. Nonlinear systems. Departement of Electrical and computer Engineering, Michigan State University. 2002.

[8] Freeman R, Kokotovic PV. Robust nonlinear control design: state-space and Lyapunov techniques. Springer Science & Business Media; 2008 Jan 11.

[9] Tedrake R. Lyapunov Analysis. In: Underactuated Robotics: Algorithms for Walking, Running, Swimming, Flying, and Manipulation [Internet]. MIT; 2024 [cited 2024 Nov 11]. Available from: https://underactuated.mit.edu/lyapunov.html.

[10] Slotine JJ, Li W. Applied nonlinear control. Englewood Cliffs, NJ: Prentice hall; 1991 Jan.

[11] Nikravesh SK. Nonlinear systems stability analysis: Lyapunov-based approach. CRC Press; 2018 Sep 3.

[12] Ross TJ. Fuzzy logic with engineering applications. John Wiley & Sons; 2005 Apr 8.

[13] Bai Y, Wang D. Fundamentals of fuzzy logic control—fuzzy sets, fuzzy rules and defuzzifications. Advanced fuzzy logic technologies in industrial applications. 2006:17-36.

[14] Sakouchi A, Bounadja E, Djahbar A, Moualdia A. Artificial intelligent-based backstepping control of parallel-connected multi-machine wind generation system using a new fifteen-switch rectifier. Wind Engineering. 2024 Oct 7:0309524X241270424.

[15] Koganti S, Sravanthy G, Teja Santhosh D, Yashaswini N, Nagaraju V, Prasad Reddy J G, Kumar NMG, Naik D A. Design and Performance Analysis of Fuzzy Based Hybrid Controller for Grid Connected Solar-Battery Unified Power Quality Conditioner. International Journal of Renewable Energy Research-IJRER, 2023, 13(1): 1-13. https://doi.org/10.20508/ijrer.v13i1.13318.g8655

[16] Ch Rami R, Prakash R B R, Srinivasa Varma P, Dilip Kumar M, Giri Prasad A, Shiva Prasad E. Maximum Power Point Tracking for Permanent Magnet Synchronous Generator based Wind Park Application. International Journal of Renewable Energy Research-IJRER, 2022, 12(2): 846-862. https://doi.org/10.20508/ijrer.v12i2.12872.g8469.

[17] Majout B, El Alami H, Salime H, Zine Laabidine N, El Mourabit Y, Motahhir S, Bouderbala M, Karim M, Bossoufi B. A review on popular control applications in wind energy conversion system based on permanent magnet generator PMSG. Energies. 2022 Aug 26;15(17):6238.

[18] Aziz D, Jamal B, Othmane Z, Khalid M, Bossoufi B. Implementation and validation of backstepping control for PMSG wind turbine using dSPACE controller board. Energy Reports. 2019 Nov 1;5:807-21.

[19] El Mourabit Y, Derouich A, El Ghzizal A, El Ouanjli N, Zamzoum O. Nonlinear backstepping control for PMSG wind turbine used on the real wind profile of the Dakhla-Morocco city. International Transactions on Electrical Energy Systems. 2020 Apr;30(4):e12297.

[20] Bounadja E, Boudjema Z, Djahbar A. A New DPC-SVM for Matrix Converter Used in Wind Energy Conversion System Based on Multiphase Permanent Magnet Synchronous Generator. Iranian Journal of Electrical & Electronic Engineering. 2019 Sep 1;15(3).